Friction stir welding processes in AA7050 thick plates

[blank page]

Faculdade de Engenharia da Universidade do Porto

Friction stir welding processes in AA7050 thick plates

By

Vitor Manuel Pereira Correia

A thesis submitted in partial fulfilment for the

Degree of Integrated master in Mechanical Engineering

Faculty of Engineering, University of Porto, Portugal

[blank page]

Friction stir welding processes in AA7050 thick plates

By

Vitor Manuel Pereira Correia

A document written fin partial fulfilment for the Degree of Master of Science in Mechanical Engineering
at

Helmholtz-Zentrum Geesthacht – Zentrum für Material- und Küstenforschung

Geesthacht, Germany

Integrated Master Degree in
Mechanical Engineering

SUBMITTED TO

Faculty of Engineering, University of Porto, Portugal

Revised Version
September 2015

[blank page]

Abstract

Friction stir welding processes in

AA7050 thick plates

Correia, Vitor

M.S., Department of Mechanical Engineering

Supervisor at HZG: Luciano Bergmann

Co-advisor at HZG: Dr. Jorge dos Santos

Co-advisor at FEUP: Prof. Dr. Paulo Tavares de Castro

A parameters study on friction stir welding processes on 8 mm thick plates of the aluminium alloy AA7050-T7451 was done. Conventional friction stir welding (FSW) and double-sided friction stir welding (DS-FSW) welds were produced and the mechanical properties and metallurgical features were evaluated. Relationship between welding parameters and the properties of the welded joints were undertaken in order to lead to a better understanding of the implications of the process in the final outcome of the weld process. From the parameters study, significant efficiency was achieved and a comparison between the two welding variants was done. For the best set of parameters found and for both variants, FSW and DS-FSW, temperature measurements during the welding process and distortion assessment, through the optical system PONTOS, were performed.

Keywords: parameters study; friction stir welding (FSW); aluminium alloys; AA7050; double-sided friction stir welding (DS-FSW); hardness; microstructure; temperature measurement; distortion assessment

[blank page]

Resumo

Friction stir welding processes in

AA7050 thick plates

Correia, Vitor

M.E., Departamento de Engenharia Mecânica

Supervisor no HZG: Luciano Bergmann

Co-orientador no HZG: Dr. Jorge dos Santos

Co-orientador na FEUP: Prof. Dr. Paulo Tavares de Castro

Foi realizado um estudo de parâmetros envolvendo processos de soldadura por fricção linear em placas de 8 mm de espessura da liga de alumínio AA7050-T7451. Uniões por soldadura foram realizadas pelo processo convencional de soldadura por fricção linear (FSW) e pelo processo de soldadura por fricção linear em dupla-face (DS-FSW) sendo as suas propriedades mecânicas e metalúrgicas avaliadas. Foram desenvolvidas relações entre parâmetros de soldadura e propriedades das ligações soldadas com vista a melhor entender as implicações dos processos no desfecho final do conjunto soldado. Do estudo de parâmetros, foram alcançados valores significativos de eficiência sendo feita uma comparação entre as duas variantes. Para o melhor conjunto de parâmetros encontrado e para ambos os processos, FSW e DS-FSW, foram realizadas medições de temperatura durante o processo de soldagem e avaliação da distorção, através do sistema óptico PONTOS,

Palavras-chave: estudo de parâmetros; friction stir welding (FSW); ligas de alumínio; AA7050; double-sided friction stir welding (DS-FSW); dureza; micro-estrutura; medição de temperatura; avaliação da distorção

[blank page]

Acknowledgements

I would like to express a special and immense gratitude to:

Prof. Dr. Paulo M.S. Tavares de Castro, co-advisor of this thesis at FEUP, Portugal, for giving me the amazing opportunity to come to Germany to produce my master's thesis. For all the support, for his contribution and for his comprehension while I stayed at HZG, I couldn't ask more.

Dr. Jorge dos Santos, co-advisor of this thesis at HZG, Germany, who, without any kind of problem, opened the possibility of working in his department and with all his staff with whom I have learned a lot. For the kindness that always demonstrated since my first day in Germany and for the comprehension and dedication to my project whenever I asked.

Luciano Bergmann, supervisor of this thesis at HZG, Germany, for the orientation of my project and guidance in all the steps of my experimental work. Without him none of my experimental work would be possible as well the results from it taken.

Eduardo Feistauer, PhD candidate, for his precious help during the preparation of samples and his always important tips.

Leon L. Hütsch, for his promptitude and professionalism that always demonstrated whenever his opinion was requested and specially for his tremendous assistance on my distortion assessment.

Stefanie Hanke and **Junjun Shen** my co-workers at HZG, for helping me with the SEM analysis.

Menno Peters, for his dedication and efficiency in the innumerable times I requested his help during my experimental work.

Tiago Ramos, my colleague in FEUP and LOME, Portugal, for precious help with the structure of my thesis.

Finally I would also like to express my gratitude to all my colleagues at HZG that during my stay had in one way or another helped me and made, ultimately, this work be possible.

[blank page]

À minha família, mãe, pai e irmã

[blank page]

Contents

[blank page]

List of Figures

[blank page]

List of Tables

[blank page]

Nomenclature

ν	tool transverse speed or welding speed [mm/s]
ω	tool rotation rate [rad/s] or [rpm]
AS	advancing side
BM	base material/metal
DXZ	dynamically recrystallized zone
FCP	fatigue crack propagation
FSW	friction stir welding
H.I.	heat input
HAZ	heat-affected zone
HZG	Helmholtz Zentrum Geesthacht
JLR	joint line remnant
LOP	lack of penetration
LTD	long transverse direction
MIN	minimum-hardness region
mm/s	millimetres per second
PM	parent material/metal
R	(maximum/minimum) stress ratio
RD	rolling direction
ROL	remnant oxide layer
RS	retreating side
SCC	stress corrosion cracking
SEM	scanning electron microscope
SOF	region of lower hardness than base material

SOF softened region

SSFSW stationary shoulder friction stir welding

STD short transverse direction

SZ stir zone

TMAZ thermo-mechanically affected zone

TWI The Welding Institute

UFG ultra-fine-grained

Chapter 1

Introduction

It is fairly well known that high-strength aluminium alloys such as 2XXX and 7XXX series are widely used in aerospace structures such as fuselage, vertical stabilizers, wings, etc. Unfortunately, such high-strength aluminium alloys are quite difficult to join by conventional fusion welding process due to the great tendency of hot crack during and after the welding process. Conventionally, and as a consequence, significant amount of joining in aerospace structures has been and still is achieved by means of riveting which results in increased manufacturing complexity and high costs. The emergence of friction stir welding, in 1991, provided an opportunity to alter the traditional approach of joining leading to lighter assemblies, reduction on the number of parts as well the production cycle times, greater joint strength and lower manufacturing costs [1].

The 2XXX and 7XXX alloys, which develop the highest strength levels [2] are the main alloys used for metallic airframe components and have been the focus of many studies in both similar and dissimilar butt and lap joint configurations [1]. In such studies and for aircraft applications in general workpiece sheets (under 6.35 mm thick) for fuselage skins and stringers and workpiece plates (above 6.35 mm thick) for wing skins, bulkheads and wing spars [2] are the starting point of all the manufacturing processes. The 7XXX series aluminium alloys, in particular, show higher strength when compared to other classes of aluminium alloys and are commonly selected for the fabrication of upper wing skins, stringers and horizontal/vertical stabilizers [3]. A wing is essentially a beam that transmits the entire applied air load to the central attachment to the fuselage; depending on whether the aircraft is flying or at rest, the wing covers are subject to alternating tensile-compressive loads which requires from the material there used a slow crack growth, long critical length and residual strength as well a good corrosion resistance and stress corrosion cracking (SCC) [2]. The 7050 aluminium alloys, covered in this document presents a good balance of strength, stress corrosion cracking resistance and toughness [3] making it ideal for wing structural parts.

Since the first implementations of FSW process in aerospace industry, around 1998 [1], its repeatability and reliability coupled by its ability of successfully joint lightweight alloys made the it particular attractive for aerospace applications and since then many commercial aerospace manufactures have implemented the use of FSW or are evaluating the technology for a possible use on future aircraft. The work here presented and consequently this document appears as a consequence of the attempt made by the aircraft manufactures in trying to improve their joining processes, in particular friction stir welding processes, in more and more metallic materials and with better mechanical properties in order to be competitive with the ascension of the composite materials and meet the requirements of the airline customers.

1.1 Project and project goal

The main objective of this work was to produce sound welds by friction stir welding processes in 8 mm thick plates of the high-strength aluminium alloy AA7050-T7451. The work was part of a bigger project by EMBRAER which defined that butt welds were to be obtained by conventional friction stir welding (FSW), double-sided friction stir welding (DS-FSW), stationary shoulder friction stir welding (SSFSW), double-sided stationary shoulder friction stir welding (DS-SSFSW) and finally bobbin-tool friction stir welding (BT-FSW). In this document only the FSW and DS-FSW variants were covered.

The welds had to respect some specifications concerned not only with welding parameters but also with mechanical properties of the weld itself as well some issues related with the productivity of the process. A welding speed - the speed along the weld joint - of at least 5 mm/s was one of specifications that had to be respected beforehand as a welding parameter; welds obtained with lower speeds were considered insufficient from the point of view of productivity. The original project also specified that the weld efficiency should be preferably higher than 80% which, in reality meant that the mechanical properties of the welded zone and the zone nearby the weld should be of at least 80% of that of the base material. Finally a requirement regarding the tool live was specified; 25 m of effective weld should be the minimum of the tool life. This last specification is obviously directed to the productivity that must, naturally be as high as possible.

The current project had a significant content of experimental work nature which was aimed at real industrial applications where results always play a significant role; friction stir welding techniques to produce successfully welded joints on 8 mm thick plates for structural wing applications was the main goal of this work since depending on the quality of the results technical and experimental information could be used for the next aircraft generation by EMBRAER.

1.2 Document structure and organization

This document is divided in 5 main chapters, being this the first one. Throughout Chapter 2 a brief introduction to aluminium alloys for aerospace applications and an overview of the friction stir welding process, particularly applied in high-strength aluminium alloys, is made.

Chapter 3 introduces a fairly detailed description of the equipment set-up and the experimental procedure performed during all the experimental work.

In Chapter 4, are presented all the results arising from the experimental work followed by a brief discussion.

Chapter 5 presents the final conclusions of this dissertation as well some of the recommendations for future work.

Chapter 2

Literature Review

This chapter aims to introduce the place of the aluminium alloys in the aerospace industry, some of the reasons why that happens as well as some of the particularities of the high-strength aluminium alloys. A significant part of this section was dedicated to an overview on the friction stir welding (FSW) joining process, some of its basic principles, the main experimental parameters, microstructure features, thermal history and metal flow among various others. Although the friction stir welding process was described in general terms a special reference was made with regard of its applications on high-strength heat-treatable aluminium alloys.

2.1 Aluminium

2.1.1 Aluminium and Aerospace Industry

Aluminium alloys have been, for more than 80 years, the primary material for the structural parts of aircraft. Well known performance, well established design methods, manufacturing and reliable inspection techniques are some of the reasons that made that happen. In more recent years though, composite materials have started to appear and to be used more widely in different parts of aircraft such as fuselage, wings as well as other structural components in place of aluminium alloys. Although the gradual increase of composite materials reduces the role of aluminium up some extent, high-strength aluminium alloys remained unshakable in some parts of airframe construction due its competitive properties and relatively low cost production.

Cost reductions related with aircraft industries are of extreme importance and have become a driving force in many airlines companies. These cost reductions can be achieved by various ways such as the decreasing of fuel consumption, maintenance cost, operational costs, decreasing the frequency of periodical controls, increasing the service life or even carrying more passengers at a time. It is commonly known that weight reduction can reduce fuel consumption and at the same time increase payload and the ranges involved. Additionally, improved and optimized mechanical properties of the materials can result in the increase of the period between maintenance and therefore reduce significantly repair costs. Since the material has a great impact in cost reduction, airframe manufacturers and material producers are focused on the development of new materials to meet customer requirements and consequently a current challenge is to develop new materials that can be used in fuselage and wing construction with improvements in both structural performance and life cycle cost. As stated by Campbell in his work [4] “ the decrease in density is about 3–5 times more effective than increasing tensile strength, elastic modulus or damage

tolerance" and thus it seems perfectly acceptable to think that an effective way of reducing the aircraft weight is by reducing the material density of the material used. A fairly direct parameter that also significantly affects cost is undoubtedly the airframe durability. Campbell, also mentioned in his work that the cost of service and maintenance over the 30-year life of the aircraft are estimated to exceed the original purchase price by a factor of two [4]. Therefore, both material producers and aircraft designers, are working in harmony to reduce weight, improve damage tolerance, fatigue and corrosion resistance of the new metallic alloys; the idea is in a near future the primary aircraft structures present an extended service life and require reduced frequency of inspections.

As previously mentioned composite materials are increasingly being used in aircraft primary structures. This attractiveness on the use of composites in the manufacturing of high performance structures relies on their superior mechanical properties when compared to metals. Higher specific stiffness, specific strength, fatigue and corrosion resistance are some of them. Although composite materials are thought to be the preferable material for wing and fuselage structures, their significantly high production costs, relatively low resistance to impact and complex mechanical behaviour, mainly due to change in environmental conditions (moisture absorption, soft/brittle transition when exposed to hot/cold environments) make designers to explore alternative techniques and material systems where metal materials and particularly aluminium alloys can be of extreme importance and have a fundamental role in the structural composition of aircraft. For these reasons aluminium producers and aircraft manufactures keep investing and put great effort in trying to improve more and more the thermo-mechanical properties of the aluminium alloys they produce as well trying to improve technologies that are already available and invent new ones.

2.1.2 Aluminium alloys

Aluminium is a light weight material with a density of approximately 2700 kg/m^3; both, pure aluminium and its alloys have the face centred cubic (FCC) structure, which is stable at temperatures up to its melting point, that is of approximately 650°C. Just only a few elements have sufficient solid solubility in aluminium to be major alloying elements; copper, magnesium, silicon, zinc an lithium are some of them. Chromium, manganese and zirconium although possessing lower solid solubility are also important transition elements which normally form compounds that help to control the grain structure of the aluminium alloy.

Aluminium alloys are normally classified into one of three groups: wrought non-heat treatable alloys, wrought heat-treatable alloys and casting alloys [4]. In this document an exhaustive explanation of all of them will not be made; since the aluminium alloy studied is AA7050-T4751, which is an high-strength heat-treatable aluminium alloy, this document will be mainly directed to such alloy or similar alloys in both properties and composition.

As previously mentioned, aluminium alloys are classified into the wrought non-heat treatable alloys that cannot be strengthened by precipitation hardening and so, they are hardened primarily by cold working; wrought non-heat treatable alloys include the series 1XXX, 3XXX, 4XXX and 5XXX. Since these kind of aluminium alloys are mainly hardened by cold working, load-bearing structural applications even at moderately elevated temperatures should be avoided since the cold worked structure could start softening (i.e. annealing). The wrought heat-treatable alloys, unlike the previous ones, can be precipitation hardened in order to develop quite high-strength levels. These alloys include the 2XXX series (Al-Cu and Al-Cu-Mg), the 6XXX series (Al-Mg-Si), the 7XXX series (Al-Zn-Mg and Al-Zn-Mg-Cu) and the aluminium-lithium alloys known as 8XXX alloys series. The 2XXX and 7XXX alloy series are those which develop the highest strength levels and therefore are the main aluminium alloys used in metal-

lic airframe components. The Al-Cu alloys of the 2XXX series, the Al-Mg-Si (6XXX) and the alloys Al-Zn-Mg of the 7XXX series are considered medium strength alloys and are classified as being fusion weldable whereas the Al-Cu-Mg (2XXX) and Al-Zn-Mg-Cu (7XXX) are generally higher strengthened and the fusion welding process is considered quite impossible. Problems with the weldability of the such aluminium alloys will be addressed latter.

The process of strengthening hardening plays a crucial role in high-strength aluminium alloys and, as will be discussed in more detail further in this document, consists of three steps: (1) solution heat treating, (2) rapidly quenching to a lower temperature and finally (3) the aging. In solution heat treating, the material is heated up to a temperature capable of put the soluble alloying elements in solution and held in this situation for a determined period of time; then it is quenched to a lower temperature in order to trap the alloying elements in solution and finally during the aging the alloying elements previously trapped in solution precipitate forming a uniform distribution of very fine particles. This distribution of precipitates strengthens and hardens the treated alloy by creating obstacles to dislocation movement [4].

2.1.2.1 Designation

Wrought aluminium alloys are designated by a four digit numerical systems developed by the Aluminium Association. The designations can be observed in Tab. 2.1 [2]. The first digit defines the major class of the series (example 2XXX - two thousand series). The second digit defines variations in the original basic alloys: it can be zero (0) for the original composition, one (1) for the first variation, two (2) for the second variation and so on. The third and fourth digits designate the specific alloy within the series; there is no special significance to the value of those digits except for the 1XXX series.

Series	Main alloying element
1XXX	99.00% Al
2XXX	Copper
3XXX	Manganese
4XXX	Silicon
5XXX	Magnesium
6XXX	Magnesium and Silicon
7XXX	Zinc
8XXX	Others

Table 2.1: Designations for aluminium wrought alloys.

Frequently attached to the designation series of the aluminium alloys is the temper designation. This designation consists of a letter followed by certain digits that are concerned with the tempers particularities In the case of the heat-treatable alloys this designation consists of the letter "T" followed by one, two, three or even four digits that specify the kind of temper made in that alloy in particular. Below its shown the temper designations for the heat-treatable aluminium alloys [2].

T1	Cooled from an Elevated Temperature Shaping Operation + Natural Age
T2	Cooled from an Elevated Temperature Shaping Operation + Cold Worked + Natural Age
T3	Solution Treated + Cold Worked + Natural Age
T4	Solution Treated + Natural Age
T5	Cooled from an Elevated Temperature Shaping Operation + Artificial Age
T6	Solution Treated + Artificially Aged
T7	Solution Treated + Overaged
T8	Solution Treated + Cold Worked + Artificial age
T9	Solution Treated + Artificial aged + Cold Worked
T10	Cooled from an Elevated Temperature Shaping Operation + Cold Worked + Artificial Age

Table 2.2: Temper designations for heat-treatable aluminium alloys.

2.1.2.2 Manufacturing process

A quite significant number of aerospace aluminium structures have their beginning in the form of sheets or plates that are submitted to engineering processes, such as FSW, resulting in the final product. Sheets and plates that are the beginning point for engineering applications result from a typical and relatively complex manufacture process. In Fig. 2.1.1 the manufacture process for the heat-treatable aluminium alloys (such as 2XXX and 7XXX series) is presented.

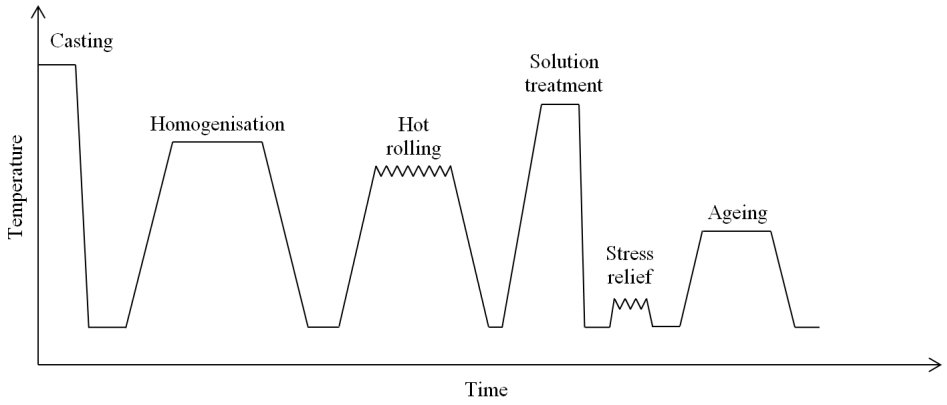

Figure 2.1.1: Schematic diagram of typical manufacture processing of a heat-treatable aluminium alloy

After the initial casting of the metallic material a homogenisation is carried out at 450-500°C [5] (which may vary depending on the alloy composition) in order to reduce the micro-scale segregation formed during the casting process leading to a more uniform structure. In the hot rolling process, ingots up to 1 m in thickness are reduced to 50-150 mm using multi passes at approximately 400°C [5]. The grain structure develops an elongated pancake-type morphology and constituent particles are broken up and dispersed in the rolling direction which generally have a substantial effect on some of the mechanical properties, especially fracture toughness and corrosion resistance in the through thickness direction. After the hot rolling process the heat-treatable aluminium alloys are submitted to a heat treatment procedure and, since this last step is the ultimate responsible for the mechanical properties a more detailed explanation of the heat treatment is presented following.

Heat treating

In generic terms "heat treating" refers to the heating and cooling operations that are performed in metallic materials in order to change mechanical properties, metallurgical structure or residual stress

state. In aluminium alloys in particular the term "heat treating" usually refers the precipitation hardening of the heat-treatable alloys.

Solution Heat Treating and Aging

Certain conditions must be satisfied by the aluminium alloys in order to the precipitation hardening be possible. To begin with, the alloy must contain at least one element or compound in sufficient amount that has a decreasing solid solubility in aluminium with decreasing temperature, that is, elements or compounds that must have an appreciable solubility at high temperatures and minimal solubility at lower temperatures [2]. Copper, zinc, silicon and magnesium are some of the elements that have that behaviour and $CuAl_2$, Mg_2Si and $MgZn_2$ are some of the common compounds that also have a decreasing solubility with the decreasing of temperature. Unless such condition is satisfied aluminium alloys can not be strengthened by heat treatment. The second condition, and no less important, is that the element or compound that is put into the solution during the solution heat treating operation must be capable of forming fine precipitate; if so, a progressive hardening takes place until a maximum hardness is reached. Depending on if the maximum hardness is not reached or exceeded it is said that the alloys are underaged or overaged respectively. Under-aging can be a result of an insufficiently high temperature for the correct aging time or the correct temperature but an aging time too short or a combination of the two. Overaging is usually a result of aging at excessive temperatures.

When an aluminium alloy satisfies both the conditions mentioned above, it is classified as a heat-treatable alloy. That is the case of the 2XXX, 6XXX, 7XXX and some of 8XXX series.

As stated before the precipitation hardening is conducted in three steps:

1. Heating to the solution heat treating temperature and soaking for a period of time long enough to put the elements or compounds present in the alloy into solution;

2. Quenching to an inferior temperature (room temperature, boiling water, etc.) in order to keep the alloying elements/compounds in solution;

3. Aging at ambient temperature (natural aging), or a moderately elevated temperature (artificial aging) to cause the supersaturated solution form a very fine precipitate in the aluminium matrix.

The solution heat treating temperature should be as high above the solid solubility curve as possible without, however, melting the lowest melting point eutectic constituents. If so, the material is invariably ruined. On the other hand, if temperature is too low the solution process will be incomplete and the aged alloy will not develop as high a strength as would be expected. The adequate temperature must be maintained long enough in order to allow diffusion to establish an equilibrium solid solution.

After the complete dissolution of the elements/compounds the alloy is quenched to a relative low temperature in order to keep the elements in solution. The quenching step is quite a delicate one because it should be at the same time sufficiently fast to keep the hardening elements in solution and minimizing the residual quenching stresses that are responsible for significant distortions [6]. Generally, high levels of strength and toughness are obtained by using high quench rates. Resistance to corrosion and stress corrosion cracking (SCC) are also in the majority of the case improved by faster quenching rates although in certain copper-free 7XXX series alloys the resistance to stress corrosion cracking is in reality improved by slow quenching. Fast quenching rates can be achieved by using cold water whereas hot or boiling water is normally used to reduce distortion sacrificing then some strength and corrosion resistance. Some precautions concerning the premature precipitation during quenching must made in order to obtain the expected properties from it. A long transfer time between the furnace and the quench tank as well low

volume of liquid in it (tank) are to avoided if premature precipitation is to be eliminated. The 2XXX and 7XXX alloys, for instance, should be cooled at rates exceeding the 427°C/s through the temperature ranges of 400-290°C [2].

The aging step can be conducted at either room temperature (known as natural aging) or at a specific temperature (higher than room temperature) that is know as artificial aging. The 2XXX aluminium alloys can be aged by either natural or artificial aging whereas 7XXX alloys although capable of harden at room temperatures are all given artificial aging treatments. T3, T4, T8 and T9 (see Tab. 2.2) are all tempers possible to be made in 2XXX alloys. The 7XXX alloys are usually aged at 121°C for periods of time up to 24h or more, producing the T6 temper. Thick products forms for the 7XXX alloys that contain more than 1.25% copper in its composition are provided in the T7 overaged condition. Although overaging reduces the strength properties it improves the corrosion resistance, fracture toughness and dimensional stability. Some typical aging parameters for aerospace plate products are shown in Tab. 2.3 [5]. Peak strength may be achieved by means of one-step or two-steps aging treatments although improved combinations of properties may be achieved by more complex treatments such as retrogression, re-aging or interrupted aging.

Alloy	Temper	First aging step	Second aging step
AA7075	T6	121°C, 24h	-
AA7150	T6	121°C, 24h	154°C, 12h
AA7050	T76	121°C, 3-6h	163°C, 12-15h
AA7050	T74	121°C, 3-6h	163°C, 24-30h
AA7050	T73	121°C, 4-24h	177°C, 8-16h
AA7075	T73	107°C, 6-8h	163°C, 24-30h

Table 2.3: Typical aging parameters of aerospace plates 7XXX alloys.

2.1.2.3 Weldability

Weldability can be defined as the ability to produce a weld free of discontinuities and flaws/defects that ultimately results in a joint with acceptable mechanical properties [2]. Aluminium alloys though possessing a relatively low melting point may be rather difficult to weld satisfactorily for a number of reasons. The fact of presenting a surface oxide layer makes it necessary to remove lest it not contaminate the welding process, so the surface oxide must be thoroughly removed by either chemical methods or manually by means of brushing the areas that are to be welded. The high coefficient of thermal expansion of aluminium also appears as a possible reason to induce flaws/defects since it may result in significant residual stresses leading to welding cracking or distortion. Allied to the high coefficient of thermal expansion is the high thermal conductivity which means that a high heat input during the welding process is required which aggravates the possibility of welding cracking and distortions. Aluminium's high solubility for hydrogen when in liquid state leads to porosity while its high solidification shrinkage (in fusion processes) leads to high cracking ranges which is the consequence of the impossibility of produce welds by fusion welding process on a significant number of the highly alloyed, high-strength 2XXX and 7XXX series aluminium alloys.

In aircraft structural joints the mechanical fastening such as riveting has been the preferred method for long time; aluminium alloys with significant use in aircraft are, as already mentioned, the 2XXX and 7XXX series. Both of the series possess alloys that may be fusion welded, such as the AA2014, AA2195, AA7004 and AA7039 but a significant part of them are considered not fusion weldable due the weld cracking and excessive strength loss. As referred just now the riveting is fairly accepted as the traditional technique of joining fuselage and wing structures which are generally composed by aluminium alloys. Riveting, however presents some setbacks since increases significantly the weight of the airframe and

cause stress concentration which invariably leads to fatigue crack initiation. Since the riveting technique presents some setbacks that aircraft manufactures want to overcome and since fuselage and wing parts are made of high-strength 2XXX and 7XXX series aluminium alloys that in general have low or insufficient levels of weldability a joining process capable of overcome this two barriers would be considered a great development in aircraft construction. Such process could be the friction stir welding process, a joining process that will be presented in the following section.

2.2 Friction stir welding

Friction-stir welding (FSW) is a relatively new solid-state, hot-shear joining process, invented at TWI (The Welding Institute, UK). FSW is considered to be the most significant development in metal joining in the last two decades and is considered a 'green' technology due to its energy efficiency, environment friendliness and versatility [7]. Since its invention, in 1991 when was mainly applied to aluminium alloys, FSW found applications in a wide variety of materials and industries, including aerospace, automotive, railway and maritime. The FSW process exhibits a number of attractive advantages when compared to other welding processes, perhaps, the most significant of all is the ability to weld alloys that are difficult or quite impossible to weld using fusion welding techniques [1].

As a solid-state process, the joining takes place at temperatures bellow the melting point of the material, and as a result does not experience problems related to re-solidification, typical of other welding processes where melting point is reached (such as porosity, embrittlement, cracking, etc.). In addition, the lower temperature of the process enables to get final joining with lower distortion and lower residual stresses. During the FSW process no filler material is required and its environment friendliness is explained by the lack of fumes, arc flash, spatter and shielding gas that are invariable associated with most fusion welding techniques and that are synonyms of pollution.

The key benefits of the friction stir welding can be summarised as follows [7, 8]:

- Low distortion of the workpiece;
- Can be applied to all the major aluminium alloys avoiding problems such as porosity, hot cracking, element loss, etc.;
- Ability to weld the difficult to fusion weld 2XXX and 7XXX aluminium alloys;
- Does not rely significantly on specialised welding skills;
- No shielding gas or filler wire required;
- Fine microstructure;
- Excellent metallurgical properties in the joint area (able to compete with other welding processes);
- High welding speed and joint completion rates;
- Good dimensional stability and repeatability;
- Minimal or no joint preparation;

As in any other welding processes there are, of course, in FSW, issues that appear as a drawback or less positive points. The fact that friction stir welding appears as a fully mechanised process prevents its use in applications of difficult access or when quite complex geometries are to be welded, something

that is best suited to a manual process. The absence of filler material is also placed in the disadvantages category since in some cases, such as fillet welds, the welding can not be easily produced. Another substantial feature that since the beginning was pointed out as a disadvantage in FSW was the exit hole (key hole) at the end of each weld. In practice and although the key hole issue appears as something less positive in the process no major or significant problems has been observed since it can be easy removed from the rest of the sound welded plate.

2.2.1 Basic principles

Although there are several process variants, some of which will be presented and discussed in this work, conventional FSW was the earliest demonstrated technique, and it has remained the most basic and widely applied technique both in research and industry [1]. As may be very easily understood all kinds of variants of the conventional FSW are in one way or another related by some of basic principles, the principles of conventional FSW.

The basic concept of FSW is remarkably simple. FSW is a process in which a non-consumable rotating tool with a specially designed probe[1] and shoulder is plunged, constantly pressed into and against the abutted or over-lapped plates and generation of heat occurs through both friction and plastic deformation as the tool is translated along the welding direction of two rigidly clamped plates properly placed on a backing plate. The tool has two primary functions which are heating the workpiece (a) and produce the movement of material that will result in the final weld (b).

In Fig. 2.2.1 [9] is displayed a conventional FSW square butt joint. In it is represented some of basic features of the process. The existence of two different sides in relation to the joining area can be observed in the Fig. 2.2.1 [9]; the side of the weld where the local direction of the tool rotation is the same as the traversing direction is called the 'advancing side'. Similarly, the side where the directions are opposite, and the local movement of the shoulder is against the traversing direction, is called the 'retreating side'. This can lead to asymmetry in heat transfer, material flow and the properties of the two sides of the weld [9]. The process is thus, by definition asymmetrical, as most of the deformed material is extruded past the retreating side of the tool.

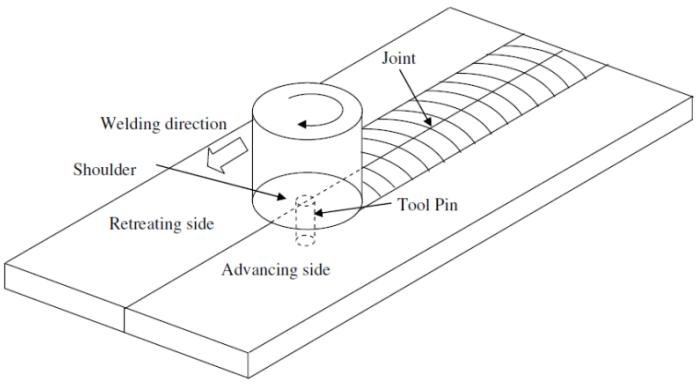

Figure 2.2.1: Schematic diagram of FSW process.

In FSW the frictional heat is generated, principally due to the high normal pressure and shearing action of the shoulder. The frictional heating causes a softened zone of material to form around the probe which cannot escape as it is constrained by the tool shoulder. As the tool traverses along the

[1] Also known as pin

joint line, material is constantly swept around the tool probe between the retreating side of the tool and the surrounding undeformed material. As a result of this process a joint is produced in a 'solid-state'. As it will be explain further in this document the various geometrical features of the tool can lead, and indeed it leads, to a extreme complexity of material movement around the probe [10]. During the solid-state welding process the material experiences immense plastic deformation at elevated temperature which leads to the generation of fine and equiaxed recrystallized grains that consequently produces good mechanical properties [11, 12, 13, 14].

2.2.2 Process parameters

FSW process involves a complex material movement and plastic deformation. Welding parameters, tool geometry and joint design have a great effect on the material flow pattern and temperature distribution having thereby significant influence on the microstructural evolution of the material.

2.2.2.1 Tool geometry

Tool geometry is one of the most or the most influential aspect when designing a FSW joining process. The tool design plays a critical role in material flow and in turn governs the traverse rate at which FSW can be conducted [7]. The tool must perform many functions related with the welding process such as the generation of heat, promotion of material mixture, breaking up the joint line, creating forging pressure, containing material within the joint and preventing the formation or at least minimizing the impact of defects or flaws (such as surface weld flash, wormholes, sheet-thinning, hooking, etc.) [1]. In short it can be said that the tool design influences heat generation, plastic flow, the power required, and the uniformity of the welded joint [9].

A conventional rotating FSW tool consists of a combination of two cylinders of a specific radius ratio known as shoulder (big cylinder) and probe/pin (small cylinder). In Fig. 2.2.2 [7] a schematically FSW tool is represented.

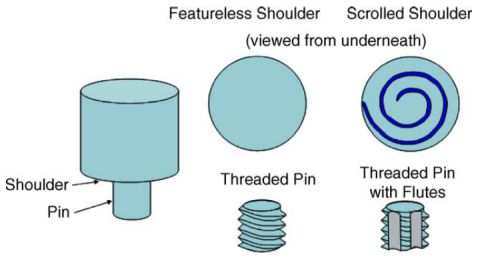

Figure 2.2.2: Schematic drawing of the conventional FSW tool.

In the initial stage of the tool plunge the heating results primarily from the friction between the probe and the workpiece; the other additional heating results form the deformation of material. The tool is then plunged till the shoulder touches the workpiece; the probe length is slightly smaller than the thickness of the plates that are to be welded so the penetration of the probe into the workpiece stops as soon as the shoulder makes contact with the surface of the workpiece. The shoulder is responsible for the generation of most of the heat and prevents the plasticized material from escaping from the workpiece, while both the shoulder and the tool probe affect the material flow [9].

The earliest tool designs consisted of a flat, featureless shoulders and cylindrical, perhaps threaded, probes, some of the first developed in the early years of the process development at TWI. With the

increase of experience and some improvements on the understanding of material flow, the tool geometry has evolved significantly and in recent years several new features have been introduced in the design of tools. These new features have been added to alter flow, mixing and reduce process loads and ultimately improve the quality of the obtained welds [7].

Some tool geometries developed at TWI are shown in Fig. 2.2.3 [9] and give us the idea of how complex and specified the tool geometry can be.

Tool	Cylindrical	Whorl™	MX triflute™	Flared triflute™	A-skew™	Re-stir™
Schematics				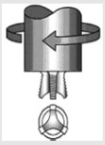		
Tool pin shape	Cylindrical with threads	Tapered with threads	Threaded, tapered with three flutes	Tri-flute with flute ends flared out	Inclined cylindrical with threads	Tapered with threads
Ratio of pin volume to cylindrical pin volume	1	0.4	0.3	0.3	1	0.4
Swept volume to pin volume ratio	1.1	1.8	2.6	2.6	Depends on pin angle	1.8
Rotary reversal	No	No	No	No	No	Yes
Application	Butt welding; fails in lap welding	Butt welding with lower welding torque	Butt welding with further lower welding torque	Lap welding with lower thinning of upper plate	Lap welding with lower thinning of upper plate	When minimum asymmetry in weld property is desired

Figure 2.2.3: Selection of tools designed at TWI.

Different geometries, different application and ways of improve certain aspects of the weld; the Whorl and MX Triflute for instance have smaller probe volumes than the tools with cylindrical probes [9]. They are believed to reduce welding force, enable easier flow of plasticized material, facilitate the downward augering effect, and increase the interface between the probe and the plasticized material, thereby increasing heat generation. It has been demonstrated that aluminium plates with a thickness of up to 50 mm can be successfully friction stir welded in one pass using these two tools [7]. Thomas et al. also suggested that the major factor determining the superiority of the Whorl probes over the conventional cylindrical probes is the ratio of the swept volume during the rotation to the volume of the probe itself.

Although cylindrical, Whorl and Triflute designs are suitable for butt welding, they are not useful for lap welding, where excessive thinning of the upper plate can occur in combination with the trapping of adherent oxide between the two or more overlapped surfaces [9]. Flared-triflute and A-skew tools were then developed to ensure the proper fragmentation of the interfacial oxide layer and a wider weld than is usual for butt welding. The Flared-triflute tool is very similar to MX Triflute with an expanded flute, while A-skew tool is a threaded tapered tool with its axis inclined to that of the machine spindle. Both of these tools increase the swept volume relative to that of the probe which lead to a expansion of the stir region resulting in a wider weld and successful lap joints [9]. In short the Flared-triflute and A-skew are believed to increase the ratio between of the swept volume and static volume of the probe, improving the flow path around and underneath the probe, widen the welding region, provide an improved mixing action for oxide fragmentation and dispersal at the weld interface, and provide an orbital forging action at the root of the weld due to the skew action, improving weld quality in this region [7]. Thomas and Dolby [15] suggested that both Flared-trifute and A-skew probes are suitable for lap, T, and similar joint designs where joining interface is vertical to the machine axis.

Motion due to rotation and translation of the tool induces asymmetry in the material flow and heating across the tool probe. It has been demonstrated that during FSW, material flows primarily on

the retreating side of the weld [9]. To overcome this problem, TWI devised a kind of new tool, the Re-stir, which applies periodic reversal of tool rotation. This reversal of rotation eliminates most problems associated with inherent asymmetry of conventional FSW although issues related with the tool live and productivity in this tool in particular were a drawback.

In more recent years many authors have studied the effect of tool design on the weldability and obtained mechanical properties and all kind of conclusions were possible to obtained. Zhao et al. [16] conclude in his work that cylindrical and tapered tool probes did not ensure effective mixing in the vertical direction what led to the appearance of defects. However, when tapered tools with threads were used, the flaws were completely suppressed. Other studies have also confirmed that tools with screw threads generate more heat and improve flow of the softer material by exerting a downward force. The choice of probe angle, which is the angle between the conical surface of the probe and its axis, is another important parameter which influences the FSW process; increasing the angle leads to a more uniform temperature distribution along the vertical direction, which helps in reducing distortion. An angle of 40° is thought to be optimum for 7XXX aluminium alloys [17].

The shoulder profiles were and are also studied in order to suit different materials and conditions. These shoulder profiles improve the coupling between the tool shoulder and the workpiece by entrapping the plasticized material within special re-entrant features [7].

Considering the significant effect of tool geometry on the metal flow, fundamental correlation between material flow and resultant microstructure of welds varies with each tool. A critical need is to develop systematic framework for tool design.

2.2.2.2 Joint design

FSW is applicable to a number of joint configurations, the most common of which are the square butt joint and the lap joint. Common joint types are possible to observe in Fig. 2.2.4. Pipe welds and hemispherical welds joints, no pictured in Fig. 2.2.4, are also common joint types. One great advantage of FSW is that typically little joint preparation is required. No matter what the joint type is, what is always necessary in FSW, is an adequate clamping system along with a rigid backing anvil, in the case of conventional friction stir welding. During the initial plunge of the tool, the forces involved are fairly large and extra care is required to ensure that plates in butt configuration do not separate. A direct consequence of that is that there is usually a large capital investment on the front end of the manufacturing process to obtain the required machinery and tooling, and set-up time relative to joining time increases when production begins.

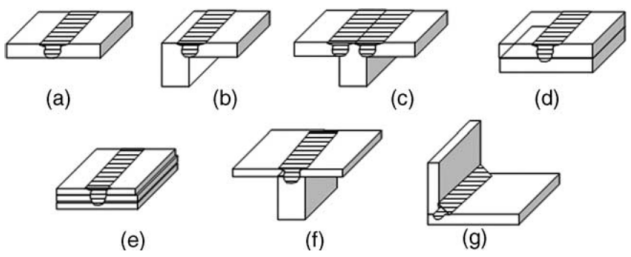

Figure 2.2.4: Joint configurations for FSW: (a) square butt, (b) edge butt, (c) T butt joint, (d) lap joint, (e) multiple lap joint, (f) T lap joint, and (g) fillet joint.

2.2.2.3 Welding parameters

Welding variables or welding parameters are the foundations of all the FSW processes and are responsible for the ultimate quality of the welding joint. In FSW two welding parameters are of extreme importance, tool rotation rate, (ω, rpm) that can be in clockwise or counter-clockwise direction and tool traverse speed, or welding speed (ν, mm/s) that is the welding speed along the line of joint [7]. The stirring and mixing of the material around the probe results of the rotation of the tool whereas the movement of the stirred material from the front to the back of the probe results of the translation of the tool. As it is easy to understand higher tool rotation rates generates higher heat inputs and consequently higher temperatures involved in the process; this happens fundamentally due the high friction heating and result in more and more intense stirring and mixing. In short, peak temperature increases with increasing rotational speed and decreases slightly with welding speed [7, 9]. The peak temperature also increases with the increase of the axial pressure.

In addition to the tool rotation rate and traverse speed, the vertical pressure on the tool, tilt angle of the tool[2] and, as discussed previously, the tool design itself are also main independent variables. The heat generation rate, temperature field, natural cooling rate, longitudinal direction force, torque and the power involved are al depend on these variables. A suitable tilt of the spindle towards trailing direction ensures that the shoulder holds the stirred material by the probe and move the material from the front to the back more efficiently. The insertion depth of probe or target depth is also a welding parameter; the insertion depth is logically associated with the probe height/length of the tool in use and is essentially the position of the tool shoulder relatively to the outer surface of the workpiece; if the insertion depth is too shallow the shoulder does not contact or at least does not contact properly the workpiece surface and that results in welds with an inner channel or surface groove since only the probe is responsible for he material stirring; otherwise, if the insertion depth is to deep, the shoulder of the tool plunges into the workpiece which is responsible for the creation of lot of flash - typical surface defect in FSW; in last case a significantly concave weld is produced, leading to local thinning of welded plates.

The torque presented in the tool during FSW is relatively simple to determine and is an important factor of the process; the torque depends on several variables such as the applied vertical pressure, tool geometry, the tilt angle, the local shear stress at the tool material interface, the friction coefficient and the extent of slip between the tool and the material. Measured torque values can provide some idea about the average flow stress near the tool and the extent of slip between the tool and the workpiece for certain conditions of welding, when other variables are kept constant [9].

The torque decreases with increase in the tool rotation speed due to increase in the heat generation rate and temperature when other variables are kept constant. It becomes easier for the material to flow at high temperatures and strain rates. However, torque is not significantly affected by the change in welding speed; the relative velocity between the tool and the material is influenced mainly by the rotational speed. Therefore, the heat generation rate is not significantly affected by the welding speed. High traverse speeds tend to reduce heat input and process temperatures.

As previously mentioned torque is not significantly affected by the welding speed variation, it increases only slightly with the increase in traverse speed because the flow of material becomes somewhat more difficult at slightly lower temperatures.

The torque on the tool can be used to calculate the power required from

$$P = T\,\omega \tag{2.2.1}$$

[2] Also known as angle of spindle or simply tool tilt

where T is the total torque on the tool and ω is the rotational speed. Significant x-direction force is an important indicator for tool wear and, in extreme cases, tool breakage. Axial pressure also affects the quality of the weld; very high pressures lead to overheating and thinning of the joint while very low pressures lead to insufficient heating and voids. Power requirement is also increased with the increase in axial pressure.

Apart from the basic and consequently fundamental welding variables that were already presented, the possibility of preheating or cooling the workpiece before and/or during the welding process appears as a new kind of welding variables which can nevertheless result in an improvement of the quality of the obtained welds. For materials such as steel and titanium, that present a high melting point, and materials such as copper that have high conductivity, the heat produced during the process of welding, by friction and stirring may be not sufficient to soften and plasticize the material around the tool which can lead, an generally leads, to the appearance of defects. In these cases it is possible to preheat and use additional external heating sources as a way of increase the process range. On the other hand, materials with lower melting point such as aluminium and magnesium alloys forced cooling system can reduce the extensive growth of recrystallized grains and dissolution of strengthening precipitates in and around the stirred zone [7].

2.2.3 Heat generation

During FSW process, heat is generated by both friction between the tool and the workpiece and via plastic deformation [9]. Friction stir welding differs from the rest of the competing processes such as arc and laser welding, since these processes use an external source of heat whereas, in turn, FSW joining process generates its own heat and as a consequence the heat input is a complex function that is dependent of the process variables (traverse and rotation speed, down force, etc.), the alloy being welded and the tool design [8].

Heat is produced primarily by viscous dissipation in the workpiece material that is close to the tool as a consequence of the high shear stresses at the tool-workpiece interface. Material at the interface may stick or slip on or around the tool, (probably there may be a combination of the two) and therefore an oscillation stick-slip behaviour may occur as local melting rapidly reduces the shear stress which leads to a steep drop in the local heat input and consequently temperature and a self-stabilising behaviour is reached [8]. The local interfacial heat generation is then the product of frictional force and sliding velocity [9]. A great problem in the calculations of the exact heat generation is that the friction coefficient can not be determined from fundamental principles since the value of the friction coefficient may, and indeed vary, with temperature, relative velocity and a number of other factors [9]; some investigators have considered this kind of effect by adjusting the friction coefficient, however no direct method to estimate the coefficient of friction or how it changes with temperature or relative velocity was possible to be obtained.

The exact heat input or heat generation is a complex issue that is not yet solved; process modelling has been used to explore the sensitivities of the heat generation but problems related with the limited quality of the constitutive data has been a barrier [8]. So, for a given workpiece material and plate thickness the operator can essentially deal process variables such as tool design, down force, tilt angle, tool plunge, rotation speed and traverse speed. Empirical attempts invariably explore a number of these variables which ultimately lead to a range of values of these same variables that produces sound welds. This window is usually designated as being 'hot welds' and 'cold welds' which are associated with high rotation speed and low welding speed (excessive flash production) and low rotation speed and high traverse speed respectively (excessive tool wear and in extreme cases tool breakage) [8].

2.2.4 Material flow

The material flow during friction stir welding is quite complex. The complexity is depending on the tool geometry, process parameters and ultimately the materials to be welded. The understanding of the material flow characteristics is of practical importance for optimal tool design and high structural efficiency welds achievement.

In friction stir welding the majority of the material flow (extrusion) occurs between the rotating probe on the retreating side and the surrounding material which is too cold and not enough stressed to deform resulting in the transport of plasticised material leading to the generation of the weld. Three types of flow affects the global transport of plasticised material during the FSW process. First, near the tool, a slug of plasticised material rotates around the tool; this movement is caused by the rotation of the tool itself and the resulting friction between tool and workpiece. The second type of material flow is a result of the rotational motion of the threaded probe that tends to push downwards the material immediately around the probe having as consequence an upward motion of an equivalent amount of material that is originally located farther way from the probe and finally there is the relative motion between the tool and the workpiece (traverse speed). As said, the global motion of the plasticised material is a simultaneous interaction of these three effects.

2.2.5 Temperature distribution

As already said, the FSW process results in an vigorous plastic deformation and friction between the rotating tool and the workpiece material to be welded. Naturally, both these factors contribute to the increase of temperature within and around the stirred zone and are the ultimate responsible for the weld achievement. Since the temperature distribution directly influences the microstructure present on the welds (such as the grain size, grain boundary, coarsening and dissolution of precipitates), consequently influences the mechanical properties in them present, so, to obtain information about the temperature distribution during the welding procedure is of extreme importance. Temperature measurements within the stirred zone are, however, very difficult to perform due to the intense plastic deformation produced by the rotation tool combined with its translation. Therefore, the real and effective maximum temperatures present within the stirred zone during a stir welding process are impossible to be measured and instead they have been either estimated from the microstructure of the produced weld or recorded by embedding thermocouple in the regions adjacent to the rotating probe (workpiece and tool).

In 1998, Mahoney et al. [18] developed a study that aimed to evaluate the changes due FSW process in the tensile properties on the AA7075-T651 (6.35 mm thick plates). In his work a series of tensile tests were performed and fractographic examinations were made using, for instance, and as tool analysis, the temperature distribution around the stirred zone. The peak temperature distribution adjacent to a FSW on a 6.35 mm plates of AA7075-T651 obtained by Mahoney is shown bellow [18].

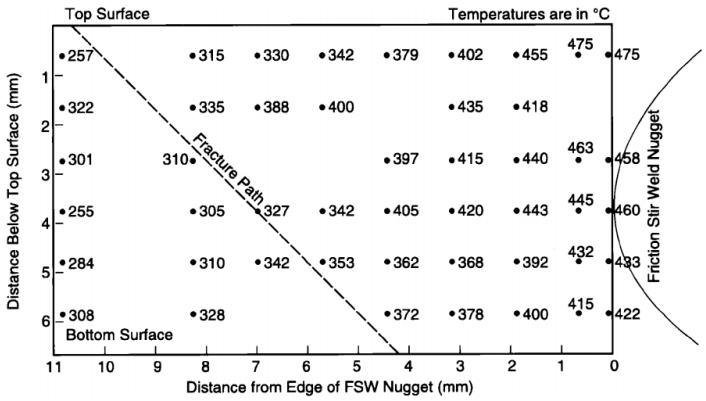

Figure 2.2.5: FSW peak temperature distribution obtained by Mahoney (1998).

As may be observed, temperature measurements were conducted around the stirred zone both as function of distance from the centre line and through thickness of the workpiece plate. Some pertinent observations can be made when looking at Fig. 2.2.5 [18]; to begin with, the maximum temperatures were recorded at locations close to the stir zone (nugget); something quite logical, as expected, the temperature decreased with the increasing distance from the stirred zone. Secondly, the temperature at the edge of the nugget decrease from the top to the bottom surface and finally an absolute maximum temperature was discovered near the intersection point between the stir zone edge and the top surface (which is naturally intrinsically related to the shoulder influence).

A common procedure when temperature fields and heat inputs are to be measure is to embed thermocouples in a region sufficiently close to that to be weld. A great number of investigations in this scope have been made [19, 20, 21, 22] and similar results to those of Mahoney were frequently obtained. For instance Tang et al. [19] demonstrated that thermocouples placed at equal distances from the joint line but on opposite sides of it showed no significant difference in the registered temperature something that in other works [23] seemed not to be true since reports of a temperature differences between process sides of the joint where monitored.

In short, and paraphrasing some of the subjects already mentioned in this work it is possible to conclude that many factors influence the thermal profile of a certain weld during the friction stir welding process. It is then, possible to be said that a maximum temperature occurs within the core of the stirred zone (which is generally below the melting point), that the shoulder is the main responsible for the heat generation, that the maximum temperature increases with the increasing of the ration of tool rotation speed/welding speed and finally that a maximum temperature rise occurs at the top surface of the workpiece with tendency to drop through through thickness in direction to the bottom surface.

2.2.6 Macroscopic weld features

The microstructural classification and consequently the definition of the different macroscopic regions on the friction stir welded transverse sections was and has been the cause of considerable confusion since the invention of the friction stir welding process. In contrast to what happens in conventional fusion processes, where the microstructural regions can, generally, be easily divided in different areas and macroscopic zones, namely, the fusion zone, where fusion occurs, and non-fused zone (heat-affected zone, HAZ) the classification of friction stir welds zones has not been proved that simple. The first attempt made to classifying FSW microstructures was made by Threadgill [24]. The 1997 document by Threadgill though pioneer was solely focused on aluminium alloys and significantly limited to features

distinguishable by light microscopy [8]. Later works concerning other metallic materials demonstrated, however, that a different behaviour and optically visible microstructural zones were seldom similar to those of the aluminium and therefore the initial classification made in 1997 was inadequate; the new classification system should be able of accommodate all materials. In the present situation aluminium is treated as a special case [25].

The intense plastic deformation and high-temperature exposure within the stir zone during the FSW process results in recrystallization within the core of the stirred region and precipitate dissolution and coarsening within and around the stir zone. Based on microstructural characterization of grains and precipitates, three distinguishable zones (this is, macroscopic areas) have been identified: the stir zone (nugget), the thermo-mechanically affected zone (TMAZ) and the heat-affected zone (HAZ). The three macroscopic zones just now referred may be observed in Fig. 2.2.6. The following figure corresponds to one of welds produce during the project here exposed.

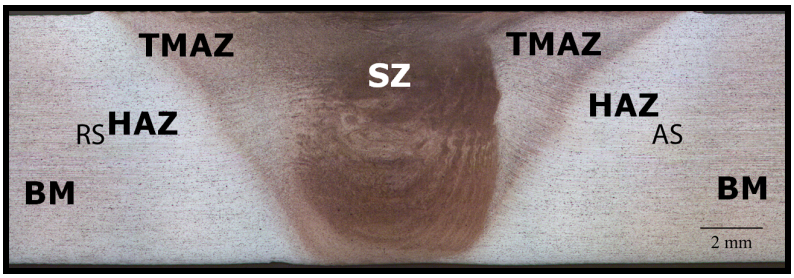

Figure 2.2.6: Typical friction stir welding macrograph showing the microstructural classification of the different distinguishable macroscopic zones.

In addition to the three previously mentioned zones it is, naturally, possible to observe the presence of the base material/metal (BM) or parent material/metal (PM) that is the material/metal remote form the weld, which is unaffected by deformation of the weld and although it may experience a thermal cycle is not affected by heat in terms of detectable changes in microstructure or ultimate mechanical properties.

This particular section of the document is aimed to introduce to the reader the different macroscopic zones that can be found in a transverse cross-section of a weld; although there is direct relationship between the microstructural evolution and the macroscopic features (regions or zones) no extensive explanation at the microstructural level will be made; a more detailed analysis of the microstructural evolution will be presented further on this document.

2.2.6.1 Stir zone

The stir zone is the core of all the welds produce by FSW. The intense plastic deformation and frictional heating generated during the FSW process results in a recrystallized fine-grained microstructure within the heart of the stirred zone. This region is known and is frequently referred as nugget zone (weld nugget) or even dynamically recrystallized zone (DRX); a term that have been more recently suggested [26] and used extensively in the literature although the term stir zone or simply nugget have remained widely used and understood.

Shape of stir zone

The shape of the stir zone is intrinsically dependent on the process parameters, tool geometry, temperatures involved before and during in the process and ultimately the conductivity of the material that

is to be welded. According to Mishra et al. [7] the stir zone can be classified into two types in terms of general shape, a basin-shaped stir zone that widens near the upper surface and the elliptical shape stir zone, Fig. 2.2.7. Various authors and researches have reported the formation of both shapes for different materials and process parameters. They suggested that the upper surface of the workpiece experiences extreme deformation and friction heating as a consequence of the tight contact with the tool shoulder and thereby the generation of the basin-shaped stir zone. More recently some investigations were conducted in order to ascertain the effect of the FSW parameters on the microstructure and obtained properties. Some of the results indicated that lower tool rotation (300-500 rpm resulted in a basin-shaped stir zone whereas for high tool rotation speed (>700 rpm) the elliptical-shaped stir zone was observed; that seems to indicate that with the same tool design different stir zone shapes can the obtained only by changing processing parameters [7]. Although investigations reported the appearance of both shapes and some studies even tried to ascertain some particular properties of the microstructure of the stir zone it seems appear low or not conclusively basis of which the shapes leads to better mechanical properties.

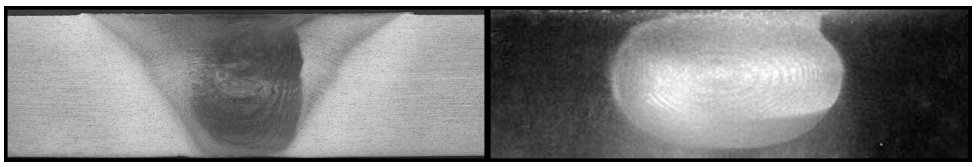

Figure 2.2.7: Two types of stir zone shape: basin-shaped (left) and elliptical shape (right).

'Onion ring' structure

A fairly common observation in the stirred region in FSW is the appearance of a series of circular or elliptical features in the transverse cross metallographic sections of the welds that are known as 'onion rings' (see Fig. 2.2.8). These have been linked to the nature of material flow during the welding process but the detailed mechanism of pattern formations and its significance is not quite completely understood and consequently remains an occasional topic of interest in the literature. A series of investigations have shown a number of different possibilities for the origin of the ring patterns; some claim that the ring patterns are an etching response to variations in the grain size between the rings [8] and others defend that a characteristic of the rings include texture effects and variations of material density. It was also shown [27] that the stir zone may also contain fractured constituent particles and that the 'onion rings' are formed as a variation in their distribution. Khrisnan [28] asserted that the 'onion rings' structures are a result of the extrusion that occurs during FSW process and that, for each rotation of the tool, a cylindrical section of material is extruded around the probe and the characteristic banded structure within the stir zone results from oxidation on the surface of each semi-cylinder. Measurements of the spacing between consecutive rings has been found to be equal to the weld pitch (the tool advance along the weld joint in one rotation) which seems to be accordance with the argument that there is a purely kinematic basis for the formation of each ring. Eq. 2.2.2 shows the weld pitch equation

$$weld\,pitch = \frac{\omega}{v}\left[\frac{1}{\mathrm{mm}}\right] \tag{2.2.2}$$

with ω being the rotation speed in (radian s^{-1}) and v the welding speed in $\mathrm{mm\,s}^{-1}$.

Although a lot of studies and investigations have been carried out in the last few years the practical significance of the phenomenon have been remained rather limited as the mechanical properties obtained

within the stir zone are generally good and no relation whatsoever was observed between the 'onion rings' structure and the variations of mechanical properties.

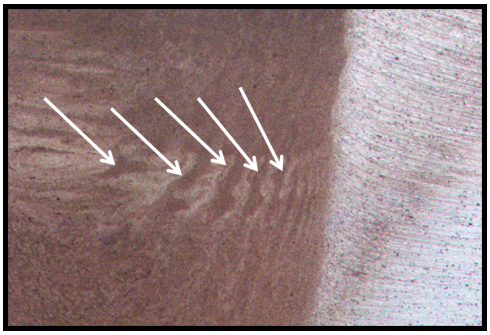

Figure 2.2.8: 'Onion rings' on a cross-section of a FSW - advancing side - (HZG).

2.2.6.2 Thermo-mechanically affected zone

The presence of a transition zone - TMAZ - between the heat-affected zone and the stir zone is unique of the friction stir welding process. The thermo-mechanically affected zone (TMAZ), is a region affected by both heat and deformation. This area extends across the weld from the HAZ of the advancing side to the HAZ of the retreating side. 'As a minimum this zone will correspond with the width of the shoulder on the upper surface, and with the probe diameter at the root' [25], in the case of conventional friction stir welding. 'In the case of aluminium it is possible to generate considerable plastic strain without re-crystallization in this region, and there is generally a distinct boundary, at least at a macroscopic level, between the recrystallized and deformed zones of the TMAZ.' [8]. The TMAZ is then characterized by a highly deformed structure as can be observe in Fig. 2.2.9. The elongated grains of the base metal were deformed, in and upward the flowing pattern around the stir zone. As it was previously mentioned although TMAZ is subjected to plastic deformation, recrystallization generally does not occur due the insufficient deformation strain though dissolution of some precipitates might occur with significant frequency. It is, then, natural to expect that the extent of dissolution depends on the thermal cycle experienced by the TMAZ during the welding process.

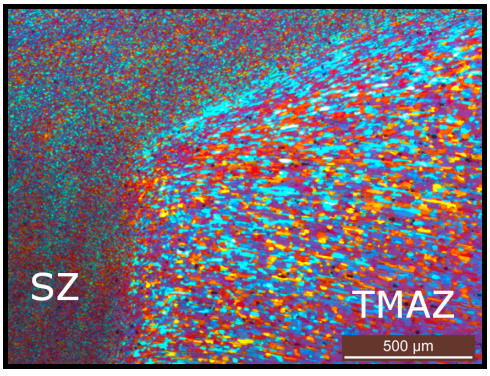

Figure 2.2.9: Detail of a thermo-mechanically affected zone in DS-FSW 7050-T7451 (HZG).

2.2.6.3 Heat-affected zone

Farther from the centre of the welding zone - joint line - and immediately beyond the TMAZ is the the heat-affected zone HAZ. This region is sufficiently close to the weld for the thermal cycle caused

by the weld itself to cause a modification of the microstructure and the properties of the base material but far enough to not experience plastic deformation. Is then a region affected only by heat, where no macro plastic deformation should be visible by light microscopy although there may be detected some deformation on a micro scale [8]; the grain structure in HAZ is consequently the same as the base material, however for high temperatures and high thermal exposure a significant effect on the precipitate structure might occur. Mahoney et al. [19] defined that HAZ is the region that experience a temperature rise above 250°C for the case of heat-treatable aluminium alloy.

2.2.7 Microstructural features

As in any other welding process, the mechanical properties and ultimate quality of the weld are defined at the microscopic level, which is determined by the thermal cycle of the welding process and, as previously mentioned in the case of the FSW can generally vary by simply changing the process parameters or the welding variables. Welding parameters must be therefore chosen in order to give the best microstructure possible and that must be, naturally, free from defects. In the majority of the materials, the welding process has some adverse effects on the microstructure and consequently intrinsic properties within and around the welded zone; therefore the weld parameter to be chosen is often a compromise between sound welds at economical production rates and producing acceptable microstructures and mechanical properties [8].

As previously exposed in this document, friction stir welds and, in particular, welds in aluminium alloys, contain a series of microstructures along the transverse section of a welded joint which, as shown, can be divided in macroscopic regions according to visual and properties inspection.

In the outer zone of the weld just after the base material can be found the HAZ that is, as mentioned, a remote zone from the centre of the weld and thus there is no obvious changes to the grain structure and usually as a consequence its presence can only be detected by a change in hardness and etching response. As the weld centre is approached clear evidence of plastic deformation can be seen in the grain structure; in the outer part of the thermo-mechanically affected zone (TMAZ) the original grains remain identifiable in the deformed structure though there is a formation of sub-grain structures and significant associated rotation of the parent grains. When the 'heart' of the weld line is reached a recrystallized stir zone with a fine equiaxed structure can be found as a result of high strains, temperatures and time of exposure.

2.2.7.1 Grain size

As briefly mentioned above during the FSW process the core of the stirred material experience a dynamical recrystallization which results in a generation of fine and equiaxed grains [14, 29]. Friction stir welding variables and process parameters such as tool geometry, workpiece condition (composition, temperature, thermal properties), vertical pressure applied onto the workpiece and the existence or not of artificial cooling are some of the process parameters responsible for the size of the recrystallized grains in the stirred zone in stir welded materials.

For aluminium alloys the typical recrystallized grain size in the core of a welded zone is in the micro range for the case of non-cooling process; ultra-fine-grained (UFG) microstructures can be achieved by using external cooling systems [7].

It is relatively easy to find in literature a fairly large number of studies concerning the effects of some process parameters on the size of the obtained grains in the welded zone. Studies concerning the temperature of the workpiece before and during the process (cooling) and the reduction of frictional heat generation by modifications on the tool design (sharpened probe's tip [21, 30]) and reduction of

diameter tool [31] have demonstrated a significant reduction on the grain size. These conclusions are consistent with the general principles of the recrystallization which says that the grain size decreases with the decreasing of annealing temperature.

In more recent years [20, 29, 32] investigations studied in more detail the influence of processing parameters on the microstructure of FSW aluminium alloys. It was possible to conclude that the recrystallized grain size can be reduced by a simple decrease of the tool rotation at a constant tool traverse speed or seemingly with de decreasing of the ratio of tool rotation rate/traverse speed [32]. As is easily understandable higher tool rotation rate or higher ratio of tool rotation rate/traverse speed results in a significant increase in the degree of deformation and particularly in a increase of the peak temperature reached on the thermal cycle. According to the recrystallization principles the increase in the degree of deformation results in a reduction of the recrystallized grain size whereas, on the other hand, the increase in peak temperature leads to the generation of coarse recrystallized grains and remarkable grain growth.

The grain size distributions also depends of the region in which they are inserted on the cross-section weld. For instance the grain size tends to increase near the top of the weld zone (next to the shoulder) and it decreases with the distance on either side of the weld-zone centreline, which corresponds approximately to temperature variation. When studying a 6.35 mm thick of an 7050 aluminium alloys Mahoney [33] not only reported a variation in grain size from the bottom to the top but also from the advancing side to the retreating side. The vertical variation in grain size can be related, and is believed to be associated, with the temperature profile and heat dissipation in the stir zone; since the bottom of the workpiece is in direct contact with the backing plate the peak temperature is lower and the thermal cycle shorter when compared to the top which effectively retards the grain growth which results in a smaller recrystallized grains. Naturally, with the increase of the plate thickness the temperature difference from bottom to top are increased which aggravates the difference between the grain size.

2.2.7.2 Precipitate dissolution and coarsening

As presented before the FSW process is responsible for a significant increase of the temperature within the stir zone due to friction between tool and workpiece and plastic deformation around the rotating probe. At such temperatures the original precipitates present in the aluminium alloy can coarsen or dissolve into aluminium matrix depending on the alloy and maximum reached temperature.

Previous works concerning the study of the effect of FSW process in the microstructure of aluminium alloys reported that homogeneously distributed precipitates are generally smaller in the base material than in the stir zone, however, the appearance of large precipitates in the stir zone was considerably lower when compared with the parent material. This seems to indicate the occurrence of both dissolution and coarsening of precipitates during the welding process. Other investigations, such as the case of Sato et al. [19] studied the microstructural evolution of a AA6063-T5 and noticed that no precipitates were found in the stir zone which indicated that all them were dissolved into an aluminium alloy during the friction stir welding process.

In the 7XXX aluminium alloys, more exactly the AA7050-T7451 aluminium alloy, which is the same in study in this document, Jata et al. [34] observed the absence of strengthening precipitates in the stirred region which as in the previous works was an indicator of complete dissolution of the precipitates. The FSW is responsible for a combination of dissolution, coarsening and re-precipitation of strengthening precipitates [7].

2.2.8 Hardness profiles

As previously referred aluminium alloys are classified into heat-treatable alloys (precipitation-hardenable) and non-heat treatable alloys (solid-solution-hardened). A series of investigation and research studies demonstrated that there is a different response on the hardness profiles for the precipitation-hardened and solid-solution-hardened aluminium alloys. The FSW process is responsible for the creation of a softened region around the weld centre in a significant number of heat-treatable aluminium alloys. As previously mentioned, such softening is believed to be caused by a coarsening and dissolution of strengthening precipitates during the thermal cycle of the welding process [7, 8, 9, 14, 29]. Sato et al. in his work [19] stated that the hardness profiles in an friction stir welded AA6063-T5 alloy was strongly affected by the precipitate distribution rather than the grain size present within the welded zone which in reality meant that a special attention must be given to precipitate distribution. Different regions can be found in a typical hardness profile. Sato et al. labelled the heat-treatable alloys hardness profiles by BM, where the same hardness as the base material can be found, LOW for the regions of lower hardness than base material, MIN where the minimum-hardness is found and finally SOF that is the softened region.

In the case of the solid-solution-hardened aluminium alloys the FSW process does not generally result in a softening in the welded zone. In studies concerning this kind of materials hardness profiles were roughly uniform and in cases the hardness in the stir zone appeared slightly higher than that of the parent material of the workpiece [35, 36]. Microstructural factors governing the hardness in the solid-solution-hardened aluminium alloys friction stir welded materials have been investigated, namely by Svesson et al. [36] and a structure of fine equiaxed grains with lower density of large particles were found in the stir zone. In the same document the authors suggested that the hardness profile was mainly dependent on the dislocation density since the material then in study, AA5083, had is dominant hardening mechanism strain hardening.

Since the aluminium alloy in study in this document is inserted into the heat-treatable alloys, more specifically 7XXX series, a special attention must be given to the kind of microstructure and hardness profile that result from the FSW process in this kind of materials rather than solid-solution-hardened alloys so the latter will not be discussed in such detail.

2.2.8.1 Hardness profiles in heat-treatable alloys

Heat-treatable aluminium alloys, as mentioned, derive much of their strength from the presence of fine precipitates that are formed during the heat treatment in which they are subjected (age hardening). As already shown, the thermal cycles that the workpiece material experiences during the welding process can lead to the precipitate coarsening or precipitate dissolution and further, during or after the cooling of the workpiece, to re-precipitation, something that is closely dependent on the peak temperature and duration of the cycle.

The transverse hardness profiles are a very common feature when a FSW study is being made and frequently appears as a tool for the first interpretation of some of the significant changes that occur during the stir welding process. Most friction stir welding of 7XXX has been performed on base materials which are in either the T6 or T7XX type of tempers, which means that the base metal has been aged to some specific strength level which is correlated with the precipitate distribution. In the last years, the effects of the FSW process on the strength and hardness distribution have been thoroughly studied and has been demonstrated that the kind of distribution can be manipulated up to some extent by the choice of the welding parameters. Precipitation hardened aluminium alloys that were subject to the FSW process exhibit a characteristic hardness profile that has a "W" shape where a local or absolute maximum in the stirred region and a minimum in the HAZ on either side of the centreline can be observed, Fig. 2.2.10.

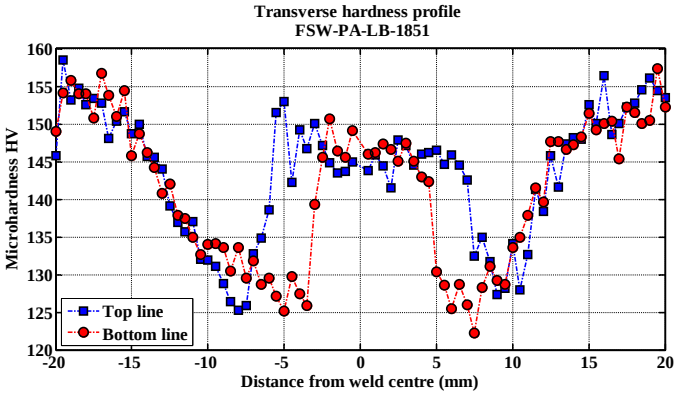

Figure 2.2.10: Characteristic hardness profiles of FSW heat-treatable aluminium alloys (HZG).

In certain cases, however, corresponding to low power welding conditions the characteristic "W" shape may not be produced and consequently the hardness is roughly the same in the stir zone and in HAZ and throughout the rest of the hardness profile; this essentially results from insufficient peak temperature in the stir zone, which is in the overaging regime rather than in the solution treatment range and thus the precipitates in the stir zone are not even dissolved and re-precipitated, only coarsen. In order to produce the characteristic "W" shape, then, the stir zone have to be heated up to or heated sufficiently up to the solution heat treatment temperature [37]. The capacity of reach a sufficiently high temperature in order to perform a solution treatment in the stir zone requires a minimum power level of the welding process which is invariably dependent on the welding speed and tool design. As mentioned just above, the lower values of hardness are found in the HAZ; there, the hardness is generally reduced significantly below that of the base material due, once more, the coarsening of the base metal precipitate distribution. Both coarsening and dissolution lead to a drop in the hardness, but strength recovery only occurs following dissolution; the hardness profiles are therefore quite consistent with the precipitate coarsening being dominant in the HAZ (lower peak temperatures) and dissolution in stir zone (where the peak temperature is frequently above the solvus of the initial precipitates), followed by natural aging [8]. The magnitude of the plunge of hardness values in the HAZ are closely connected to the welding speed and generally not associated with the peak temperature that the core of the stir experiences [38]. Is easily understandable that low welding speed causes the material to endure longer time in overaging temperature regime which is responsible for the aggravation of the hardness plummeting in the heat-affected regions and is then possible to conclude that low welding speed has as a consequence low HAZ hardness; faster welding speeds, on the other hand, generally lead to colder welds and narrower HAZ causing an increase in the stir zone hardness due to the reduced deformation temperature and increased strain rate [8, 37].

Since natural aging is commonly to be observed in the stirred region, which appears as a strength recovery, it might be expected that post-welds treatment would be a reasonable option to promote even better properties on the obtained weld; however this kind of procedure is not largely applied since a complete re-solution heat treatment is not often possible or even economically viable.

2.2.9 Flaws in friction stir welds

As it happens in most materials joining processes, as the case of fusion processes, FSW may lead to the occurrence of flaws and defects. In this section of the document it will be presented to the reader some of the common flaws and defects liable to appear in FSW process; an essential subject since the ultimate quality of the produced welds are intrinsically depended on the flaws magnitude.

As stated before in this document, FSW, being a solid-state joining process, is able to preclude the

classic problems of the fusion processes such as the significant porosity and hot cracking though is not at all free from the possibility of appearance of other kinds of flaws/defects that are then defined as characteristics of the stir welding process. As stated by Threadgill et al. in their thorough review on the friction stir welding of aluminium alloys [8] a distinction between flaws and defects must be made. According to Threadgill et al. review '*a flaw or imperfection is a feature that one would prefer not to be in the weld, but it may or may not compromise the integrity of the weld. If after evaluation, the flaw is deemed unacceptable, then it becomes a defect. ... Flaws or discontinuities should be characterised as defects only when specific acceptable criteria, related to the engineering application, are exceeded, and the presence of a flaw compromises the integrity of the structure.*'.

In friction stir welding flaws or defects may be of any orientation, size or shape, [1] although as in any other joining process the FSW process moves in linear fashion along the joint line and therefore there is a tendency to produce defects which propagate for some length and have their major dimension parallel to the travel direction. Some of the recurrent FSW flaws/defects are excessive flash, excessive concavity, tool inclusions, foreign substances, voids, wormholes, lack of penetration (LOP), root defects and kissing bond defects which may occur in the root or in the weld interior.

2.2.9.1 Joint line features

It is significantly frequent and even natural that the material to be welded by friction stir welding has an oxide layer in its surface. After stir welding this oxide layer can sometimes be observed, when a cross-section of a particular weld is studied, as a partially dispersed visible trace of the original joint line. This trace or group of traces are normally denominated as remnant oxide layers (ROL), joint line remnants (JLR), entrapped oxides, residual oxides, lazy-S curves or even kissing bonds [1]. Joint line remnants are features that extend form the weld root, at the particular location of the original union between the butting plates, throughout the core of the stirred region and in some cases are not more than a string of inadequately dispersed oxide particles that had as origin the oxide layer present in the surfaces of the abutting plates. This features are affected by the welding speed (increasing the welding speed reduces the disruption of oxide per unit of advance of the tool), tool shoulder and tool design [39, 40, 41]. In some cases the simple cleaning, grinding or machining of the abutting surfaces just before perform the welding can completely eliminate the layer oxide problem.

In order to produce a sound bond is important to adequately disrupted the oxide layer between the butting surfaces of the plates and in the great majority of cases is that exactly what happens. In fact, normally, the original joint line suffers an increase in length some 3-5 times its original size and the oxide is broken up and completely scattered so that most of the original joint line is indeed metal to metal bond and thus sufficiently strong [8].

Correct depth of penetration of the probe is an essential issue in order to ensure that mixing occurs through all the thickness of the plates; when a too short probe is used, when the tool plunge is incorrectly set or even when there is a misalignment between the tool and the joint line a root flaw can be produced which is an obvious indicative of lack of proper bonding. As a result of this lack of penetration, especially localized at the bottom of the weld, there might be a region when travelling to the top of the weld where an effective bond exists but is weak. This is generally designated as kissing bonds.

2.2.9.2 Formation of voids

Other critical features that are somewhat frequent in FSW process are voids, particularly in early stages of a parameters study. Voids or empty volumes can be observed in different zones of a cross-section

of a weld but are particularly common on the advancing side, near the base of the probe and a sort of cracking, lack of material near the top surface that is a consequence of the trailing edge of the tool shoulder. Except for critical cases voids can not be detected by visual inspection of the surface of the welds but are generally fairly easy to uncover by a simple study of its cross-section. Inadequate welding pressure, high welding speed, low rotation rate and unappropriated clamping system are some of the of factors that have been identified as contributing to void formation [20, 22, 39, 42]. Insufficient welding pressure has as consequence inadequate tool shoulder forging action in order to achieve full consolidation. In turn when high welding speeds are applied in combination with low rotation rate the material receives low work per unit of weld length and under such conditions the plasticised material may not reach an appropriated temperature. In cases where the welding speed is extremely high or the welding pressure is frankly low the result of the welding process might be an extension of the tunnel (void) up to upper surface of the workpiece forming a groove type of defect that has in all cases as consequence the complete rejection of the produced weld.

2.2.9.3 Other types of flaws

Flash is produced by the displacement of material from the centre of the joint line on the top surface of the workpiece to either side of the shoulder influence, Fig. 2.2.11

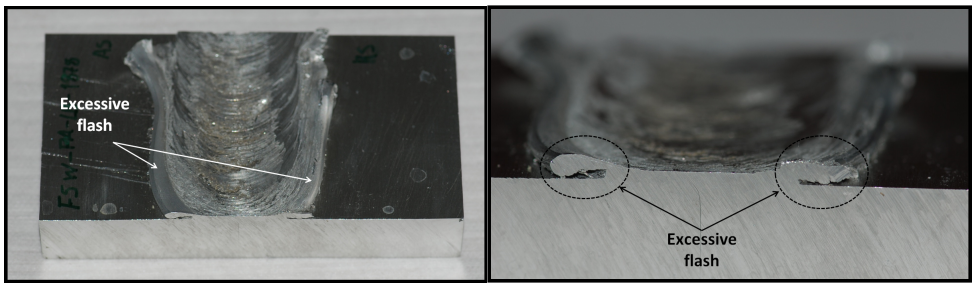

Figure 2.2.11: Friction stir weld presenting excessive flash (HZG).

Excessive flash is not necessarily considered a bad feature; in some cases high flash levels are deliberately produced in order to ensure adequate penetration, especially in welds where the fit-up is significantly poor. Excessive flash may result from a number of reason such as too deep insertion depth, improper tooling or parameter settings. Reduce the rotation rate of the tool and use scrolled shoulders are examples of things that were proved to reduce the amount of flash produce during the welding process [1]. Although excessive flash may be not considered a critical feature in some cases is also important to notice that may result in a significantly concave weld which (due the conservation of volume) causes thinning of the weld. Both the excessive flash and excessive face concavity can be easily detected by visual inspection.

In the FSW process the tool is considered non-consumable, however as a consequence of the great friction involved in the welding process wear does occur to the tool in use which may lead to dimensional changes which, in turn, may cause weld flaws/defects. Moreover as severe wear of the tool take place some particles of the tool material are left behind within the already welded material; in some less rigorous applications this might not be a relevant issue but in other cases the embedded tool particles have a significant detrimental effect on the joint properties and are not acceptable. In addition to tool material particles the presence of other substances such as oil, grease or even dirt can also affect the FSW joint produced.

In Tab. 2.4 [8] some of the common flaws that may be found when welds of two abutted plates are produce by FSW are presented.

Flaw type	Location	Causes
Void	Advancing side at edge of SZ	Low forging pressure Welding speed to high Plates clamped improperly
Void	Beneath top surface of weld	Welding speed to high
Remnant joint line	stir zone	Inadequate removal of oxide Inadequate dispersal of oxide by tool
Root flaw	At the base of the stir zone	Probe too short Incorrect tool plunge depth Poor tool alignment

Table 2.4: Characteristic flaws that can be found in butt joint welds.

As can be observed the most common and frequent flaw types are in general caused by the use of non-optimized parameters and inadequate welding variables; when appropriate parameters are used the amount of flaws are reduced significantly and in some cases even completely eliminated.

2.2.10 Properties

As is being mentioned in this document FSW process results in a significant microstructural evolution within and around the stirred zone (stir zone, TMAZ and HAZ). As a consequence and as in any other joining process substantial changes occur in post-weld mechanical properties. In this section of the document and introduction and analysis of the appearance of residual stresses and distortion will be made as well the changes in the typical mechanical properties such as strength, ductility and fatigue behaviour.

2.2.10.1 Residual stresses

During the fusion welding processes, quite complex thermal and mechanical stress are developed in the weld and surrounding region due to the localized application of heat and constraint. After the welding process residual stresses appear and are often at, or very close to the parent material or weld material yield strength [8]. The presence of residual stress in a welded plate affects its distortion behaviour and its ability to sustain applied load while maintaining structural integrity. While compressive stresses may in some circumstances be beneficial, tensile stresses tends to cause crack initiation and its propagation leads to a catastrophic failure [9]. In the case of the friction stir welding process it is believed that residual stresses are significantly decreased when compared with fusion welding processes, something that is related to the low temperature solid-state process of FSW. However, when compared to more compliant clamps used for fixing the parts in the conventional (fusion) welding processes, the quite rigid clamping system used in FSW exerts a much higher restraint on the workpiece; that restriction of movement prevents the contraction of the welded stir zone and the heat-affected zone during the cooling step in both longitudinal and transverse directions resulting consequently in the appearance of residual stresses in both longitudinal and transverse directions. The existence of significant high values of residual stresses have a significant effect on the post-weld mechanical properties, in particular fatigue and fracture toughness, so it is of capital importance to investigate the residual stress distribution in the FSW welds if a complete analysis of the process is required.

Determination of residual stresses is a complex area. Residual stresses present in a weld can be measured by destructive methods (e.g. hole drilling method, contour method) or non-destructive methods such as neutron diffraction and synchrotron X-ray diffraction techniques [8]. Since diffraction techniques

are frequently expensive and conventional hole-drilling is only suited to uniform plane stress around the produced hole, Moiré interferometry incremental-hole-drilling method is also possible to be used to assess residual stresses in friction stir welds [9].

Several authors have determined residual stresses by non-destructive techniques using, essentially X-ray diffraction. A broad agreement in the results is possible to be observed even for different materials. The results are then all in agreement that the largest variation are in the longitudinal stresses, wherein being mostly tensile in the HAZ, lower in the stir zone and compressive in the parent material [8]. James and Mahoney [43] measured residual stresses (using X-ray diffraction) in the FSW 7050-T7451 and they found that the residual stresses in all of the welds were significantly low when compared to those generated during fusion welding processes; the reason was attributed to the lower heat input during the FSW process and recrystallization accommodation of stresses. They also revealed that at the transition between the fully recrystallized and partially recrystallized regions (TMAZ and HAZ) the residual stresses were higher than those observed in other regions of the weld and that, in general the longitudinal residual stresses were tensile and transverse residual stresses were compressive.

The characteristic profile of the longitudinal residual stresses across a friction stir weld are shown in Fig. 2.2.12 [8].

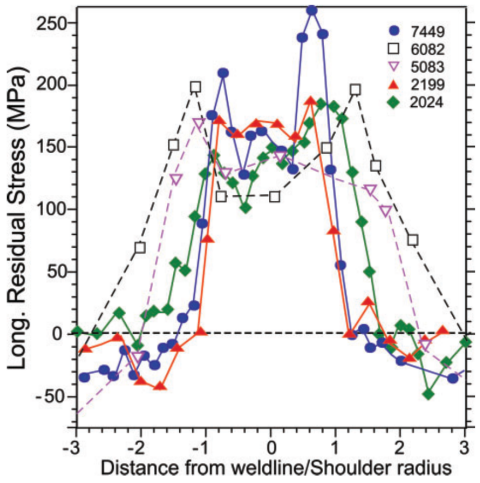

Figure 2.2.12: Longitudinal residual stresses for friction stir welds in different aluminium alloys.

As already referred the longitudinal stresses present the largest variations and are then typically much greater than the transverse [44]. From a quick look of Fig. 2.2.12 [8] it is possible to observe that longitudinal residual stresses exhibit an "M" shaped profile across the weld; the stresses tend to be tensile over a region extending just beyond the diameter of the tool shoulder embracing the stir zone and the TMAZ reflecting the extent of the hot region caused by the shoulder. The maximum magnitude values are frequently found just within or just beyond the shoulder radius which means that quite often the peak stress values lie within the HAZ although, in farther regions form the centreline the minimum value are also possible to found there. Lower levels of compressive residual stresses are generally found in the base material just beyond the heat-affected zone influence. The width of the tensile zone and the magnitude of stresses are closely related with the processing conditions [8]. Donne et al. [44] in his work measuring residual stresses on the dissimilar FSW of AA2024-T3 and AA6013-T6 concluded, among other things, that with the decreasing of the welding speed and tool rotation rate, the magnitude of the tensile longitudinal residual stresses were decreased. More recently, Peel et al. [45] investigating the residual stress distribution on FSW AA5083 obtained similar results since he concluded that the residual stresses increased with the increasing of the tool speed and moreover that the transverse residual stresses did

not exhibit dependence on the traverse speed. Still in the same work Peel et al. found an asymmetry in longitudinal residual stress profiles with the stresses being approximately 10% higher on the advancing side.

Distortion

The amount of distortion present in a workpiece that was friction stir welded is invariably linked with the residual stresses in it present. In most cases aluminium alloys that are friction stir welded present low distortion levels when compared with arc welding or any other fusion process. In case of low thicknesses, however, some quite significant distortion may occur in FSW welds where the design leads to an asymmetry in restraint or heat sink.

In short, as a solid-state welding process, there is a appreciable room for manipulating the residual stresses and distortions during the welding process. Thermal and mechanical tensioning have been found to be successful in the purpose of reduce and reverse the state of stress [8].

2.2.10.2 Strength and ductility

Tensile properties of friction stir welds are, generally, mentioned as capable of equal or even exceed those reported for fusion weld processes [8]. Mahoney et al. [18] studied the effect of the friction stir welding process on tensile properties of the aluminium alloys 7075-T651. Specimens were obtained for the longitudinal direction (along the welding direction) and for the normal (transverse to the welding direction) direction. As can be easily understandable the longitudinal tensile specimens only contained the fully recrystallized zone, that is the stirred region, whereas the transverse tensile specimens contained the microstructures of the four, already mentioned regions of a typical cross-section friction stir weld, that are the base material, HAZ, TMAZ and stir zone. On the 1998 document, Mahoney et al. [18] came to the conclusion that for the longitudinal direction a reduction in the yield and ultimate strength was possible to observe while the elongation was mainly unaffected. The reduction of strength was attributed to the reduction of the pre-existing dislocations and the elimination of the very fine hardening precipitates. A recovery of the lost tensile strength was achieved by a post-weld aging treatment. In the case of the transverse tensile specimen a reduction in both strength and ductility was observed. Moreover, the strength and ductility values observed in the normal direction were substantial lower than those founded on the longitudinal orientation. In contrast to what happened in the case to the longitudinal tensile specimen the post-weld treatment did not restore any of the lost strength during the welding process leading even to a further reducing of the ductility. As emphasized before the tensile specimens in transverse orientation contain the four different microstructures and so the obtained ductility is invariably an average strain over the gage length of the various regions [8]. As might be expected different regions have different resistances to deformation due to different grain size and precipitate size and being HAZ the region that has the lowest values of strength (due to substantial coarsened precipitates) is there that, during tensional stresses, strain occurs. So in the low strength heat-affected zone high levels of strain are possible to be observed resulting eventually in necking and rupture. As a consequence in a well projected weld the fracture must always occur in the HAZ. For the particular case of the heat-treatable alloys (such as 2XXX, 6XXX or 7XXX in the T6 or T7 condition) the cross-weld tensile test (transverse tensile specimens) the fail frequently occurs at the side of the stir zone, or at the HAZ/TMAZ boundary [8]. The failure mechanism is a ductile shear failure, showing 45° facets, although, for thicker specimens the faceting might be more complex. The elongation is invariably lower than that which can be found in the base material due to concentration of strain in softer regions. Although the intrinsic strength and ductility

of the advancing and retreating sides are known as different (the retreating side has lower strength) and although some authors [7] believe that the fracture is prone to happen always at the retreating side others, such as Threadgill et al. [8] claim that failure can occur on either the advancing side or retreating side although for a series of welds they will all generally occur in the same side.

2.2.10.3 Fatigue

The friction stir welding process being mainly concerned with engineering applications, such as bridge construction, transport vehicles, platforms and extreme demanding aerospace structures, where cyclical load variations are quite frequent, the knowledge of the FSW structures' fatigue properties is of critical importance. In this section a brief introduction of some of the research made under the fatigue behaviour of FSW welds will be presented. The primary purpose is to discover the main implications and fatigue properties changes of the process when related with parent material and its place among the rest of the joining processes.

One of the most common ways of evaluating the fatigue behaviour is through stress-number of cycles to failure (S-N) curves. In past few years a great number of materials where covered in several investigations where the S-N behaviour was conducted. These works resulted in important observations and allowed to conclude some general fatigue behaviours. One of them is that in simple S-N fatigue tests on cross-section welds samples, the fatigue performance of friction stir butt welds is often a bit worse than that of the base material tested under the same conditions (the fatigue strength of the FSW weld is then lower than that of the base material). Some investigations [46] reported, however, that milling a thin layer of the top surface or both the top and bottom surfaces (removing the superficial irregularities) resulted in a better fatigue performance approaching that of the parent material. These kind of observations clearly suggest that the fatigue life is closely related to surface crack nucleation (presence of substantial superficial irregularities) and that a poor fatigue behaviour can occur even in welds where there are no inherent defects or internal flaws. The failure is then associated with an initiation event at geometric stress concentration at either side of the weld (surface quality); when superficial irregularities are machined away the failure frequently occurs in the region of lowest strength. Hori et al. [47] reported that the fatigue strength of friction stir welds decreased with the increase of tool traverse speed/rotation rate ratio due the aggravation of the lack of penetration phenomenon and the increase of non-welded groove on the root side of the weld; once skimmed the bottom surface the fatigue strength of the FSW weld remained virtually unchanged by the welding speed/rotation speed ratio. Another quite important observation possible to be made was that the fatigue strength of the FSW welds was higher than that of other joining processes; as an explanation for this fact is a finer and more uniform microstructure in FSW welds.

As previously stated when introducing the appearance of residual stresses on the FSW structures, its presence (residual stresses) can play a very significant role in the overall of fatigue behaviour. Donne et al. [48] found that the presence of residual stresses were by far the most important effect in their compact tension fatigue specimen in which fatigue crack propagation (FCP) varied significantly with R (maximum/minimum stress ratio); once the residual stresses were taken into account very little variation in fatigue performance was observed as dependent of FSW process parameters.

One of the most important subject in fracture mechanics is the fatigue crack propagation behaviour. The knowledge and understanding of how a crack propagates is of practical significance in engineering structures. Jata et al. [34] collected some fatigue crack growth data in a study carried out on eccentrically loaded single edge tension tests on the aluminium alloy 7050-T7451 (7XXX series) with the crack running through different regions longitudinally to the weld direction. At the load ratio of 0.33 they found that the fatigue crack propagation in the stir zone was inferior, while the growth rate in the HAZ is superior

to that of the parent material. In the stir zone the microstructure and intergranular failure mechanism dominates the crack growth whereas the compressive residual stresses dominate the crack growth within the heat-affected zone.

2.2.11 Process variants

Since its development, the conventional FSW process has evolved and expanded into a quite significant number of process variations that included modifications in tool geometry/design, changes in the joining methodology as well as types of welding surfaces materials to be weld. Stationary shoulder FSW, double-sided FSW, friction stir processing, friction stir spot welding and bobbin-tool friction stir welding are some of the process variations that, as previously referred, have the same basis as the conventional friction stir welding process. In this section only the variants present in the EMBRAER project will be subjected to a brief introduction.

2.2.11.1 Double-sided FSW (DS-FSW)

The double-sided FSW (frequently simplified as DS-FSW) is probably the simplest variation of the conventional friction stir welding process and in reality no conceptual change of the conventional joining process is verified.

In contrast to what happens in the conventional FSW process where the joining takes place in a single pass (which means that the welding process is through all the thickness) in the double-sided FSW only half of the thickness is welded at a time which means that at least two passes are needed to complete the joining process. The fact that only half of the thickness is welded at a time has as a consequence that the plates to be welded must be turned at the end of the first pass; generally the same tool and process parameters are used for both passes (i.e. tool rotation rate, welding speed, probe length, etc.) however some particular changes between passes could be set in order to improve the overall welding process. The need for at least two passes to complete the joining process results in a significant amount of time that is spent in the turning of the plates between passes which appears as a drawback of the process; moreover if a fully automated system is to be applied to produce DS-FSW joining process an inevitable increase in complexity and required funds will be predictable. These drawback may, however, be justified since the DS-FSW approach was intended to induce the serration of the geometric discontinuities and to induce a significant microstructure homogeneity at the stirred zone [49] which may be responsible for significant improvements on the post-welded properties.

As stated before no significant change in the process variant is observed when compared with the conventional friction stir welding process, in fact, the DS-FSW is the result of two passes in conventional FSW for each side of the workpiece (e.g. abutted plates). Welding only half of the thickness at a time has as a consequence, naturally, the reduction of the tool size and in turn the reduction of the heat input (H.I.) for each pass resulting in a more homogeneous microstructure and larger properties uniformity across the cross-section of the welded plates. Being considerably simple to produce double-sided friction stir welded structures and being an approach that could lead to significant improvements in the post-welded properties DS-FSW has been studied in the past few years and ways of improving it and turn it profitable in comparison with the conventional FSW are some of the goals of the FSW researchers.

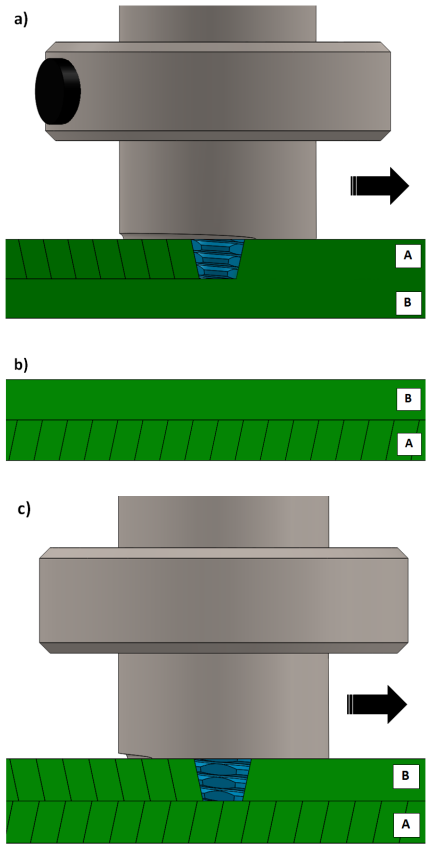

Figure 2.2.13: The three steps of the DS-FSW process.

2.2.11.2 Stationary shoulder FSW (SSFSW)

Stationary shoulder friction stir welding process, usually designated simply as SSFSW, is a variant of the conventional FSW. As mentioned before in the standard FSW process the majority of the generated heat is a result of the deformation under the shoulder; the heat is then conducted down and through the banking plate which leads to a significant temperature gradient between the top and the bottom surfaces of a weld. Moreover, in association with significant temperature gradient the high heat input proportion caused by the shoulder tends to expand the HAZ which is responsible for the ultimate decrease of the weld properties. With the previous problematic issues in mind Russell et al. proposed in 2008 the SSFSW process. The main purpose of it was to reduce the large through-thickness temperature gradient that was normally observed when welding low thermal conductivity titanium alloys [50]. In contrast to what happens in conventional FSW in the SSFSW process the probe (pin) is rotated through a bearing assembly in the tool shoulder, which (the shoulder) is fixed to the head of the welding machine; in conventional FSW the probe and the shoulder rotate simultaneously. During the welding process the non-rotating shoulder (so stationary shoulder) slides across the surface of the workpiece while only the tool probe rotates inside it. In this variant the shoulder is then responsible for little heat production whereas nearly all originated energy from plastic work is provided by the probe. In SSFSW then, the functions of the tool become somewhat separated in that all heat is generated by the probe and the shoulder provides the forging pressure [1].

Although SSFSW was developed having in mind applications in low conductivity materials some advantages seemed to appear when welding much more conductive materials such aluminium alloys. When welding with stationary shoulder a narrower and more parallel through-thickness thermal field would be

expected which ultimately leads to a reduction of the HAZ width and lower levels of distortion which improve the weld properties. Good surface finish and significant versatility to create a different number of joints (butt joints, corner joints, T-joints) when provided the proper tool geometry (i.e. shoulder) are also some of the advantages of the stationary shoulder process.

2.2.11.3 Bobbin-tool FSW (BT-FSW)

Bobbin-tool friction stir welding is a variant of the conventional FSW in which the tool probe extends through the workpiece an reaches a second shoulder on the base side that replaces the anvil or backing bar and consequently this process is also know as self-reacting FSW [1]. This process configuration employs then two rotating shoulders which are connected by a probe; the upper shoulder (acting on the upper surface of the parent material) and a lower shoulder (acting on the lower surface of the parent material) which are responsible for the process loads remain confined within the tool [51]. This appears as one of the main advantages of the process since can lead to a reduction of the size and complexity of the tooling necessary to welds large structures [1]. The BT-FSW set-up makes it capable of joining closed hollow extrusions or complex structures without the introduction of any sort of backing elements [52, 53] while additionally has the ability to weld a workpiece simultaneously from both sides eliminating the occurrence of root flaw and lack of penetration typical of the conventional FSW[52] resulting in a more uniform through-thickness mechanical properties [54]. In Fig. 2.2.14 is presented a representation of the BT-FSW tool/process.

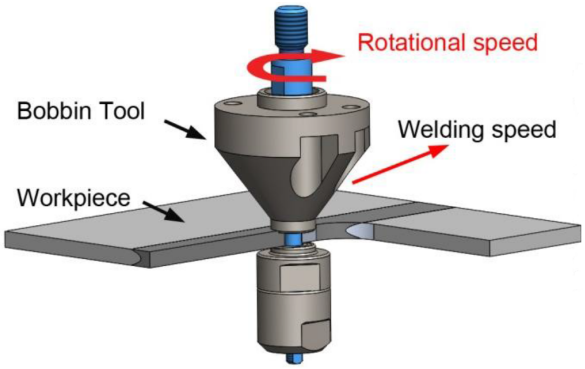

Figure 2.2.14: Bobbin-tool process representation.

[blank page]

Chapter 3

Experimental procedure

3.1 Methodology

The experimental work developed at the HZG facilities followed a methodology that is presented in Fig. 3.1.1.

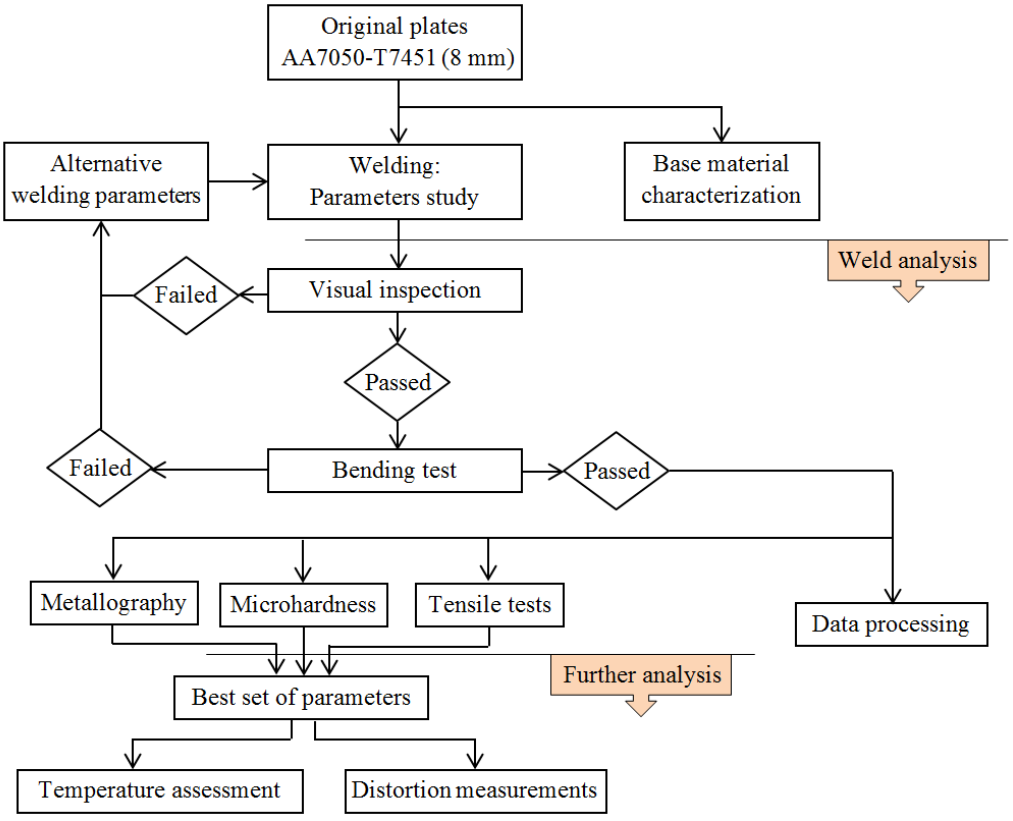

Figure 3.1.1: Flow chart of the methodology followed on the parameters study.

Original 1200 mm × 200 mm × 8 mm (8 mm plate thickness) plates of the aluminium alloy AA7050-T7451 were the initial point of all work. At the beginning material samples of the original plates were

extracted so to ascertain the real chemical composition and mechanical properties of the material to be welded in order to avoid possible errors when comparing with the pre-established values for the same material. A quite significant number of welds were to be produce in order to develop a study of welding parameters; previous works were the basis for the production of the first welds and the experimental procedure was then carried out taking into account the results that were being successively obtained since a full DoE analysis would imply number of tests incompatible with the available time to accomplish the experimental work; after and for each weld (for a certain welding parameters) the evaluation of the weld (weld analysis) was made firstly through simple visual inspection and then through the bending test procedure. The relatively fast and simple bending test procedure, to be properly discussed later, allowed a fast separation between the undoubtedly unsatisfactory welds (the ones that failed) from the welds that could present satisfactory results and that should be further studied, namely, through the metallographic analysis, microhardness assessment and tensile testing. After the best set of parameters have been found further analysis were performed so to measure the distortions resulting and the temperatures involved during the welding process (solely for the best set of parameters both for the single-sided FSW and DS-FSW).

3.1.1 Base material characterization

As previously mentioned all friction stir welds were performed on 8 mm thick plates of the hot-rolled and then aged 7050-T7451 aluminium alloy. In this section a brief introduction of the base material characteristics will be quickly discussed and the analysed properties exposed.

3.1.1.1 Chemical composition

Material samples were cut from one of the delivered plates to ascertain the real chemical composition. The chemical analysis was carried out internally (HZG). The literature composition ranges and upper limits for the selected alloy [55] as well the results of the internal chemical analysis are presented in the table below. Good accordance between the chemical analysis and the internationally established values was obtained.

Chemical Element	Established	Chemical analysis (HZG)
Al	87.3 - 90.3	89.4
Cr	< 0.04	-
Cu	2 - 2.6	2.37
Fe	< 0.15	0.07
Mg	1.9 - 2.6	2.05
Mn	< 0.1	0.008
Si	< 0.12	0.04
Ti	< 0.06	0.04
Zn	5.7 - 6.7	5.99
Zr	0.08 - 0.15	0.11

Table 3.1: Chemical composition of the 7050-T7451 alloy in weight percentage (weight %).

3.1.1.2 Metallographic characterization

A metallographic analysis of the three material directions - rolling direction (RD), long transverse direction (LTD) and short transverse direction (STD) - was made. As mentioned before in this document,

section 2.1.2, 7XXX aluminium alloys (7050-T7451) plates are obtained by hot-rolling which is responsible for the elongation of the grain structures along the rolling direction. In Fig. 3.1.2 its presented the grain directionality possible to find on the 7050-T7451 plates. Elongated grain structure along the rolling direction and more equiaxed grain for the STD and long transverse directions are typical of grain directionality due to rolling process.

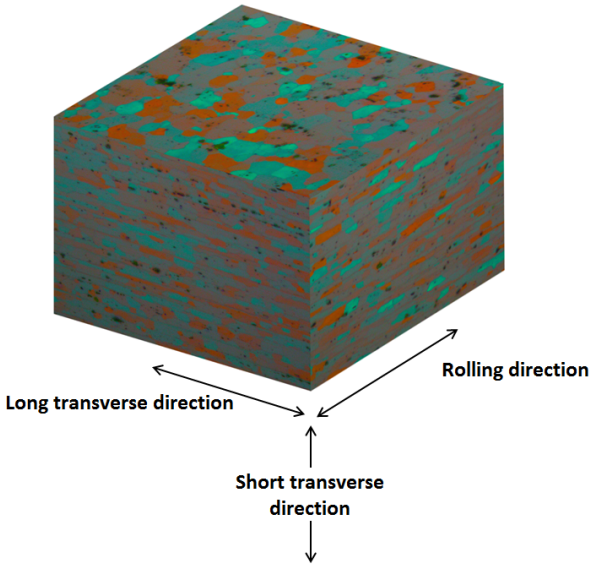

Figure 3.1.2: Grain directionality on the 7050-T7451 studied plates.

The arrangement of the three material directions in the plates can be observed in the figure below; RD perpendicular to welding direction; LTD parallel to welding direction; short transverse direction through thickness direction.

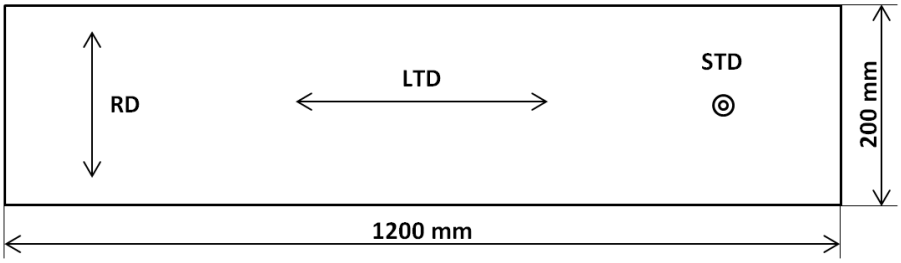

Figure 3.1.3: Material direction arrangement on the 7050-T7451 plates.

3.1.1.3 Mechanical properties

Four tensile specimens for both the rolling and long transverse directions were manufactured by the workshops at HZG to determine the tensile properties of the material to be welded (such as Young's modulus, yield strength, ultimate strength and elongation). In Tab. 3.2 are presented the properties obtained for both the RD and LTD as well the literature values for the same material [55]. With exception of the elongation which revealed a significant higher value than predicted by established value good accordance between the laboratory test and established values was obtained.

Property	Manufacturer	Mechanical analysis (HZG) RD	LTD	Unit
Young's modulus	71 - 74.6	68.9 ± 0.2	69.7 ± 0.3	GPa
Yield strength	393 - 462	451.0 ± 0.8	449.8 ± 0.5	MPa
Tensile strength	455 - 524	507.1 ± 0.8	513.0 ± 0.3	MPa
Elongation	2 - 10	16.4 ± 0.5	16.0 ± 0.7	% strain
Fatigue strength (10^7 cycles)	130 - 150	–	–	MPa
Fracture toughness	23.1 - 42.9	–	–	MPa$\sqrt{\text{m}}$

Table 3.2: Some mechanical, impact and fracture properties of the AA7050-T7451.

In addition to the tensile tests, hardness assessment for all directions (RD, LTD and STD) was performed. Tab. 3.3 presents the predefined (literature) and measured values for the different directions; the values presented were the result of microhardness measurements for 30 points over each directional surfaces.

	HV
Literature	135 - 155
Rolling direction (RD)	157.3 ± 3.2
Long transverse direction (LTD)	158.5 ± 3.1
Short transverse direction (STD)	159.2 ± 2.3

Table 3.3: Hardness assessment of the base material.

As can be observed the hardness values for each spacial direction are very similar and in average approximately 158 HV. For the mechanical properties assessment of the performed welds the values related to the rolling direction were used as a comparison since, with exception of hardness, all mechanical properties were determine for the cross-section direction (RD); for the case of hardness the LTD value was used since the hardness assessment is performed in the welding direction, LTD.

3.1.2 Welding procedure

Square butt welds were made at the interface between sets of two plates (along the plates length). All welds were performed in a FSW gantry system machine at HZG facilities (Germany). Some characteristics of the FSW machine are presented in Tab. 3.4. Before being placed in welding position each pair of plates was submitted to a thorough and meticulous removing of the oxide layer on the surface to be welded. A strong manual clamping system was used in order to ensure a proper placement of the workpiece throughout the welding process (see Fig. 3.1.4). A tilt angle of 1° was set for all welds; all welds were produce in room conditions.

Axial force (Z)	80 kN
Force along welding direction (X)	20 kN
Bi-directional rotational speed	3500 rpm
Max. spindle torque	340 Nm
Welding speed range	1 - 160 mm/s
Max. continuous weld length	2350 mm
Tilt angle range	-3° to +3°

Table 3.4: Technical data of the HZG FSW gantry machine.

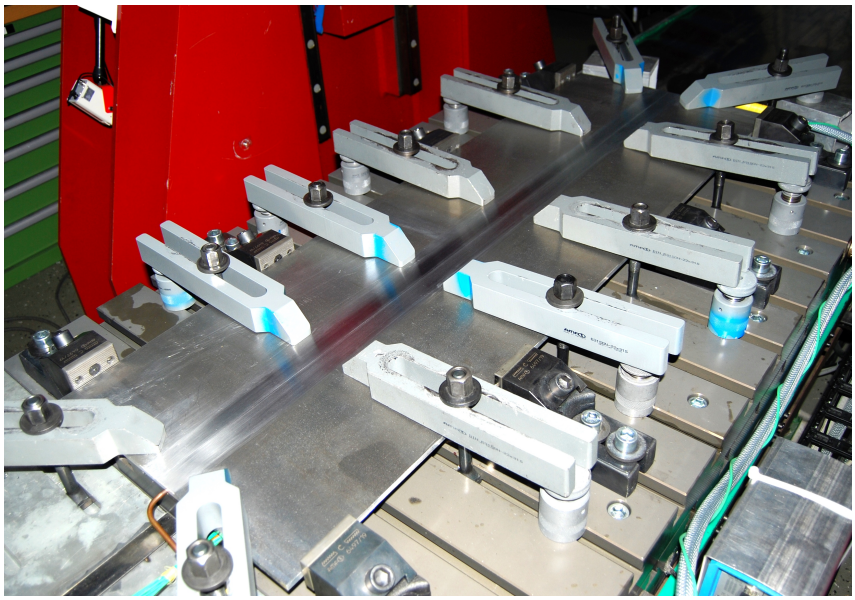

Figure 3.1.4: Clamping system used (HZG)

It should be to mentioned that for each weld produced an internal designation (HZG) was defined. The original HZG designation is of critical importance since raw data of welding procedure is store in that designation system and thus throughout this document that designation will be always present. The welding designation appears as a set of letters followed by four digits (welding number) intending to unmistakably identify a particular weld (FSW-PA-LB-XXXX for the case of conventional FSW; DS-FSW-PA-LB-XXXX for the double-sided FSW).

3.1.2.1 Conventional FSW

In order to establish a satisfactory weld a significant number of experiments (welds) were produced in the conventional FSW parameter study. In Tab. 3.5 are presented, by designation order (chronological order) the experimental welds performed.

The conventional friction stir welding tool was a two-piece design (shoulder and probe) which allowed the probe length regulation. A Triflat design, with a 20 mm diameter scrolled shoulder (HOTVAR - H13 tool steel) with a tapered (three flats), threaded probe (MP-159) with a diameter of 8 mm at the intersection with the shoulder was the tool used in all the conventional friction stir welds (see Fig. 3.1.5 and Fig. 3.1.6). The precise geometrical features of the tool can be found in annex. With an exceptional case which is properly indicated all welds were performed by force control. Since the length of the probe was possible to regulate, probe length appeared as a welding parameter.

Designation FSW-PA-LB	Welding speed (mm/s)	Rotational speed rpm	Vertical load kN	Probe length mm	Observations
1838	5	700	35	7.8	-
1839	6	800	-	7.8	Probe broke
1840	6	800	16	7.8	Position control
1841	6	800	25 - 35	7.8	-
1842	6	800	25	7.8	-
1846	6	800	25	7.85	-
1847	8	800	25	7.85	Probe broke
1848	8	1000	25	7.85	-
1849	8	1000	25	7.87	-
1850	7	900	25	7.87	-
1851	5	700	25	7.87	-
1860	5	700	30	7.87	-
1861	6	800	30	7.87	-
1862	7	900	30	7.87	-
1863	8	1000	30	7.87	-
1864	5	700	20	7.87	-
1865	6	800	20	7.87	-
1866	7	900	20	7.95	-
1867	8	1000	20	7.95	-
1868	7	900	25	7.95	-
1869	8	1000	25	7.95	-
1870	8	1000	30	7.95	-

Table 3.5: Welding parameters for conventional FSW.

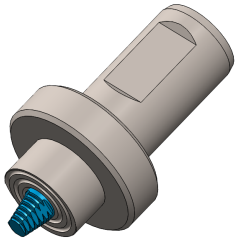

Figure 3.1.5: FSW tool representation.

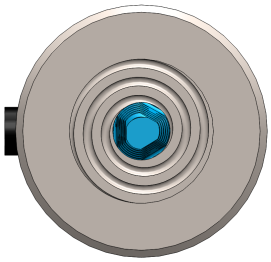

Figure 3.1.6: Bottom view of the FSW tool (representation).

3.1.2.2 Double-sided FSW

A similar approach to that of conventional FSW was made for the case of double-sided FSW; the same tool material and tool design was used, however, this time a 15 mm and 6 mm diameters were used for respectively shoulder and probe (at the intersection with the shoulder). The precise geometrical features of the different parts of the tool can be consulted in annex. For each pass the plates had to be loosened, turned around by the welding direction, and clamped again. For each complete weld the same welding parameters were used for both A (first pass) and B sides (second pass). In the following table are presented the performed welds and its respective welding parameters.

Designation DS-FSW-PA-LB	**Welding speed mm/s**	**Rotational speed rpm**	**Vertical load kN**	**Probe length mm**	**Observations**
1852-A/B	5	800	15	4	-
1853-A/B	5	700	15	4	-
1854-A/B	6	800	15	4	-
1855-A/B	7	900	15	4	-
1856-A/B	8	1000	15	4	-
1857-A/B	9	1100	15	4	-
1858-A/B	10	1200	15	4	Probe broke
1872-A/B	10	1200	15	4	-

Table 3.6: Welding parameters for double-sided FSW.

3.1.3 Weld analysis

After a set of plates has been welded an analysis of the obtained product had to be done in order to ascertain the condition of the weld (and the basic welding parameters such as tool plunge and probe length) and ultimately the properties of the sound welds. As mentioned in 3.1 immediately after the welding process has finished a very simple and fast visual inspection of the welds was made to ascertain whether there were evident lack of penetration (LOP) - at the welding root (bottom surface) in the case of the single FSW - and/or cracking within the shoulder trail surface; if that happened the weld was immediately rejected and other welding parameters were tested; otherwise the weld was then submitted to the bending test procedure.

3.1.3.1 Bending test

The bending test procedure is a very simple and quick way of evaluate the ductility of the joints and possible defects that they might have, particularly lack of penetration (LOP). In order to ascertain whether there was or not LOP all single-sided friction stir welds were subjected to the three point root bending test according to the 'Destructive tests on welds in metallic materials - Bend test (ISO 5173:2009 + Amd. 1:2011) English translation of DIN EN ISO 5173:2012-02'. Following the bend test standard specifications, samples of 400 mm long and 35 mm width were cut from the original welded plates and bend test performed using l=62 mm. The tests were carried on a hydraulic press HIDROALFA, model 20. In Fig. 3.1.7 is shown a sketch of the performed bending test.

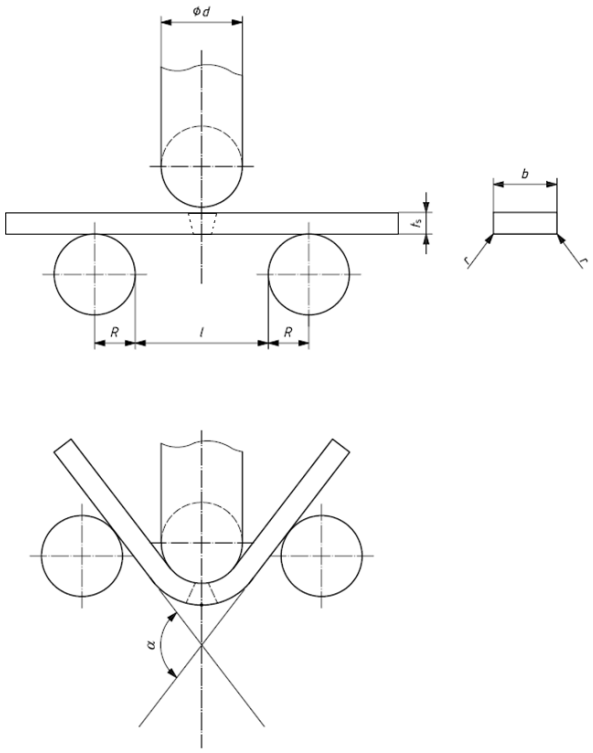

Figure 3.1.7: Transverse (three-pointed) root test.

Specimens that presented a brittle fracture or that presented a fracture along the junction line of the two plates (at the root, naturally) were immediately rejected for presenting lack of penetration.

Double-sided friction stir welds were not subjected to the bending test (since the ascertainment of LOP procedure have no effect).

3.1.3.2 Metallographic analysis

Metallurgical characterization of those welds that had a positive response to bending test was performed with the purpose of revealing the aspect of its cross-section and unveil possible flaws produced during the FSW process. Cross-section samples for metallography evaluations were cut (45 mm × 15 mm × 8 mm (thickness)) by diamond abrasive wheels in a Struers Discotom-6 automatic machine and posteriorly embedded in a cold mounting resin (Demotec 30) so as to allow the analysis of the cross-sections through thickness looking on the welding direction. The embedded samples were then ground and polished on a automatic grinder; the details of sample preparation are presented in Tab. 3.7.

Step		Lubricant	Time (min)
Grinding	Silicon carbide #320	water	3
	Silicon carbide #800	water	1.5
	Silicon carbide #1200	water	1.5
Polishing	Silicon carbide #2500	water	3
	Dac	Diamond suspension 3μ	4
	Nap	Diamond suspension 1μ	4

Table 3.7: Grinding and polishing procedure.

After being properly polished the samples were etched for approximately 120 seconds using Barker's etchant. Macrographs and micrographs were obtained using an optical microscope - Leica DM IRM.

3.1.3.3 Microhardness test

Vickers's hardness (microhardness analysis) was measured on the transverse cross-sections using a conventional Zwick/Roell ZHV microhardness machine. Hardness measurements were made with a spacing between indentations of 0.5 mm, using a 2 kg load (HV 0.2) and a dwelling time of 10 seconds.

Two centred indentation lines (of 40 mm long and 80 indentations each) for the case of the conventional FSW and three (of 35 mm long and 70 indentations long) for the case of the DS-FSW were performed transversely to the welding direction. Schematic sketch of the indentations lines for both conventional FSW and double-sided FSW are presented in Fig. 3.1.8 and Fig. 3.1.9 respectively.

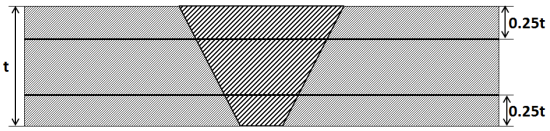

Figure 3.1.8: Indentation lines in FSW specimens.

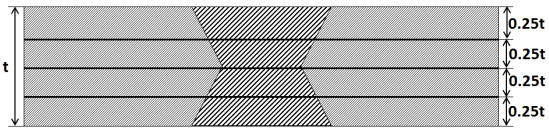

Figure 3.1.9: Indentation lines in DS-FSW specimens.

Hardness maps (topographies) were performed so to assess the influence of the welding parameters on the hardness response. The topographies were made using a spacing between indentations of 0.5 mm, using a 2 kg load (HV 0.2) and a dwelling time of 10 seconds; an UT100 automatic hardness tester was used.

3.1.3.4 Tensile test

Three specimens from each weld (for those that did not fail on the bending test) were tested in a Zwick/Roell universal testing machine with a load cell capacity of 200 kN. The mechanical assays were performed at room conditions, with a constant cross-head speed of 1 mm/min; a mechanical MTS 634.25F-24 axial extensometer with an initial length (L_0) of 75 mm was used to register the elongation values throughout the tensile test. The geometrical features of the specimens are presented in the figure below (the technical drawing sheet is possible to be found in annex); as may be observed in Fig 3.1.10 the specimens were manufactured to be tested along the rolling direction explaining thereby the use of the base material rolling direction properties as a comparison (as already stated in 3.1.1.3).

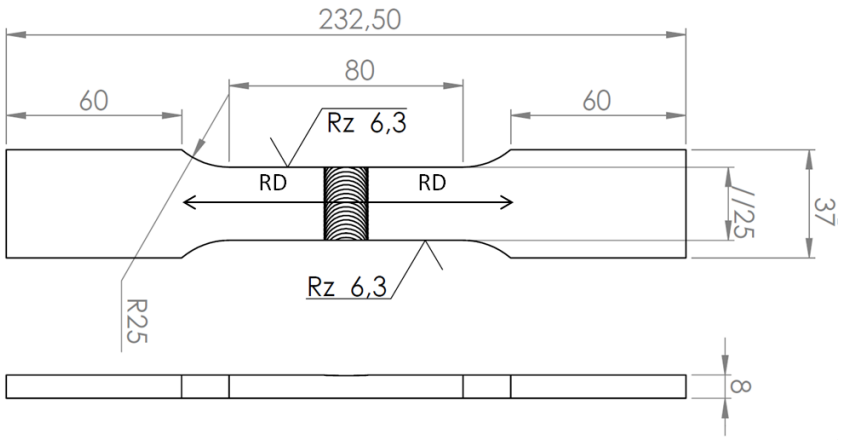

Figure 3.1.10: Geometric drawing of the specimen for FSW and DS-FSW tensile test.

3.1.4 Fracture surface analysis

Conventional FSW fracture surfaces, for four different weld pitch and the same vertical load (see Tab. 3.8) were studied in order to a ascertain the influence of the weld pitch on the fracture surface features and the mechanical properties obtained. A characteristic DS-FSW fracture was also subject to SEM analysis so to reveal in more detail the microscopic features of its rupture. Detailed fracture surfaces micrographs were obtained by a Scanning Electron Microscope (SEM) Quanta^{TM} 650 FEG.

Macrographs of two cross-sectional fractures regions were performed in an optical microscope - Leica DM IRM - so to allow to ascertain where the failure occurred.

Designation FSW-PA-LB	**Welding speed (mm/s)**	**Rotational speed rpm**	**Weld pitch mm^{-1}**
1851	5	700	14.67
1846	6	800	13.96
1868	7	900	13.46
1869	8	1000	13.09

Table 3.8: Welds that had their the fracture surfaces analysed. (same vertical load, 25 kN).

3.1.5 Temperature measurements

After the parameters study was completed, temperature measurements were carried out for the best welding parameters; two sets of plates, in a butt-joint configuration, for the FSW and DS-FSW, were prepared to allocate a series of thermocouples which registered the temperature distribution during the welding process. For each pass, and for both the conventional FSW and DS-FSW, a total of 26 thermocouples type "k" (nickel-chrome/nickel-aluminium) with 0.5 mm diameter were placed into the backing bar and into the workpiece, 8 and 18 thermocouples respectively; the thermocouples were then connected to a data acquisition system with an external amplifier and integrated AD-converter which, through a LabVIEW software, performed the evaluation of the thermal data in real time with an acquisition rate of 10 Hz. For the insertion of the thermocouples into the plates, 0.8 mm diameter and 4.5 mm deep holes were drilled in the top surface of the plates, for the conventional FSW, and in both surfaces, for the DS-FSW process case. The thermocouples placed on the backing bar were aligned with the joint line and at 1 mm from the bottom surface. The nominal position and the HZG numbering convention of the drilled holes/thermocouples is presented in Fig. 3.1.11; in total, six thermocouples were placed in three main regions to collect thermal information.

A pyrometer system (Pyrometer IMPAC IP 120) was also set in order to measure the tool temperature during all the welding process.

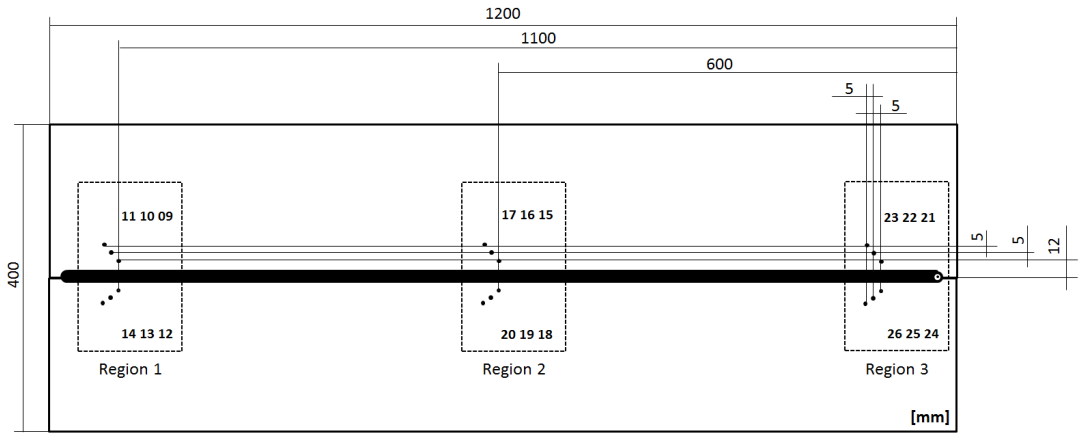

Figure 3.1.11: Thermocouple positions for each pass for 8 mm thick plates of the AA7050-T7451.

3.1.6 Distortion assessment

In order to ascertain the effect of the welding processes on the original geometry and shape of a set of the two plates, the commercial available PONTOS optical measurement system from GOM GmbH was used. A 1250×900 [mm $\times$ mm] measuring volume was used during the distortion measurements and a pixel deviation between 0.013 and 0.04 was found during the calibration, which according to the measurement systems manufacturer, gives a measurement uncertainty below 0.1 mm.

So that PONTOS could work, a number of black and white markers were randomly stuck onto the plates; these markers, which the stereo vision-based system could easily detect, worked as reference points within the plates surface allowing PONTOS measurement system to ascertain the relative position deviation between each marker. For that, after the measurement apparatus be properly mounted and calibrated, two static photos in the exact same conditions were taken, one immediately before and one immediately after the welding process being performed. In Fig. 3.1.12 is possible to observe a set of plates, about to be welded, prepared with stuck markers to perform distortion measurements using the optical system PONTOS; at that stage one photo had already been taken - the immediately before or basis state photo.

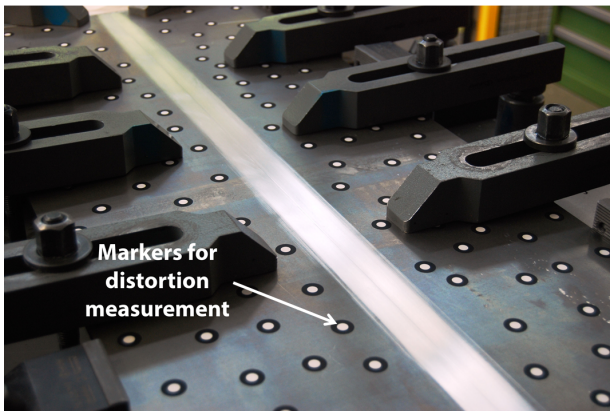

Figure 3.1.12: A set of plates ready to be welded to distortion assessment using PONTOS (HZG).

In all distortion measurements the plates were placed on measuring standing set-up which possessed static reference points, markers, at the top, bottom and right side of the camera visual field. In Fig. 3.1.13

is presented a simplified 3D representation of the PONTOS distortion measurement system used. An artificial light diffuser was used throughout all measurements.

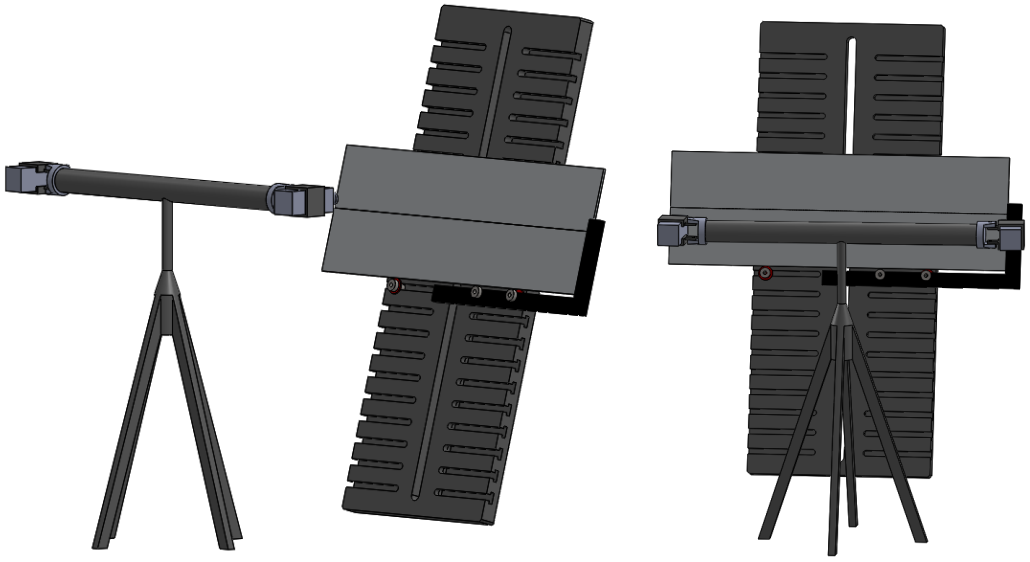

Figure 3.1.13: PONTOS Distortion assessment set-up, representation (HZG).

Chapter 4

Results and discussion

In this section the results of the parameters study for both the conventional and the double-sided friction stir welding are presented. The results and its analysis are somehow organized by experimental and chronological order being FSW and DS-FSW presented separately at first and then compared as joining processes in the light of the results and overall properties achievement.

4.1 FSW

For the single-sided FSW all welds presented a good surface finish.

4.1.1 Bending test

Below is presented a table with the outcome of the bending test procedure; the '*' represents the welds where the probe broke during the welding process; AS and RS are for advancing and retreating side respectively.

From a simple observation of the Tab. 4.1 is possible to assert that:

- For the initial phase of the study (first five welds) a probe length of 7.8 mm has proved insufficiently short;
- For a given vertical load, higher welding speeds (lower weld pitch) require longer probe length (notice welds 1846 and 1848);
- For a given probe length and for significantly high welding speeds (low weld pitch) greater vertical load is required (notice welds 1850 and 1862);
- There is no clear tendency in which side the rupture is preferably to happen;
- Although not entirely conclusively there seems to be a relationship between welding speed and the bending angle which indicates that for higher welding speeds (lower weld pitch) lower values of bending angles are obtained (see Fig. 4.1.1).

Designation FSW-PA-LB	**Welding speed mm/s**	**Rot. speed rpm**	**Load (Z) kN**	**Probe length mm**	**Bending test outcome**	**Angle (α) degree (°)**	**Side of failure**
1838	5	700	35	7.8	LOP	-	-
1839	6	800	-	7.8	*	-	-
1840	6	800	16	7.8	LOP	-	-
1841	6	800	25 - 35	7.8	LOP	-	-
1842	6	800	25	7.8	LOP	-	-
1846	6	800	25	7.85	Good	65	AS
1847	8	800	25	7.85	*	-	-
1848	8	1000	25	7.85	LOP	-	-
1849	8	1000	25	7.87	LOP	-	-
1850	7	900	25	7.87	LOP	-	-
1851	5	700	25	7.87	Good	58	RS
1860	5	700	30	7.87	Good	65.5	RS
1861	6	800	30	7.87	Good	64.4	RS
1862	7	900	30	7.87	Good	54.4	AS
1863	8	1000	30	7.87	LOP	-	-
1864	5	700	20	7.87	Good	75	AS
1865	6	800	20	7.87	Good	64.2	RS
1866	7	900	20	7.95	Good	45.3	AS
1867	8	1000	20	7.95	Good	55.3	RS
1868	7	900	25	7.95	Good	51	AS
1869	8	1000	25	7.95	Good	50	AS
1870	8	1000	30	7.95	Good	57.4	AS

Table 4.1: Results of the bending test procedure for the conventional friction stir welds.

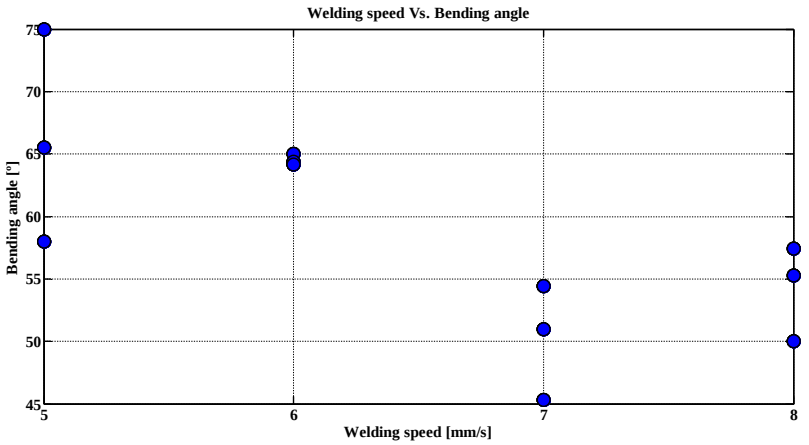

Figure 4.1.1: Relationship between welding speed and bending angle values.

The welds that failed to pass the bending test procedure were immediately set aside; only the welds that have passed will then be subjected to discussion. In Tab. 4.2 is possible to observed the 12 different welds that successfully passed the bending test with its respective welding parameters, extracted welding data (from the gantry machine) - horizontal load and torque - as well as the respective calculated heat input. The heat input was calculated using the power model based on torque values [56].

$$HI = \frac{\omega}{v} \cdot \mathrm{T} \left[\frac{\mathrm{J}}{\mathrm{mm}}\right] \tag{4.1.1}$$

where ω is the rotation speed in radian s^{-1}, v is the welding speed ($\mathrm{mm\,s}^{-1}$) and T is the torque measured by the welding machine (Nm).

Designation FSW-PA-LB	**Welding speed mm/s**	**Rot. speed rpm**	**Load (Z) kN**	**Probe length mm**	**Load (X) kN**	**Torque Nm**	**Heat input kJ/mm**
1846	6	800	25	7.85	8.39	40.2	0.56
1851	5	700	25	7.87	7.80	41.1	0.60
1860	5	700	30	7.87	7.80	44.6	0.65
1861	6	800	30	7.87	8.83	43.7	0.61
1862	7	900	30	7.87	9.80	41.6	0.56
1864	5	700	20	7.87	7.76	38.8	0.57
1865	6	800	20	7.87	8.62	36.6	0.51
1866	7	900	20	7.95	10.73	36.9	0.50
1867	8	1000	20	7.95	11.14	34.3	0.45
1868	7	900	25	7.95	10.69	39.3	0.53
1869	8	1000	25	7.95	11.59	38.1	0.50
1870	8	1000	30	7.95	11.80	39.3	0.51

Table 4.2: Welding parameters and weld data for those welds that successfully passed on the bending test procedure.

It is important to notice that Tab. 4.2, which results from the bending test procedure of the welds presented in Tab. 4.1 lay out the particularity of possessing four levels of welding pitch for three levels of vertical load resulting in the aforementioned 12 welds. The levels just mentioned are presented in form of a table (Tab. 4.3).

Level	**Welding speed mm/s**	**Rotational speed rpm**	**Weld pitch mm^{-1}**	**Load (Z) kN**		
1	5	700	14.67	20	25	30
2	6	800	13.96			
3	7	900	13.46			
4	8	1000	13.09			

Table 4.3: Levels of the effective welding parameters present in Tab. 4.2.

4.1.2 Metallographic analysis

From the metallographic study made of the cross-sections of the welds presented in Tab. 4.2 was possible to observe that a basin-like shape stir zone was present in all of them; although the shapes of the stir zone and TMAZ regions were roughly the same for all welds a quite significant difference on microstructure and volume of mixed material was verified.

Following are presented a number of macrographs and micrograph analysis in order to represent the effect of the welding parameters on the macroscopic features of the cross-sections.

4.1.2.1 Effect of weld pitch

Below are presented four macrographs intending to show the weld pitch variation effect on the macroscopic features for a constant vertical load of 25 kN. Fig. 4.1.2 to Fig. 4.1.5 are presented in decreasing order of weld pitch.

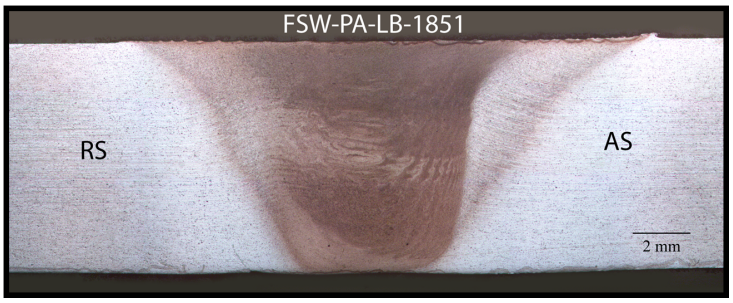

Figure 4.1.2: Macrograph of the weld FSW-PA-LB-1851 (5 mm/s; 700 rpm).

Figure 4.1.3: Macrograph of the weld FSW-PA-LB-1846 (6 mm/s; 800 rpm).

Figure 4.1.4: Macrograph of the weld FSW-PA-LB-1868 (7 mm/s; 900 rpm).

Figure 4.1.5: Macrograph of the weld FSW-PA-LB-1869 (8 mm/s; 1000 rpm).

From a quick observation of the macrographs (Fig. 4.1.2 to Fig. 4.1.5) it is possible to verify that as the weld pitch decreases (increasing of welding speed) the quality of the material mixture is significantly deteriorated. For a constant vertical load as the weld pitch decreases a slightly lower torque value was observed which had as a consequence the reduction of the heat input value (see Tab. 4.2). The reduction of the weld pitch and consequently the reduction of the heat input was then responsible for the appearance of a non-properly mixed material region in the upper part of the stir zone (darker zone) which can be observed in Fig. 4.1.4 and Fig. 4.1.5. The lack of complete mixed material presented in welds such as FSW-PA-LB-1868 and FSW-PA-LB-1869 revealed volumetric defects (voids) with significant size that could be even detected by a thorough visual inspection of its respective cross-sections which, naturally, could foresee being in the present of unsatisfactory welds.

4.1.2.2 Effect of vertical load

In the Fig. 4.1.6 to Fig. 4.1.8 are presented the cross-sections of the welds that were performed for a constant welding speed of 7 mm/s (constant weld pitch) aiming to clarify the effect of the vertical load on the aspect and features of the cross-sections. The three macrographs are ordered by ascending vertical load.

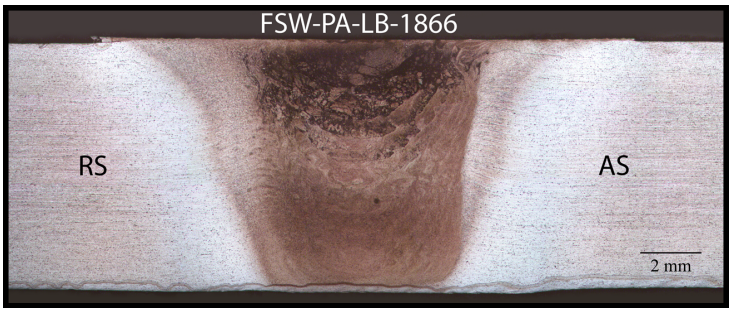

Figure 4.1.6: Macrograph of the weld FSW-PA-LB-1866 (20 kN).

Figure 4.1.7: Macrograph of the weld FSW-PA-LB-1868 (25 kN).

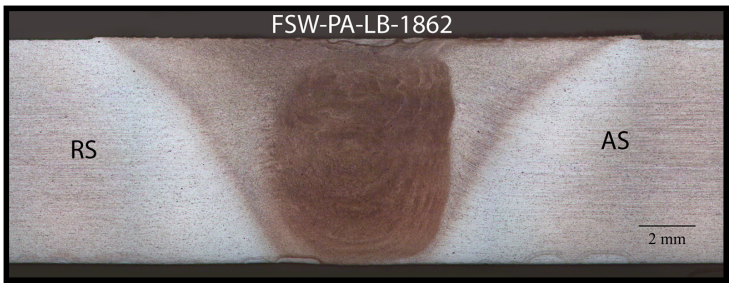

Figure 4.1.8: Macrograph of the weld FSW-PA-LB-1862 (30 kN).

Just as for the case of the weld pitch variation effect, it is possible to observe a significant difference in the appearance of the cross-sections presented above, in this case, by simply varying the vertical load parameter. For a given weld pitch, the increase of vertical load is responsible for increasing slightly the torque value which is ultimately responsible for the increase of the energy rate per length of weld (heat input). As previously mentioned, for the case of the weld pitch variation, a slightly increase of the heat input leads to a more successful material mixture. An area with significant size, presenting insufficiently material mixture (darker zone), is possible to be observed in Fig. 4.1.6 which, for the case of welding speed of 7 mm/s, also presents the lower vertical load and lower heat input. This darker region which is present mainly in the upper part of the stir zone is reduced as the vertical load is constantly increased (so as the heat input) being even suppressed for the case of 30 kN (Fig. 4.1.8).

For what was observed in the macrograph analysis was possible to conclude that a more homogeneous structure and successful mixture were obtained for high weld pitch (slow welds) and high vertical load welds; with these conditions higher heat inputs are applied to the set of plates and the stir of material is duly performed. On the other hand, for low weld pitch and low vertical load, significant amount of defects and lack of complete material mixture was observed within the upper region of the stir zone increasing its dimensions as the heat input was successively reduce. These observations were in accordance with the previously presented flaw section, particularly the Tab. 2.4. Below (Fig. 4.1.9) is presented the weld performed for the lower weld pitch and lower vertical load - lower heat input; as excepted the macrograph analysis revealed the largest region of defects and insufficient material mixture amongst all the 12 welds under analysis.

Figure 4.1.9: Macrograph of the weld FSW-PA-LB-1867 (8 mm/s; 1000 rpm; 20 kN) revealing the largest defect region.

The macrograph analysis permitted even to reveal that as the welding speed was increased a more straight and defined line was obtained between the stirred zone and the TMAZ on the advancing side (see Fig. 4.1.2 to Fig. 4.1.5). Although significantly more visible for the lower welding speeds, nearly all welds presented the 'onion ring' feature, specially on the advancing side of the welding process. This

observation is in accordance with Biallas et al. [57] that found in his work that higher tool speeds led the 'onion rings' to vanish. As exposed briefly in previous chapters such features are commonly observed in FSW cross-sections and are thought to be intimately related with the material extrusion nature during the welding process.

4.1.2.3 Microstructure analysis

As seen in the first part of this document the different macro-morphologies, SZ, TMAZ and HAZ, are intrinsically related with different microstructures likely to be discovered in higher amplifications. Below are presented the microstructures possible to be observed in two very different welds, FSW-PA-LB-1851 and FSW-PA-LB-1867, corresponding to a good and poor material mixture welds respectively.

In Fig. 4.1.10 are exposed the different microstructures present in the FSW-PA-LB-1851 successful weld; as expected, three very distinctive microstructures were observed; (A) base material/HAZ where significant sized and elongated grains were present, (B) corresponding to the stir zone (nugget region) where the original microstructure was refined due to the severe deformation and relatively high temperatures produced during the welding process resulting in equiaxed small grains and finally (C) relative to the TMAZ on the advancing side where it is obvious to notice an upward grain rotation toward the tool; as previously exposed this region is characterized by grains undergoing plastic deformation but not recrystallization. In Fig. 4.1.10(D) is shown a detail of the transition between SZ and TMAZ on the bottom region of the weld (AS); a closer look reveals a change in the grain rotation from an upward direction to downward direction close to the bottom surface.

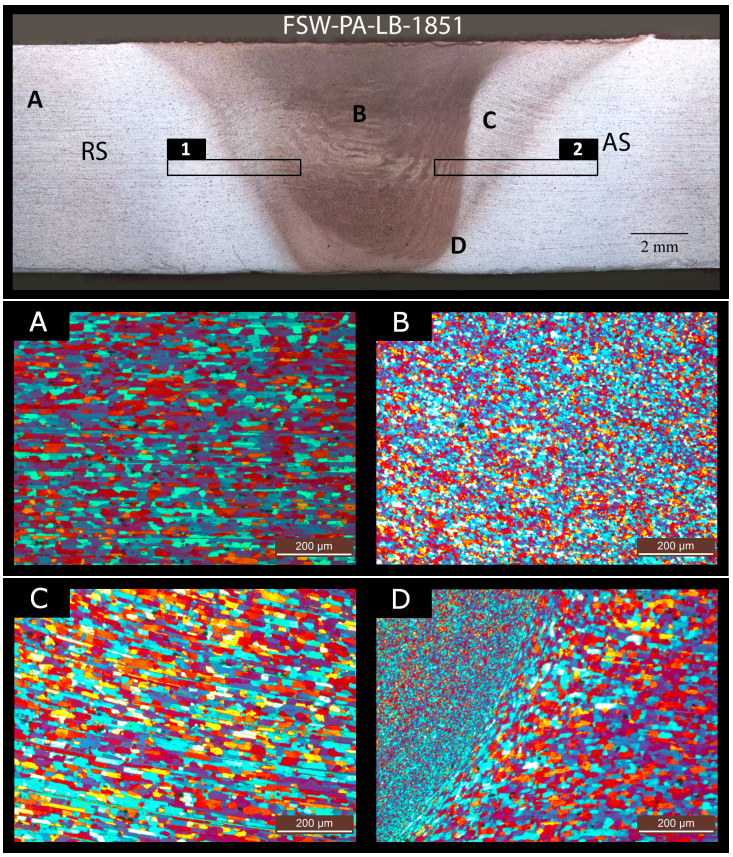

Figure 4.1.10: Micro-features of the FSW-PA-LB-1851 weld.

As previously mentioned there is a significant difference between sides of the welding process relatively

to SZ/TMAZ transition. Due to the material extrusion nature a more defined and straight line is obtained on the advancing side of the process than on the retreating side. Fig. 4.1.11 presents the grain structures boundaries for both the retreating and advancing sides (see. Fig. 4.1.10). In contrast to what happens in Fig. 4.1.11(2) no defined border between SZ/TMAZ is possible to de observed in Fig. 4.1.11(1).

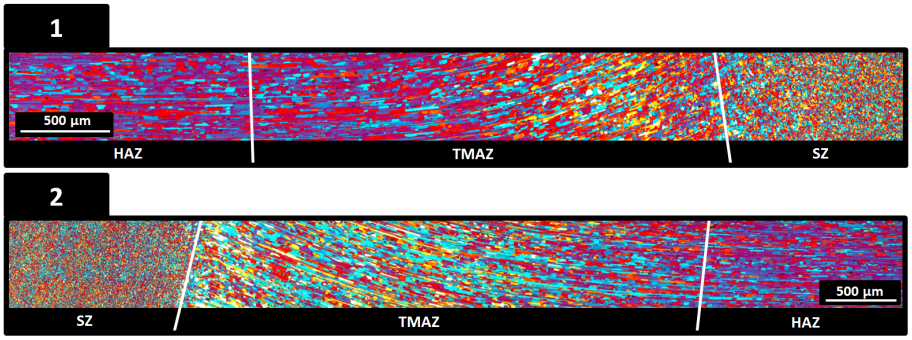

Figure 4.1.11: Cross-sectional microstructures boundaries. 1 (RS), 2 (AS).

In Fig. 4.1.12 are revealed some of the characteristic micro-features possible to be observed on the insufficiently stirred welds. As alluded before lack of mixture on the upper part of the weld could be detected due to significant sized volumetric defects; in Fig. 4.1.12(A) and (C) volumetric defects (voids - darker regions) are possible to be found on the SZ/TMAZ boundary. The stirred region microstructure became more homogeneous as it nears the bottom surface; although still with some visible defects Fig. 4.1.12(B) already presents a small and equiaxed grain.

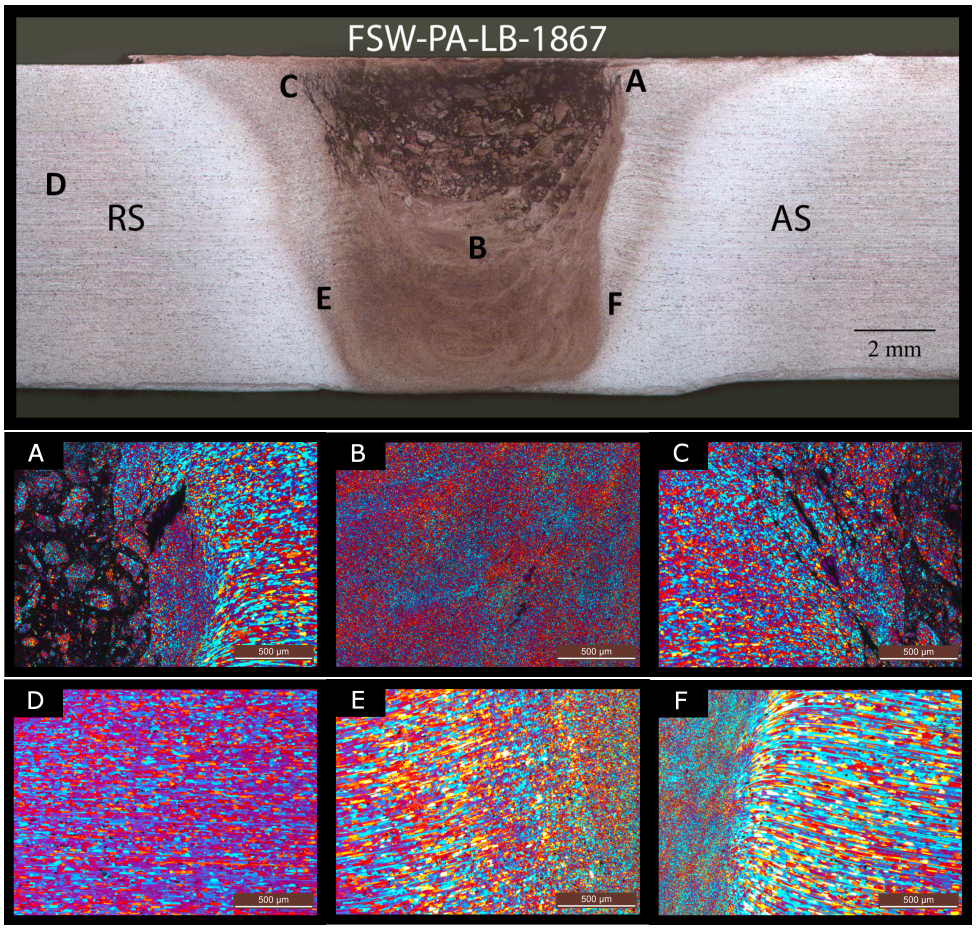

Figure 4.1.12: Micro-features relative to FSW-PA-LB-1867 weld.

4.1.3 Microhardness test

In the Tab. 4.4 are presented the results of the microhardness assessment. The minimum hardness value for each weld resulted from an average of the five lowest hardness values that could be found on either the top or bottom microhardness indentation lines. In the rightmost column is presented the hardness efficiency in relation to the base material hardness value for the long transverse direction (LTD), 158.5 HV.

Designation FSW-PA-LB	**Welding speed mm/s**	**Rot. speed rpm**	**Load (Z) kN**	**Min. Hardness HV**	**BM - 158.5 HV (%)**
1846	6	800	25	122.0 ± 2.6	77.0
1851	5	700	25	127.1 ± 2.5	80.2
1860	5	700	30	124.5 ± 1.3	78.5
1861	6	800	30	127.0 ± 2.2	80.1
1862	7	900	30	131.7 ± 6.2	83.1
1864	5	700	20	120.7 ± 5.4	76.2
1865	6	800	20	116.0 ± 4.0	73.2
1866	7	900	20	-	-
1867	8	1000	20	-	-
1868	7	900	25	-	-
1869	8	1000	25	-	-
1870	8	1000	30	132.1 ± 3.5	83.3

Table 4.4: Hardness assessment results for single-sided FSW.

A brief glance of Tab. 4.4 allows to verify that a significant number of those twelve welds presented an average minimum hardness value very close of just above the 80% of that of base material being, the efficiency goal, regarding the hardness assessment substantially achieved.

Below are presented the hardness profiles of two different welds, one corresponding to complete mixture and homogeneous structure and other where defects and lack of material mixture were found. The welds that, on the cross-section examination, revealed a homogeneous structure and a complete material mixture presented, the already expected, characteristic 'W' hardness profile shape along the indention lines. Below, in Fig. 4.1.13 is shown an example, for the weld FSW-PA-LB-1860, of the hardness profiles for both the top and bottom indentation lines.

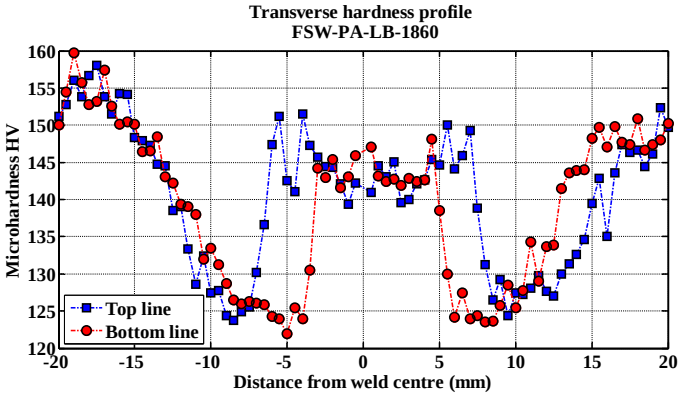

Figure 4.1.13: Hardness profiles of the weld FSW-PA-LB-1860.

As expected the hardness values dropped to its minimum on the HAZ zone, increasing again in the stir zone where the temperatures reached during the welding process led to dissolution and a new natural

aging. It is worth to notice that the top line reveals a wider hardness plateau at the centre than the bottom hardness line something, naturally, intimately related with the inverted conical-shaped SZ.

For the case of those welds that revealed significant lack of mixture on the upper region of the stir zone, such as the weld FSW-PA-LB-1867, the hardness evaluation unveiled a great fluctuation on the hardness values and an abrupt drop on the average hardness value for the top line on the centre zone (stir zone). Since good material mixture is possible to be observed on the bottom region of the macrograph the hardness profile relative to the bottom region presented the normal 'W' configuration (see Fig. 4.1.14).

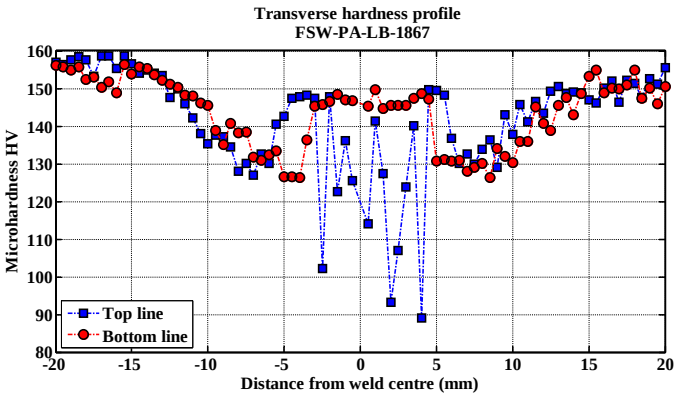

Figure 4.1.14: Hardness profiles of the weld FSW-PA-LB-1867.

4.1.3.1 Effect of the heat input

As previously mentioned the concept of heat input is the ultimate responsible for the aspect, characteristics and properties of a FSW welded workpiece. The heat input effect on the microhardness distribution is possible to be observed in Fig. 4.1.15 and Fig. 4.1.16. Although both figures have the purpose of showing the heat input effect upon the microhardness progress along the cross-sections the weld pitch and vertical load effects are shown separately. As referred in previous sections of this document, the heat input can be easily increased by either increasing the weld pitch or the vertical load or a combination of the two.

Fig. 4.1.15 presents the influence of the weld pitch variation for a given vertical load, 25 kN. The hardness maps are presented, from top to bottom, in descending order of weld pitch. Lower weld pitch leads to lower heat inputs which means less amount of heat provided to the workpiece for a given length of effective weld. As may be observed in Fig. 4.1.15 the successive decreasing of the weld pitch value and consequently the reduction of heat supplied per unit length is responsible for a significant reduction of the heat-affected zone (HAZ). A greater weld pitch leads to a greater amount of heat supplied to the joint line which consequently implies longer thermal cycles and higher temperatures during the welding process; as an immediate consequence more amount of material is subjected to significant high temperatures for longer periods of time leading to the dissolution of the precipitates which ultimately is responsible for the drop on the hardness values.

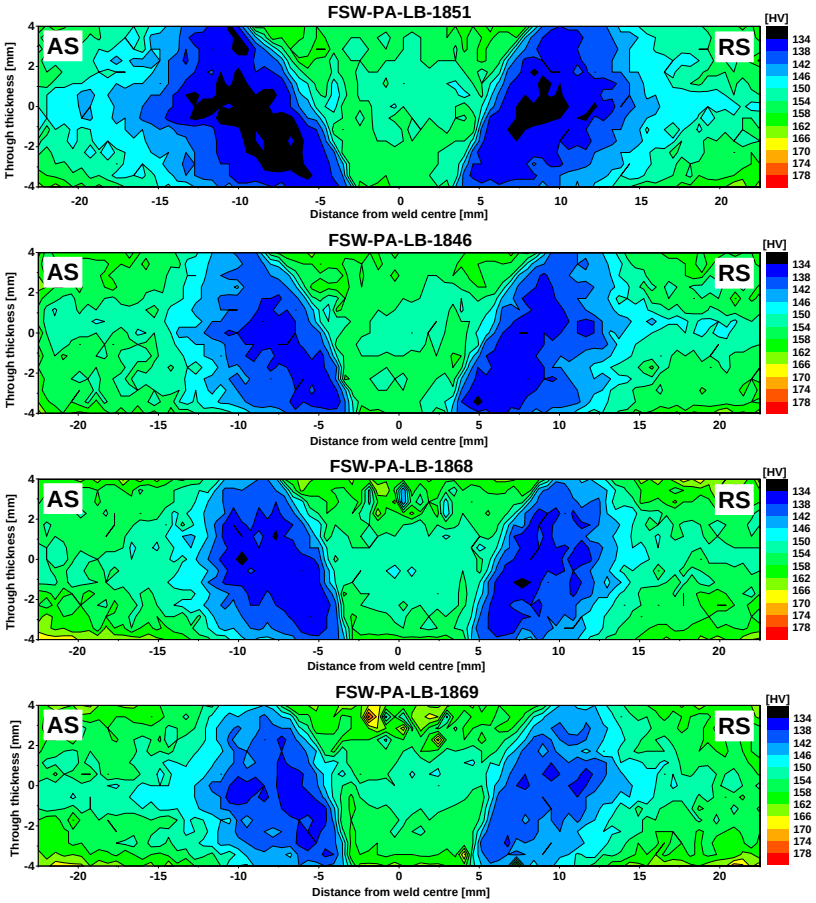

Figure 4.1.15: Influence of the weld pitch on the microhardness topography.

In spite of the two last cross-section hardness maps of Fig. 4.1.15 presenting the least area of affected material, which could lead to be considered the best welds, defects related with lack of complete mixture were identified on the metallographic analysis (section 4.1.2) something that has as a consequence the hardness values fluctuation observed in Fig. 4.1.14 and even possible to be seen on the upper part of the stir zone in Fig. 4.1.15.

Fig. 4.1.16 shows the influence of the vertical load for a constant weld pitch, 14.67 mm^{-1} (5 mm/s and 700 rpm). By this time the hardness topographies are displayed, from top to bottom, in ascending order of vertical load, 20, 25 and 30 kN respectively. As previously said, higher vertical load, induce higher values of torque which consequently increase the heat input per unit length. As it has been said for the case of the weld pitch influence, higher heat input leads to greater areas of affected material where greater drops of hardness can be observed. Since the increase of vertical load and the increase of weld pitch lead to an increase of the heat supplied to the workpiece the same conclusions given for the weld pitch case can be drawn for the vertical load case. A particular feature that can be observed in Fig. 4.1.16 is that an increase of the vertical load is intimately responsible for the widening of the stir zone, something particularly visible on the top of the cross-sections.

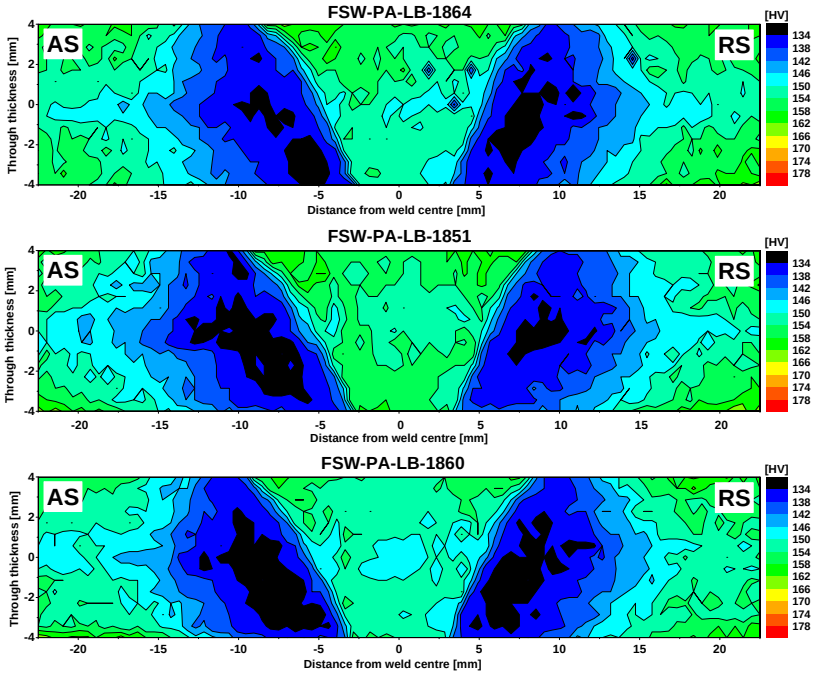

Figure 4.1.16: Influence of the vertical load on the microhardness topography.

Although an evident relation between the size of the HAZ and the amount of heat supplied per unit length was possible to be ascertained, no real tendency was possible to be drawn regarding which side, advancing or retreating, possessed greater affected area. Similar size, shape and hardness values were found in both sides of the cross-sections which indicated a good process symmetry, particularly on the thermal distribution.

4.1.4 Tensile test

In the Tab. 4.5 are presented the results obtained from the tensile tests. The percentage values represent the weld efficiency when compared with the base material values (for the RD) - 451 MPa, 507.1 MPa and 16.4% for the yield strength, ultimate strength and elongation respectively. On the rightmost column is presented the heat input for each weld.

Designation FSW-PA-LB	Weld. speed mm/s	Rot. speed rpm	Load (Z) kN	Yield S. MPa	Ultimate. S. MPa	Elongation (%)	H.I. kJ/mm
1846	6	800	25	368.7 ± 2.1 (81.8%)	415.8 ± 26 (82.0%)	1.7 ± 0.7 (10.4%)	0.56
1851	5	700	25	362.7 ± 2.5 (80.4%)	475.0 ± 2.4 (93.7%)	7.1 ± 0.4 (43.3%)	0.60
1860	5	700	30	355.3 ± 2.9 (78.8%)	467.7 ± 4.1 (92.2%)	7.4 ± 0.4 (45.1%)	0.65
1861	6	800	30	367.3 ± 3.1 (81.4%)	464.7 ± 15.3 (91.6%)	5.1 ± 2.8 (31.1%)	0.61
1862	7	900	30	366.0 ± 2.0 (81.8%)	414.0 ± 6.1 (81.6%)	1.6 ± 0.1 (9.8%)	0.56
1864	5	700	20	361.7 ± 4.0 (80.2%)	430.9 ± 20.5 (85.0%)	2.5 ± 1.3 (15.2%)	0.57
1865	6	800	20	370.0 (82.0%)	370.0 (73.0%)	0.8 ± 0.3 (4.9%)	0.51
1866	7	900	20	-	205.7 ± 16.8 (40.6%)	0.29 ± 0.0 (1.8%)	0.50
1867	8	1000	20	-	153.9 ± 0.8 (30.3%)	0.22 ± 0.0 (1.3%)	0.45
1868	7	900	25	-	353.0 ± 4.5 (69.6%)	0.58 ± 0.0 (3.5%)	0.53
1869	8	1000	25	-	297.0 ± 43.4 (58.6%)	0.45 ± 0.0 (2.7%)	0.50
1870	8	1000	30	-	281.7 ± 13.2 (55.4%)	0.41 ± 0.0 (2.5%)	0.51

Table 4.5: Tensile test results for single-sided FSW.

From a quick look at the table presented above it is possible to verify that a great range in mechanical properties values were obtained. The results appear to be in complete agreement with what was possible to assert from the metallographic and microhardness analysis; the best mechanical properties are related with the best material mixture and the best hardness properties. As shown in section 4.1.2 the quality of material mixture, which is on the basis of good hardness properties, is increased with the increasing on the amount of thermal energy supplied during the welding process and so the best mechanical properties were obtained for the highest heat inputs. In Fig. 4.1.17 and Fig. 4.1.18 are presented the relations between the heat input and the mechanical properties, ultimate strength and elongation respectively; as stated, in both cases the increase of the heat input tends to improve the properties values.

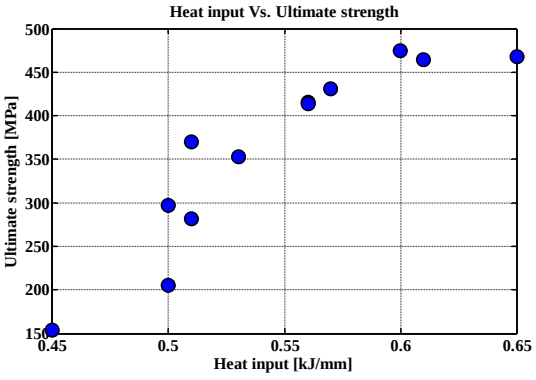

Figure 4.1.17: Heat input Vs. Ultimate Strength.

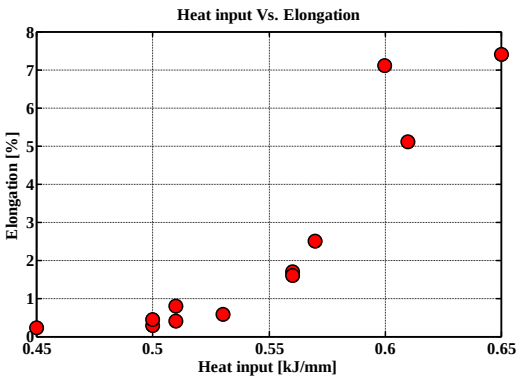

Figure 4.1.18: Heat input Vs. Elongation.

Lower values of heat input are then responsible for insufficient material mixture than in turn leads to poor mechanical properties. A weld lacking material mixture presents in its core a significant amount of volumetric defects that represent a weakened region which, for itself, explains the lower values on the mechanical properties.

The single-sided FSW process seems to be particularly severe on the elongation parameter, its highest value was 7.4% which correspond to a modest weld efficiency of 45.1%. With the exception of the elongation, which appears as the critical property, it is possible to say that substantially good results were obtained on the parameters study for the single-sided friction stir welding set; a significant number of welds, although some of them presenting very low elongation values, presented relatively high values of yield and ultimate strength with the virtual efficiency goal of 80% being mainly achieved. A couple of welds, namely, FSW-PA-LB-1851 and FSW-PA-LB-1860, which are on highest heat input range, emerge as the most successful amongst all the welds since they present the best mechanical properties; since there seemed to be no great difference between them - regarding the mechanical properties values - and since FSW-PA-LB-1851 leads to lower tool wearing it was chosen FSW-PA-LB-1851 set of parameters in detriment of those of FSW-PA-LB-1860. In this way the tool life is expected to be longer and to lead to an improvement of the productivity without compromising the mechanical properties on the performed welds.

Fig. 4.1.19 presents stress-strain curves of a number of welds in comparison with the base material response. The average Young Modulus value was 71.1 GPa.

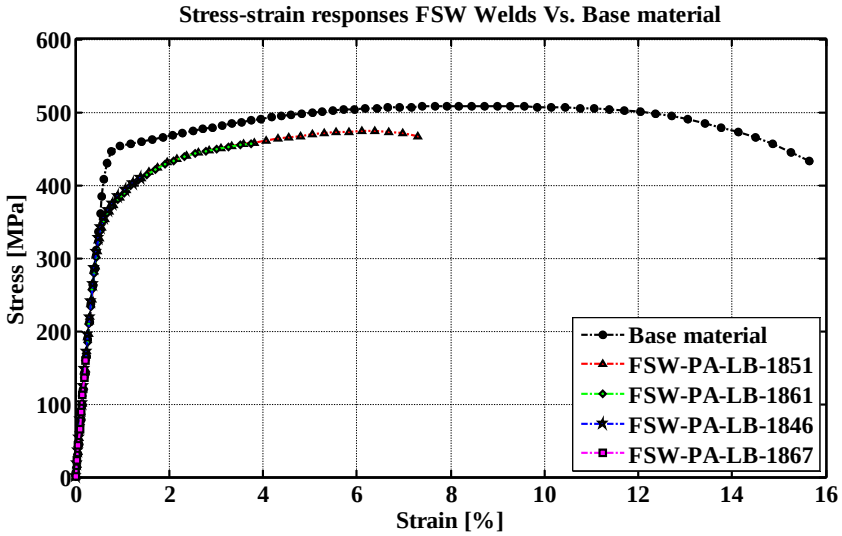

Figure 4.1.19: Tensile curves of some welds in comparison to base material's.

4.1.5 Temperature measurements

As previously stated in this document temperature measurements were conducted for the best set of welding parameters, which, as seen in 4.1.4, were the welding parameters corresponding to FSW-PA-LB-1851 (namely 5 mm/s, 700 rpm and 25 kN of welding and rotational speed and vertical load respectively). In Fig. 4.1.20 are presented, graphically, the results of the temperature measurements undertaken for the later welding parameters (corresponding to the HZG FSW-PA-LB-1886 weld). Expectedly, being a linear and stable process, similar thermal responses were detected in the three main measuring regions. During the welding process and for each region (composed by six measuring points/thermocouples) the thermal cycle observed was considerably short; peak temperatures were reached very quickly (20 to 30 seconds)

followed by a substantially fast cooling with temperatures dropping down the 50°C in approximately 1:00 to 1:10 minutes leading to a global thermal cycle of approximately one and a half minute (1:30 minutes). In the Tab. 4.6 are exposed the maximum temperatures reached for each thermocouple during the welding process.

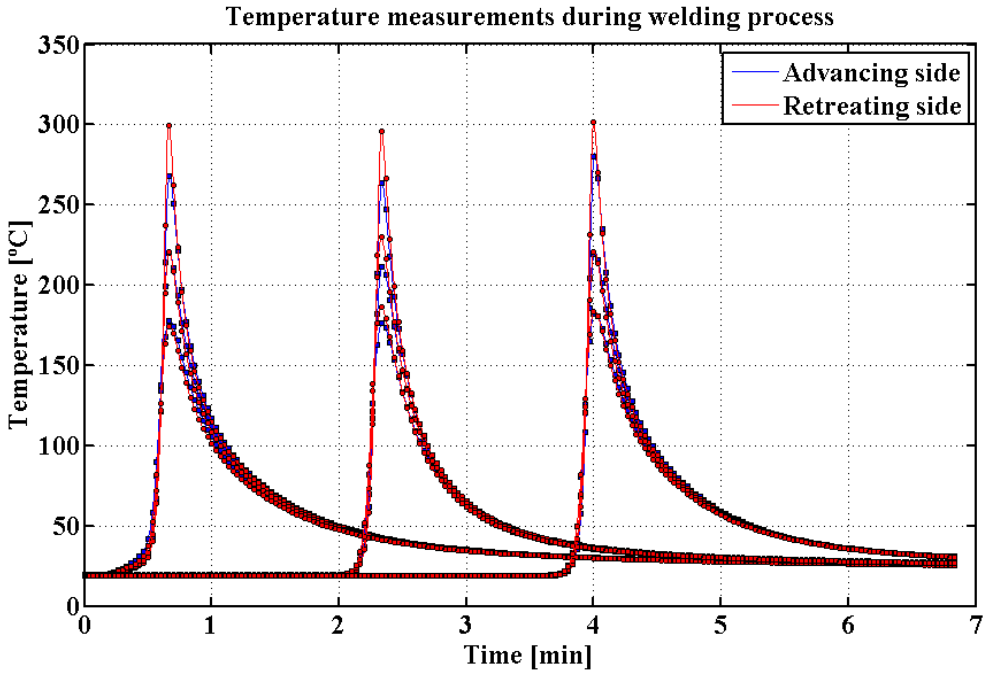

Figure 4.1.20: Temperature measurements during FSW-PA-LB-1886 weld.

Through a brief glance at both Fig. 4.1.20 and Tab. 4.6 it is possible to notice that the absolute maximum temperature reached during the process was 301.5°C for the case of the thermocouple 24 and that, for the case of the thermocouples nearest positioned to the joint line (12 mm), higher temperatures were detected on the retreating side of the welding process (thermocouples positioning can be seen in section 3.1.5).

Region	Side	Thermocouple position	Max. Temperature [°C]
1	Advancing side	9	268.6
		10	220.4
		11	178.2
	Retreating side	12	300.1
		13	220.9
		14	174.6
2	Advancing side	15	264.4
		16	212.4
		17	176.5
	Retreating side	18	295.7
		19	229.9
		20	186.2
3	Advancing side	21	282.4
		22	220.9
		23	183.0
	Retreating side	24	301.5
		25	221.2
		26	184.0

Table 4.6: Peak temperature for all measuring points.

Tab. 4.7 shows the comparison of peak temperatures of the thermocouples nearest placed to the joint line. For a given region, retreating side thermocouples recorded slightly higher temperatures than those placed on the advancing side; a global difference of 27.2°C, corresponding to 9.1%, between side temperatures could be established. Similar results were obtained by Fu at al. [58] and Brown et al. [37] in their works about 7050 aluminium alloy.

Region	Side	Thermocouple	Temperature [°C]	Difference [%]
1	Advancing side	9	268.6	10.5
	Retreating side	12	300.1	
2	Advancing side	15	264.4	10.6
	Retreating side	18	295.7	
3	Advancing side	21	282.4	6.3
	Retreating side	24	301.5	

Table 4.7: Temperatures recorded for thermocouples nearest the joint line; AS and RS comparison.

As the measurement positions moved away from the joint line, to respectively 17 and 22 mm, peak temperatures and differences between temperatures registered on either side tended to drop significantly or even to be eliminated for the later case. Fig. 4.1.21 shows in greater detail the temperature progress in one particular region (region 1).

Located ideally at 1 mm from the bottom surface of the joint line a temperature of 294.8±15.0°C was registered on the eight thermocouples located on the backing bar; that temperature was very similar to those obtained for the thermocouples closest placed to the joint line (namely 9, 12, 15, 18, 21, 24, see 3.1.5). It is important to notice that peak temperatures values are quite sensible to the exact position in which the thermocouple was allocated; geometrical accuracy of the measuring point position, depth of the drilled hole and adequate placement of the thermocouple into de drilled hole itself are all features that might, naturally, influence the results.

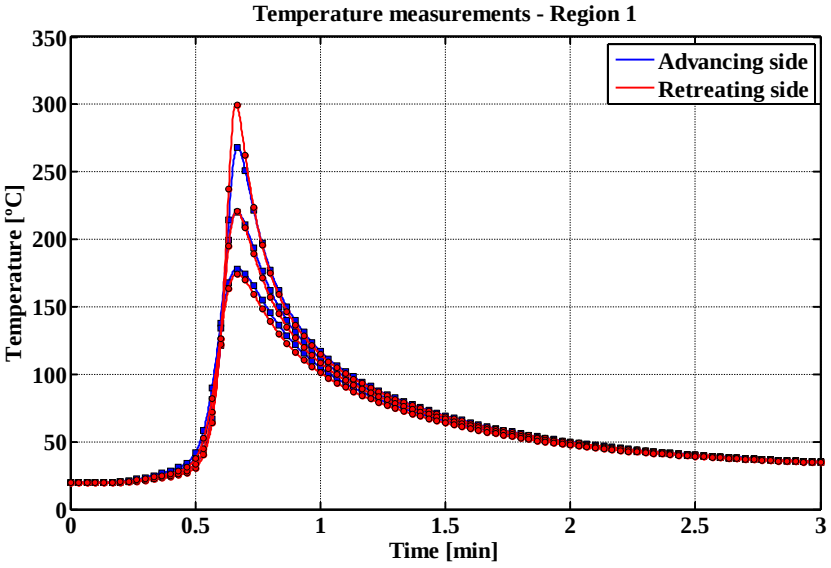

Figure 4.1.21: Temperature response to welding progress on region 1.

Below the temperature response registered on the tool during and immediately after the welding process is presented. On the welding process of a complete set of plates (which took approximately 4 minutes) the tool temperature was gradually increased from room temperature to its maximum of 375.8°C. After an initial stage where its temperature was successively increased it tended to stabilize

on a plateau with an average temperature of 365 to 370°C. Although these temperatures were naturally superior to those registered on the workpiece they represent the average temperatures obtained on the tool shoulder (roughly 2 to 3 mm from the workpiece plates) and not the maximum temperature throughout the process which happens on the core of the stir zone close to the rotational probe. Once the process was complete and the tool removed from the workpiece its temperature dropped abruptly. Notice that at Fig. 4.1.22 temperature origin starts at 150°C since the pyrometer used had its minimum detectable temperature at 160°C.

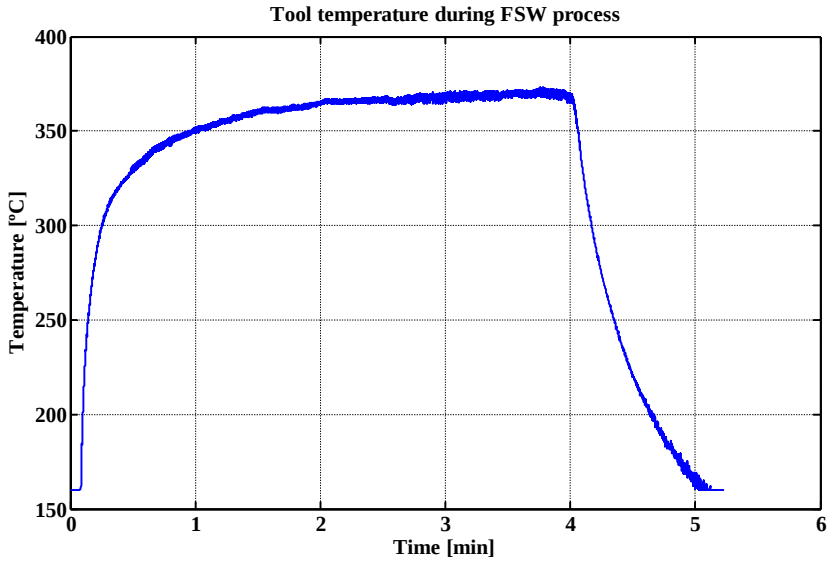

Figure 4.1.22: Temperature progress on the welding tool during FSW process.

4.1.6 Fracture analysis

With exception of the FSW-PA-LB-1851 and FSW-PA-LB-1860 cases [1], the tensile fracture occurred either through the stir zone or along the retreating side of SZ/TMAZ boundary. On the 1851 and 1860 tensile specimens the fracture position was located, without exception, at the HAZ of the retreating side. Fig. 4.1.23 and Fig. 4.1.24 present the cross-sectional morphology for both characteristic fracture cases.

Figure 4.1.23: Macro-morphology of the FSW-PA-LB-1851 weld fracture.

[1] as well one specimen of the FSW-PA-LB-1861 weld

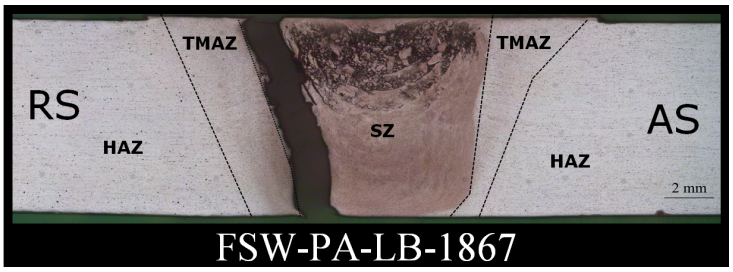

Figure 4.1.24: Macro-morphology of FSW-PA-LB-1867 weld fracture.

For the FSW-PA-LB-1851 and FSW-PA-LB-1860 type of fracture, Fig. 4.1.23, the distance of the fracture region to the central line of the weld seam corresponds to the position with the lowest hardness. The transverse tensile specimens consist of a number of different microstructural regions which seems to allow deformation to localize at the weakest region, which is the HAZ for the precipitation hardened aluminium alloys. For these welds evident necking could be observed at the HAZ on the retreating side (Fig. 4.1.23) which indicate a significant resistance to failure and a relatively ductile fracture resulting ultimately in best mechanical properties. Slightly higher temperatures registered on the retreating side could be on the basis of the side failure preference; as previously exposed a real tendency of higher temperatures on the retreating side of the process was observed which may result in slightly lower mechanical properties values leading to necking and consequently failure in that particular region. This kind of preference was also observed in previous works [37]. Although a certain tendency of failure on the retreating side was ascertained a very different kind of failure was observed on all the rest of the welds, Fig. 4.1.24. The failure occurred within the shoulder influence region and essential through the boundary SZ/TMAZ or even through the stir zone. No necking was observed on either side of the cross-sections resulting in very low elongation values. Inadequate material intermixing produced at low heat inputs was the cause for the low mechanical strength values.

Four set of parameters, obtained for a constant vertical load and for different weld pitches were subjected to a deeper fracture study. Fig. 4.1.25, below, presents the real fracture appearance of the tensile specimens by decreasing order of weld pitch. As mentioned above, the retreating side seems to be the preferable side of failure even for those welds in which failure occurred within the shoulder trailing region, (b), (c) and (d). The differences in the failure features of the four joints include the distance and manner of crack propagation. As seen before, with exception of the case of FSW-PA-LB-1851 weld in which failure occurred on the HAZ at the retreating side, the crack propagated through or on the border of the stir zone; Although (b), (c) and (d) presented this kind of failure there seems to be an increase on the resistance to crack propagation as the weld pitch and heat input are successively increased. For the weld presented in (d), for instance, the crack seems to occur in simple shearing mode which implies very poor elongation; for the (b) weld the crack propagates in a kind of 'Z' shaped manner which indicates increased resistance to crack propagation even though the fracture also occurs in shearing mode. Consequently, the elongation of the weld joint may be slightly increased.

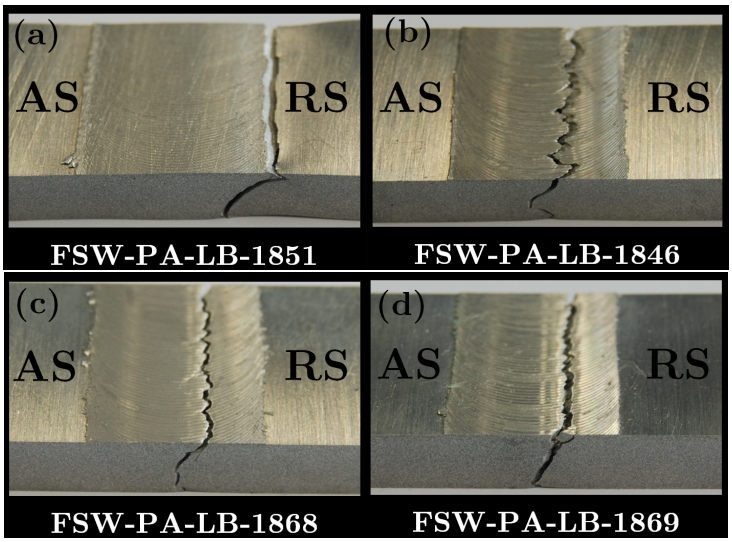

Figure 4.1.25: Cross-sectional fracture appearance resulting of the tensile test.

Further observations of the fracture surface of the tensile specimens are presented from Fig. 4.1.26 to Fig. 4.1.28. Analysis under SEM examination of the fractured surfaces of the 1851 weld revealed the presence of large amount of dimples (Fig. 4.1.26) indicating the overload and ductile nature of the fracture. The overall appearance of fracture and the macro-features of the 1851 weld fracture were homogeneously distributed throughout the fracture surface. As the analysis was expanded to successively lower weld pitch values fewer and fewer ductile features (dimples) and increasingly number of defects could be detected.

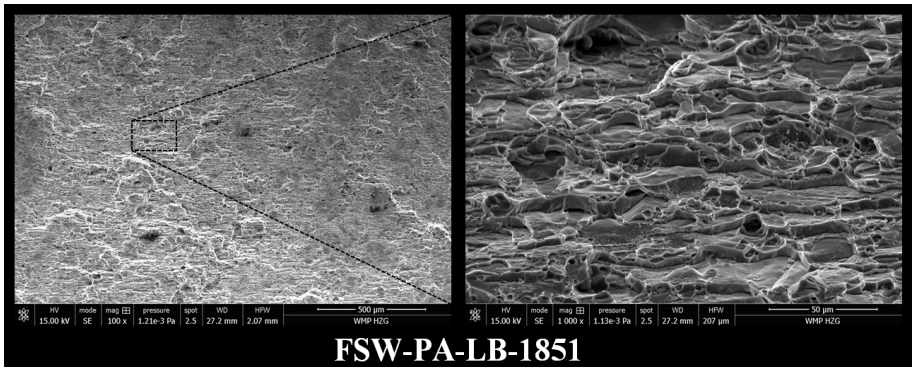

Figure 4.1.26: SEM micrographs of fractured surface of the FSW-PA-LB-1851 weld.

Fig. 4.1.27 corresponding to the second highest heat input of the four welds in analysis presented a relatively homogeneous and smooth fracture having, however, tendency to exhibit volumetric defects (voids) and consequently a rugged band region on the upper part of the fracture surface (close to the tool).

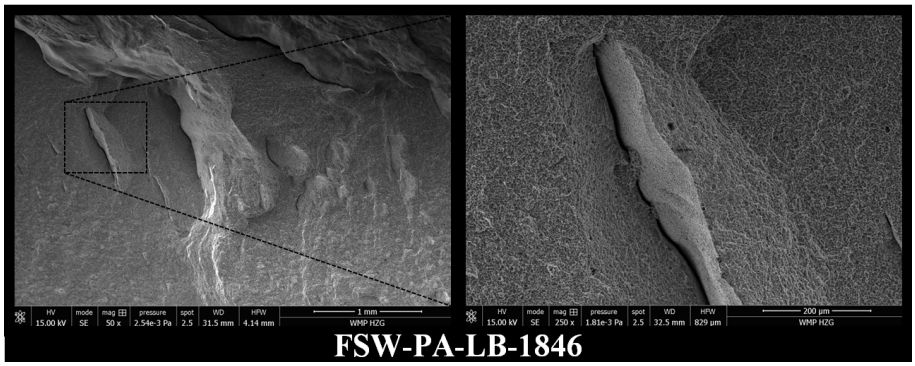

Figure 4.1.27: SEM micrographs of fractured surface of the FSW-PA-LB-1846 weld.

FSW-PA-LB-1868 and FSW-PA-LB-1869 welds presented a very similar fracture surface. As seen in section 4.1.2, significant amount of defects and lack of material intermixing was detected in both welds where volumetric defects of significant size could be observed. Similar macro-features where found for both surfaces (two figures on the left in Fig. 4.1.28) which consisted of equally spaced peak and valleys structures resulting in an overall ragged surface where which valley could or seemed to end or be originated by a volumetric defect. Such features may be and indeed they seem to be, intimately related with the extrusion nature of the process and in particular with the relation rotational/welding speed of the tool (weld pitch). This evidence suggests that these voids are the source of failure through the stir zone observed for lower heat input welds as a result of lower weld pitches. Higher amplifications revealed non or very few small sized dimples which seem to support the brittle fracture originated by volumetric defects hypothesis.

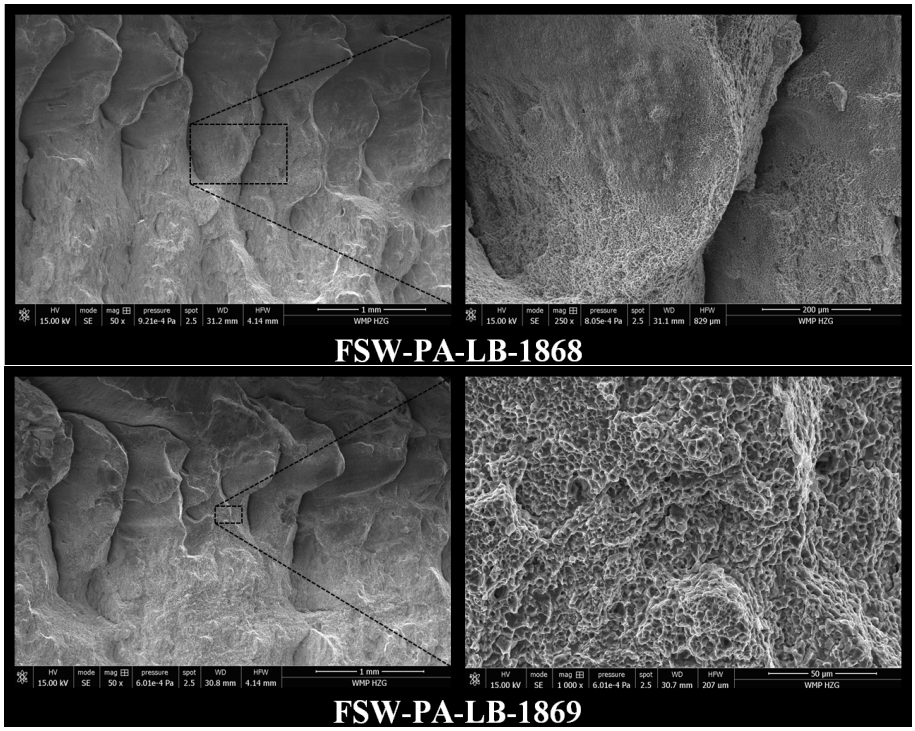

Figure 4.1.28: SEM micrographs of fractured surfaces of the FSW-PA-LB-1868/1869 welds.

4.1.7 Distortion assessment

Distortion measurements were performed using PONTOS optical measurement system; a number of black and white markers were placed randomly onto the overall surface of sets of plates which were

then welded using the best parameters combination found for the single-sided FSW (FSW-PA-LB-1851 welding parameters). Fig. 4.1.29 presents an example of the markers distribution, 182 in total, over an entire area of a set of plates (HZG designation FSW-PA-LB-1903). The markers on the upper region, are referent to the plate on advancing side whereas on the bottom region is referent to the plate of the retreating side. The middle region, not provided with markers, represents the welding joint line. The markers distribution on Fig. 4.1.29 are presented as seen from the camera visual field - top view; the weld was performed from the left side of the figure (Starting Point - SP) to the right (Finish Point - FP) following the welding direction (WD).

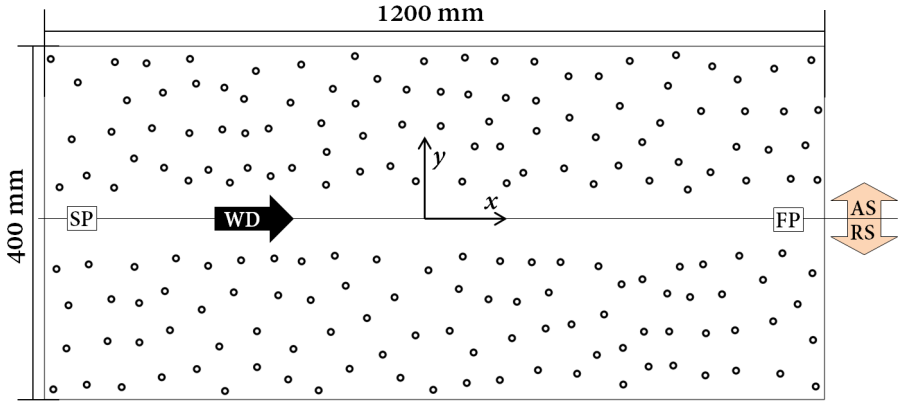

Figure 4.1.29: Representation of point distribution for distortion measurement.

In Fig. 4.1.30 and Fig. 4.1.31 are presented, in detail, top views of part of a set of plates; it is possible to verify a perfect relation between the real markers distribution - on the real specimen, already welded, Fig.4.1.30 - and the representation using the PONTOS data set, Fig.4.1.31.

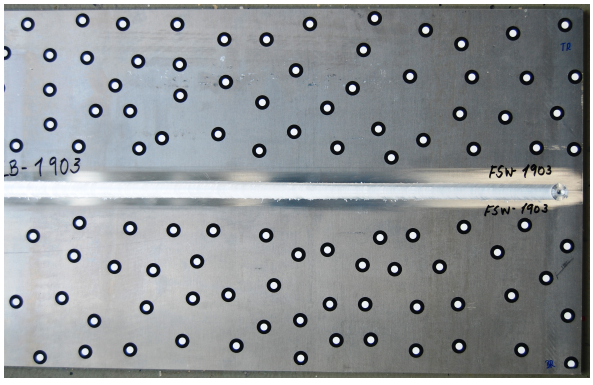

Figure 4.1.30: Markers on the real specimen (HZG).

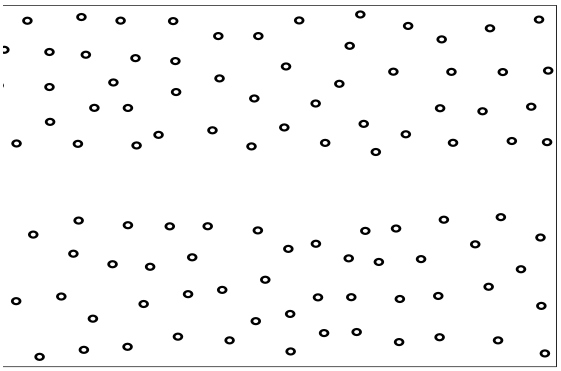

Figure 4.1.31: Representation using PONTOS data.

From Fig. 4.1.32 to Fig. 4.1.34 are exhibited, in form of distortion maps, the characteristic distortion assessment using PONTOS software data for the three spacial directions, x, y and z respectively (FSW-PA-LB-1903); the coordinate system used is represented in Fig. 4.1.29 with z axis being normal to the page plane and pointing in the reader's direction. The following figures shows the distortion progress in millimetres with the markers distribution representation presented superimposed it.

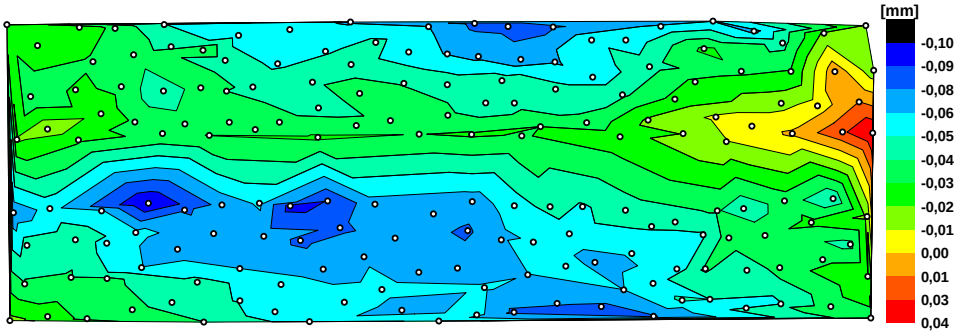

Figure 4.1.32: Distortion map relative to the x direction.

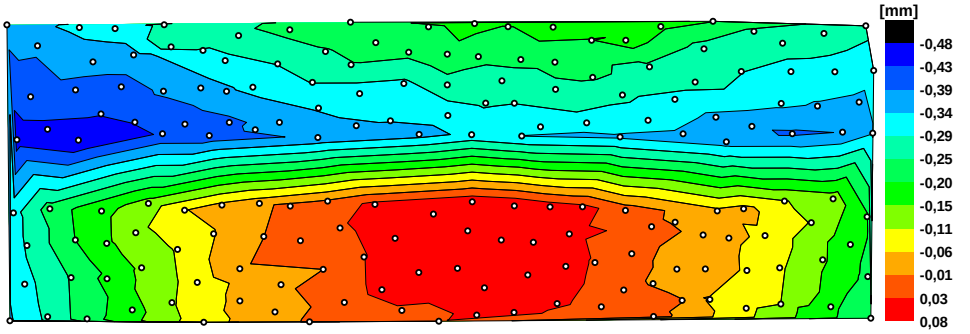

Figure 4.1.33: Distortion map relative to the y direction.

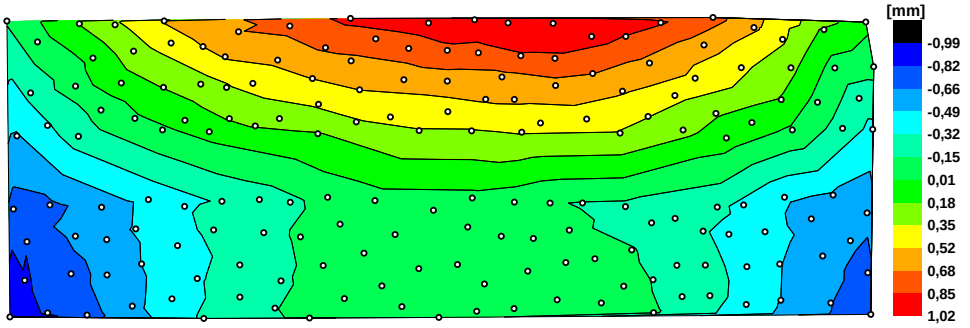

Figure 4.1.34: Distortion map relative to the z direction (normal to the page plane).

An immediate conclusion possible to draw when looking at the distortion maps presented above is that significantly low or even negligible values of distortion were obtained for the x and y directions. The maximum absolute value of distortion for the x direction was 0.1 mm; it is important to notice that this value is inserted on the measuring error band and should therefore be neglected. Insignificant values of distortion on the x direction means that the welding process had no real influence on the the axial direction even if significant axial residual stresses could be found. Although greater than those of x direction, the distortion values relative to the y direction are still, considerable low (see Fig. 4.1.33).

Fig. 4.1.34 presents the displacement distribution for the z direction, the higher values of distortion amongst the three spacial directions. It is important to notice that the distortion maps represents the displacements of each individual marker relatively to its original position on the measuring backing set-up before the welding process and that means that the values, particularly the signal of the values, are relative and intrinsically dependent on how the plates were placed on the measuring set-up. A zero or very

low value of displacement may, therefore, signify that the plate was either placed on the same measuring position or that, indeed, did not undergo distortion. The displacements values should then be considered as a whole and not referent to real punctual displacement. In order to lead a better interpretation and overcome possible misinterpretations of the the real distortion of the plates a schematic 3D representation of the distortions involved are shown in Fig. 4.1.35.

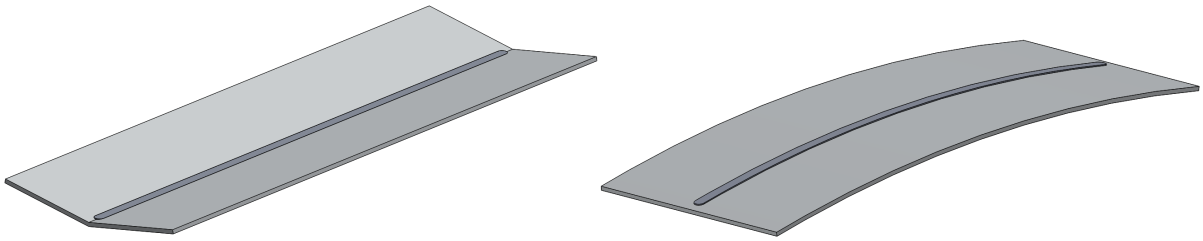

Figure 4.1.35: Schematic representation of the two kinds distortion after FSW process.

As may be observed, the displacement distribution shown in Fig. 4.1.34 results from a combination of two kinds of distortion. The welding process is responsible for leading the plates to buckle relatively to its cross section centreline resulting on a very small lifting (approximately 1 mm) of the centre when supported by the edges (short direction, y) on a flat surface and to buckle lengthwise along the joint line resulting on a visually imperceptible lifting up of the edges, 0.5 mm (long direction, x) resulting in wide V-shaped feature cross-section. The combination of the two kinds of distortion results in distortion configuration represented in Fig. 4.1.36

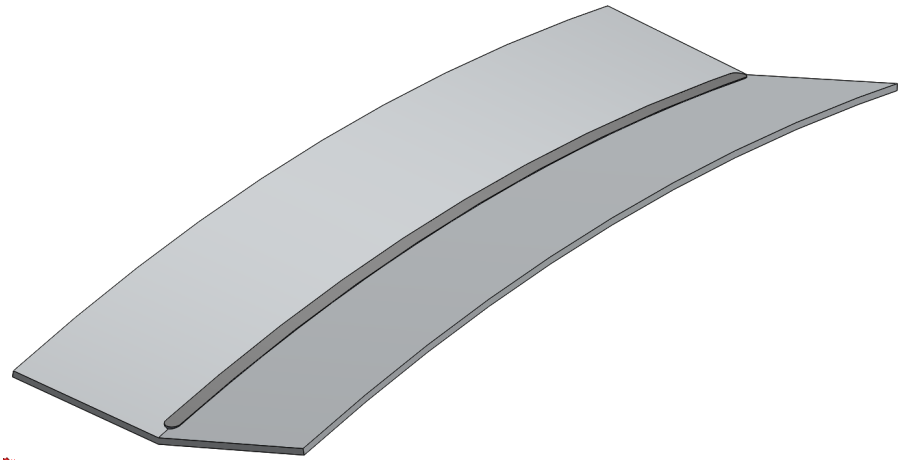

Figure 4.1.36: Schematic representation of the overall distortion after FSW process.

In Fig. 4.1.37 is presented the overall distortion map; since significantly higher displacement values were found for the z direction, the overall distortion map present very similar features to those of Fig. 4.1.34.

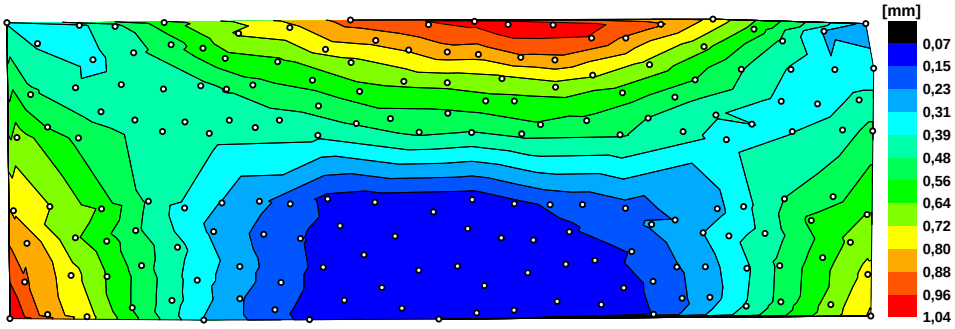

Figure 4.1.37: Distortion map relative to the global distortion xyz (absolute values).

From the distortion assessment was possible to ascertain that low values of displacement were found as a consequence of the welding process. From what was possible to verify the set the plates had tendency to reveal higher displacement values on the outer plate edges, something physically expected. Although the clamping system and the particular way in which the set of plates were loosened may had some influence over the overall distortion, no definitive conclusion may be drawn on why the plates suffered distortion in such particular shape.

4.2 DS-FSW

In this section the results obtained for the DS-FSW parameters study will be presented. Since the experimental approach performed on the DS-FSW study was very similar to that made for the single-sided FSW a similar results presentation structure was followed.

Below are presented, in form of table, the welding parameters and the collected data for the DS-FSW parameters study. The horizontal load (X) and torque values are the result of the average of both passes values whereas the heat input results from the sum on the heat input of both, A and B passes. For all welds a vertical load of 15 kN and a probe length of 4 mm were used.

Designation DS-FSW-PA-LB	**Welding speed mm/s**	**Rot. speed rpm**	**Weld pitch mm^{-1}**	**Load (X) kN**	**Torque Nm**	**Heat input kJ/mm**
1852	5	800	16.76	3.21	20.30	0.68
1853	5	700	14.66	3.55	22.72	0.67
1854	6	800	13.96	3.90	21.24	0.59
1855	7	900	13.46	4.41	19.71	0.53
1856	8	1000	13.09	4.70	19.29	0.50
1857	9	1100	12.80	4.70	17.84	0.46
1872	10	1200	12.57	4.64	18.80	0.47

Table 4.8: Welding parameters and collected weld data for the DS-FSW parameters study.

Such as for the case of the conventional FSW all the welds performed for the DS-FSW presented good surface finish.

4.2.1 Metallographic analysis

Below, Fig. 4.2.1 and Fig. 4.2.2, are presented the typical appearance of a cross-section of a weld performed by DS-FSW. Two passes in which approximately half of the thickness is welded at a time

result in an overall two mirrored basin-like shape stir zone united at sensibly half of the thickness. Unlike the conventional FSW all welds revealed complete material intermixing.

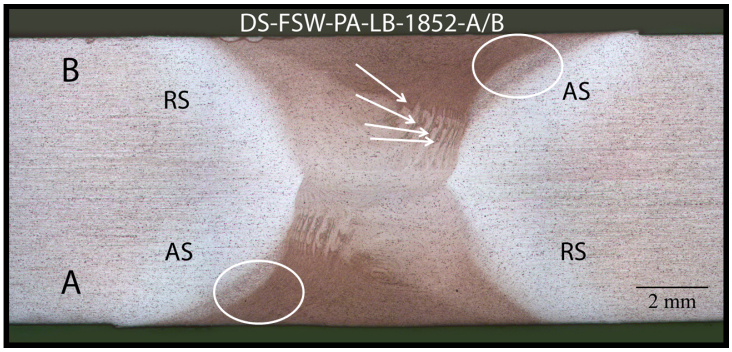

Figure 4.2.1: Characteristic macrograph of the double-sided welds (5mm/s, 800rpm).

The significant increase on the welding speed from Fig. 4.2.1 to Fig. 4.2.2 was responsible for the narrowing of the stir zone and for the reduction of the thermal effect of the tool shoulder revealed by the sharp angle at both advancing sides (white circumferences at Fig. 4.2.2). 'Onion rings' features were possible to be detected in all welds at the advancing side for both passes although easier detected for lower welding speed cases, Fig. 4.2.1.

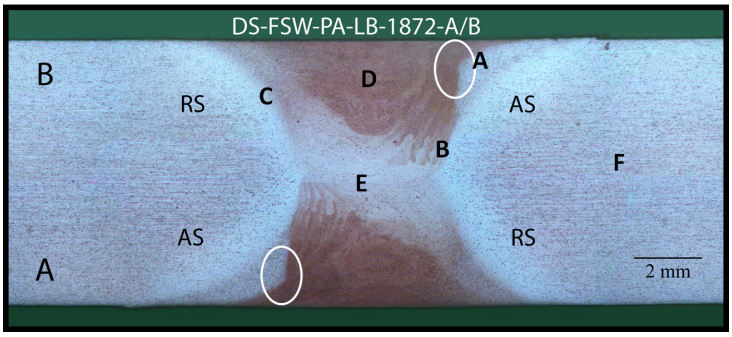

Figure 4.2.2: Macrograph of a DS-FSW (10mm/s, 1200rpm).

Fig. 4.2.3 exposes a number of micro-features characteristics of the double-side welds; since DS-FSW is the result of the two FSW passes the same three distinctive microstructures, presented in 4.1.2.3, could be observed - Base material/HAZ, stir zone (SZ) and TMAZ. These micro-features, as previously exposed are the inevitable consequence of the friction stir welding process. In Fig. 4.2.3(B) are indicated with white arrows the 'onion ring' features which present significant difference on the grain characteristic from that of in-between regions. Fig. 4.2.3(E), representing the half thickness region, shows a structure composed by small sized different orientated grains where the second pass (B) presents, naturally, greater influence on the final structure.

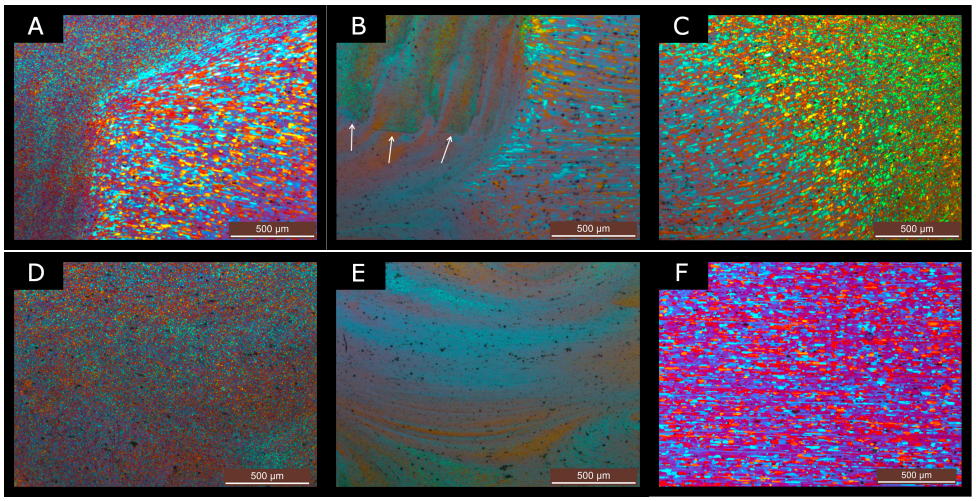

Figure 4.2.3: Micro-features relative to DS-FSW-PA-LB-1872 (see Fig. 4.2.2)

4.2.2 Microhardness test

Tab. 4.9 presents the results of the microhardness assessment for the double-sided friction stir welds. As for the case of conventional FSW the minimum hardness values presented below resulted from the average of the hardness values obtained for the lower hardness region.

Designation DS-FSW-PA-LB	**Welding speed mm/s**	**Rot. speed rpm**	**Min. Hardness HV**	**BM - 158.5 HV (%)**
1852	5	800	131.7 ± 3.0	83.1
1853	5	700	125.7 ± 1.0	79.3
1854	6	800	132.3 ± 1.9	83.5
1855	7	900	129.0 ± 0.8	81.4
1856	8	1000	133.9 ± 2.3	84.5
1857	9	1100	137.4 ± 2.5	86.7
1872	10	1200	136.0 ± 2.0	85.8

Table 4.9: Hardness assessment results for double-sided FSW.

In general, higher values of hardness efficiency were obtained for the DS-FSW process variant than for the conventional FSW (see Tab. 4.4); a variation on efficiency values from 79.3 (1853) up to 86.7% (1857) ultimately means the double stir welding process had relatively low implications on the degradation of the original base material hardness. Such as for the single-sided FSW the virtual hardness efficiency goal of 80% was then achieved.

The typical hardness profiles obtained for the double-sided welds are presented in Fig. 4.2.4. Both the top and bottom lines presented the already expected 'W' configuration with the minimum hardness values at the HAZ as result of the dissolution of the precipitates. The lower overall hardness values were detected in the middle through thickness region which could or not present a plateau at the centre corresponding to the stir zone. This behaviour is easily explained since the half thickness region experiences twice the thermal welding cycle being the last pass, in particular, responsible for the creation of a low-hardness zone in the weld centre as a consequence of its HAZ below the probe influence.

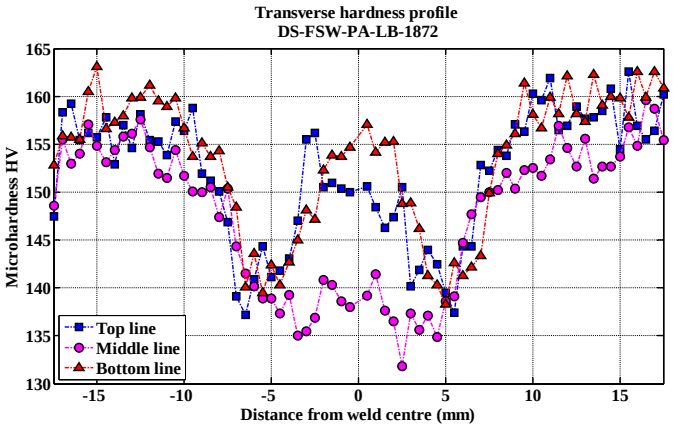

Figure 4.2.4: Hardness profiles of the double-sided 1872 weld.

4.2.2.1 Heat input effect

In Fig. 4.2.5 are exhibited three hardness topographies corresponding to three different double-sided welds. The welds are ordered, from top to bottom by descending value of heat input; since all welds were performed for a constant vertical load of 15 kN the successively decrease of the heat input is a consequence of the subsequent successive decrease of the weld pitch. As presented for the single-sided process the successive decrease of the weld pitch value leads to a reduction on the amount of heat supplied per unit of produced weld which consequently implies lower temperatures reached during the welding process which ultimately means that less and less material is subjected to sufficiently high temperatures to lead to the dissolution of the precipitates and consequently drop on the hardness.

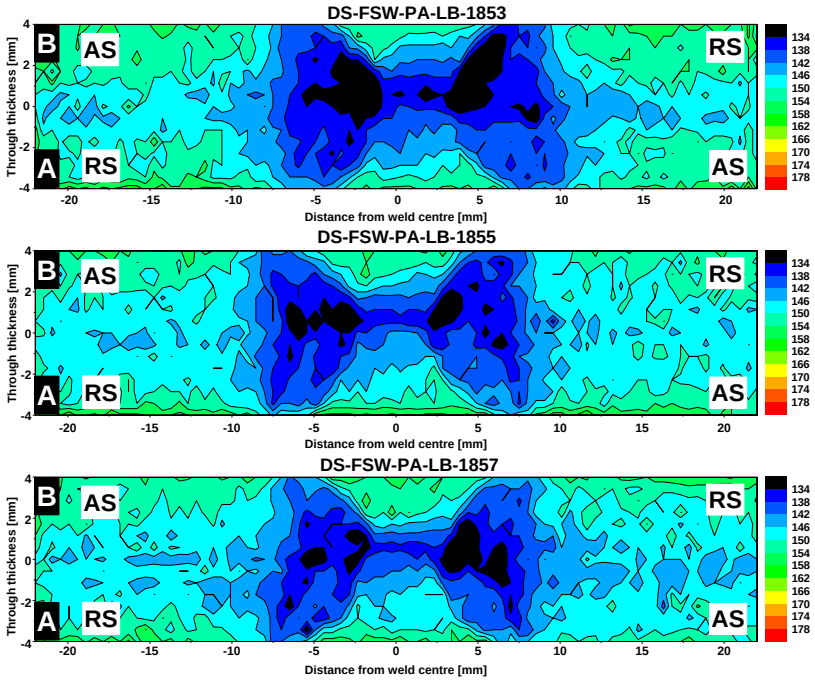

Figure 4.2.5: Influence of the heat input on the hardness distribution on a cross-section surface.

As previously referred half way through the plates thickness there is a low hardness region which approximately represents the division between passes. No conclusion was possible to be drawn regarding which side, for each pass, was more affected by the welding process in respect to the hardness response.

4.2.3 Tensile test

Tab. 4.10 presents the mechanical properties values achieved during the tensile test procedure for the double-sided welds. On the rightmost column are presented the global heat input values for each weld.

Designation DS-FSW-PA-LB	**Welding speed mm/s**	**Rot. speed rpm**	**Yield S. MPa**	**Ultimate S. MPa**	**Elongation (%)**	**Heat input kJ/mm**
1852	5	800	380.3 ± 2.9 (84.3%)	481.9 ± 2.8 (95.0%)	8.1 ± 0.1 (49.4%)	0.68
1853	5	700	380.0 ± 1.7 (84.3%)	478.9 ± 1.3 (94.4)	8.0 ± 0.2 (48.8%)	0.67
1854	6	800	407.5 ± 2.1 (90.4%)	505.5 ± 1.3 (99.7%)	9.1 ± 0.1 (55.5%)	0.59
1855	7	900	410.7 ± 0.6 (91.1%)	505.3 ± 0.6 (99.6%)	9.2 ± 0.3 (56.1%)	0.53
1856	8	1000	415.7 ± 2.1 (92.2%)	505.2 ± 0.5 (99.6%)	10.0 ± 0.4 (61.0%)	0.50
1857	9	1100	421.5 ± 0.7 (93.5%)	510.6 ± 1.3 (100.7%)	10.7 ± 0.2 (65.2%)	0.46
1872	10	1200	419.3 ± 2.9 (93.0%)	506.3 ± 0.5 (99.8%)	10.1 ± 0.2 (61.6%)	0.47

Table 4.10: Tensile test results for double-sided FSW.

An immediate conclusion when glancing at the Tab. 4.10 is that incredibly high values of tensile properties can be achieved by DS-FSW, particularly the yield and ultimate strength values. For a significant number of the welds the double-sided FSW variant seems to affect very little or virtually not affected at all the base material yield and ultimate strength properties. With the exception of 1852 and 1853 welds, for instance, the ultimate strength obtained after the welding process is virtually the same of the original workpiece.

Such as for the single-sided FSW the elongation appears as the critical feature reaching its maximum, of 10.7%, for the 1857 weld representing an efficiency of 65.2%. This represents an improvement of 30.8% when compared with the best elongation value for the conventional FSW. Since none of the welds presented clear lack of material intermixing no definitive conclusion could be drawn regarding what may cause the slightly variations on properties values between different welds. It should be noted, however, that the tensile properties, particularly the elongation, seems to be improved as the heat input is successively decreased, reaching its global maximum for the DS-FSW-PA-LB-1857 which also represents the lower heat input value weld.

In general terms it can be said that a significant improvement on the tensile properties, with special reference to the elongation, was obtained by DS-FSW variant. The best set of parameters, leading to the best mechanical properties, were those of the 1857 weld namely, 9 mm/s, 1100 rpm and 15 kN. With these parameters an improvement of 14.0%, 7.0% and 33.6% for the yield strength, ultimate strength and elongation respectively were obtained when compared with those obtained for best set of parameters found on the conventional FSW parameters study previously presented (section 4.1.4). In Fig. 4.2.6 are shown the tensile test responses of some of welds performed for the DS-FSW process as well the comparison with the stress-strain curve of the base material and the best FSW obtained weld.

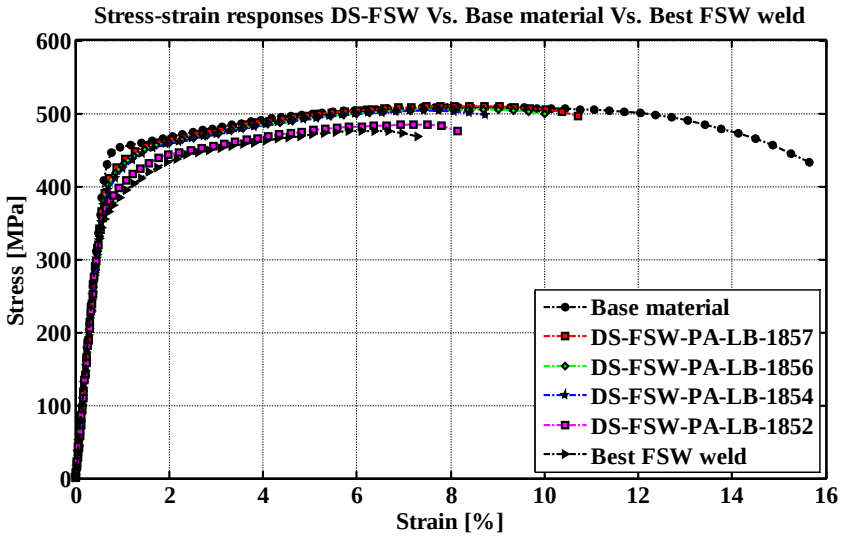

Figure 4.2.6: Comparison of the stress-strain curves of some DS-FSW welds as well as the base material and the best FSW tensile responses.

4.2.4 Temperature measurements

Fig. 4.2.7 presents the typical progress of temperature values during one pass for the DS-FSW process along the full length of a set of plates. The temperature progress representation is referent to the second pass (B) of the DS-FSW-PA-LB-1896 weld (HZG denomination) performed for the best set of parameters found in the study, which were, as seen, 9 mm/s, 1100 rpm and 15 kN; in Fig. 4.2.7 are presented just the data collected for the 18 thermocouples located in the drilled holes (see 3.1.5).

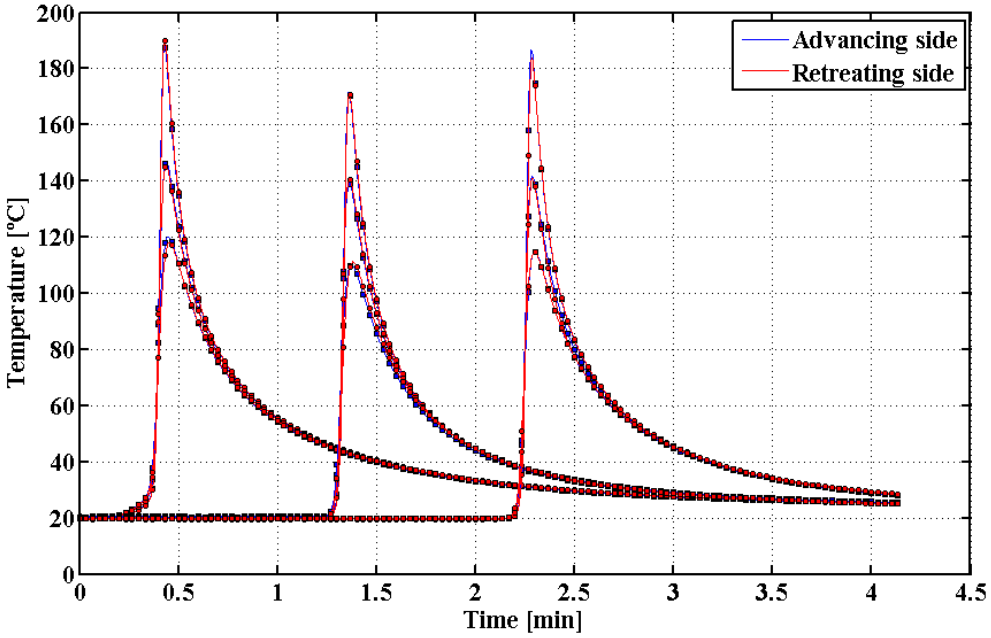

Figure 4.2.7: Temperature measurements during the DS-FSW-PA-LB-1896 (B).

The thermal cycles shape, roughly the same for all the three measuring regions, are in everything identical to those observed on the conventional FSW; peak temperatures are reached very quickly followed

by a relatively fast cooling in an overall thermal cycle of about 1:20 minutes. Peak temperatures, presented in Tab. 4.11, were significantly lower than those observed for the single-sided version (see. Tab. 4.6) something easily understandable since a smaller tool and a smaller amount of energy is supplied at a time (in each pass) when compared with the overall process of conventional FSW. The highest temperature value observed for the DS-FSW process was 190.6°C for the thermocouple number 12 which represents a global difference of 110.9°C (36.8%) when compared with the highest temperature value registered for the conventional FSW.

Region	**Side**	**Thermocouple position**	**Max. Temperature [°C]**
1	Advancing side	9	188.5
		10	146.8
		11	120.1
	Retreating side	12	190.6
		13	145.4
		14	118.0
2	Advancing side	15	171.7
		16	139.0
		17	110.3
	Retreating side	18	171.3
		19	140.8
		20	111.3
3	Advancing side	21	186.8
		22	141.6
		23	114.9
	Retreating side	24	183.7
		25	140.9
		26	114.8

Table 4.11: Peak temperatures at the measuring points, DS-FSW (pass B).

An overall difference between welding processes regarding the peak temperatures from the thermocouples nearest placed to the joint line of 89.5°C (32.9%) for the advancing side and 117.2°C (39.2%) for the retreating side was possible to ascertain. Unlike conventional FSW no real tendency or high temperature deviations were observed between the two sides of the process, Tab. 4.12. That may be explained by the fact that for both the FSW and DS-FSW the drilled holes were located at the same positions which in reality means that the thermocouples on the DS-FSW were placed farthest from the tool shoulder influence than for the FSW resulting, naturally in lower temperature values as well lower, or none, difference between the two sides of the process; as seen in 4.1.5 differences between temperatures registered on either side tend to drop as the measurement position are moved away from the initial joint line.

Region	Side	Thermocouple	Temperature [°C]	Difference [%]
1	Advancing side	9	188.5	1.1
	Retreating side	12	190.6	
2	Advancing side	15	171.7	0.2
	Retreating side	18	171.3	
3	Advancing side	21	186.8	1.7
	Retreating side	24	183.7	

Table 4.12: Recorded peak temperatures for the nearest measuring points; AS and RS comparison.

Located on the backing bar and ideally at 1 mm from the bottom surface and hence at approximately 5 mm bellow the tip of the probe the 8 backing bar thermocouples registered an average temperature of 159.9±15.1°C.

In Fig. 4.2.8 the temperature recorded on the tool during and after the welding of one of the passes is presented. For each pass and for a complete plate length weld (approximately 2:15 minutes) the maximum temperature observed was 371.8°C which was essentially the same registered on the single-sided FSW.

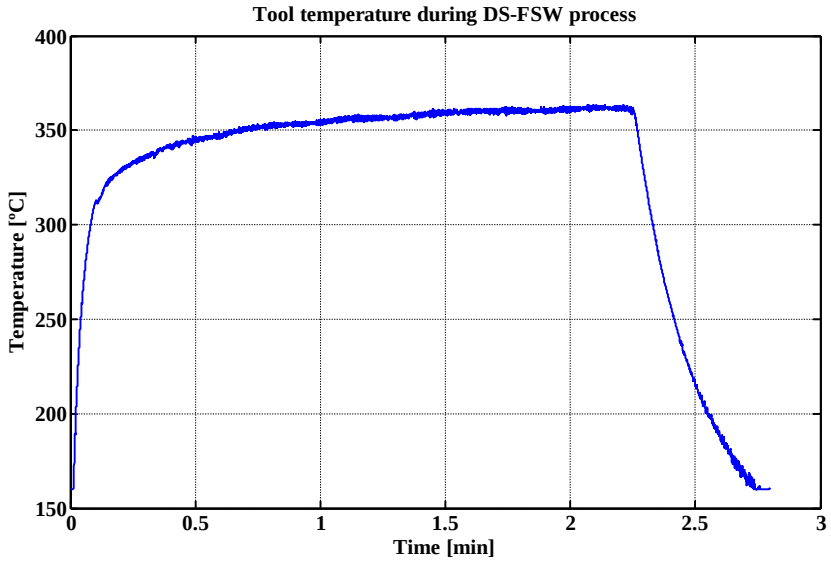

Figure 4.2.8: Temperature progress on the welding tool during DS-FSW process.

It should be mentioned that the temperature presented do not represent the ultimate temperature reached during the welding process within the core of the stir zone but rather an estimate temperature value for a given measuring position. Therefore, and since the measuring points were located in the exact same place for both processes, it is possible to conclude that a narrower affected zone is achieved by performing the DS-FSW process.

4.2.5 Fracture analysis

The double-sided tensile specimens presented two different failure locations. The fracture locations are exhibited in Fig. 4.2.9 and Fig. 4.2.10; in both cases the failure occurred, with no exception, at the heat-affected zone, which as previously shown corresponds to a weakened region where the lower mechanical values are expected to be found.

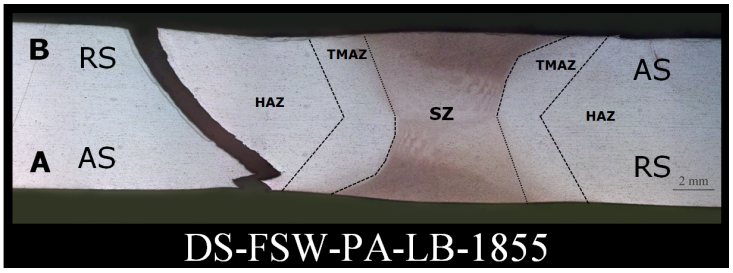

Figure 4.2.9: Macro-morphology of DS-FSW-PA-LB-1855 weld fracture.

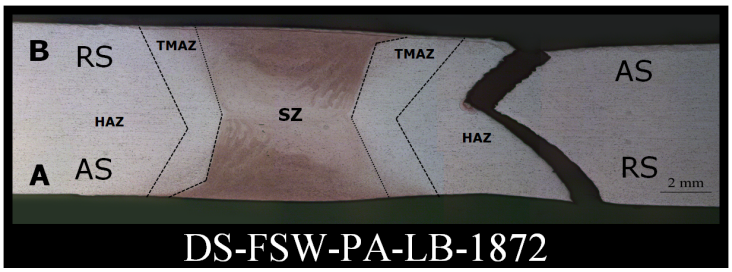

Figure 4.2.10: Macro-morphology of DS-FSW-PA-LB-1855 weld fracture.

The fractures possessed a sharp straight edge that followed (in the welding direction) the outer border left by the shoulder trail on the advancing side of either the first pass (Fig. 4.2.9) or second pass (Fig. 4.2.10) of the process (pass A or B respectively). These kind of fracture, seemed to suggest that the shoulder trails left on the advancing side of either passes were somehow responsible for a stress concentration factor, as a sort of notch, that led the fracture to follow its trail line along the welding direction. No obvious or conclusive reason seems to justify the pass preference to failure although the fracture mode presented in Fig. 4.2.9 which was observed in all tensile specimens on 5 of the 7 welds in study and thus by far the most common, corresponded to the highest heat input values; the lower heat input value welds, namely 1857 and 1872 presented the fracture mode exhibited in Fig. 4.2.10 which could imply that the pass preference to failure may be somehow related with the overall heat input value supplied. Bellow in Fig. 4.2.11 and Fig. 4.2.12 are presented the real fracture appearance of the tensile specimens.

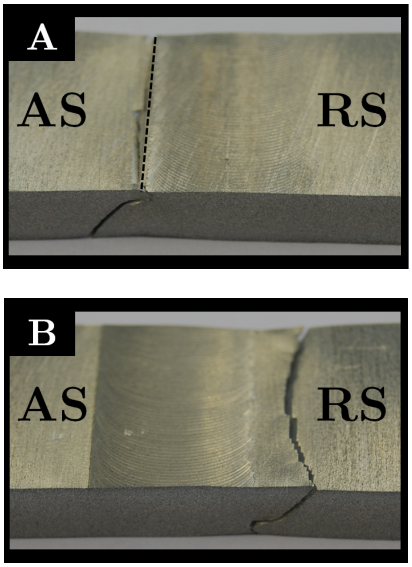

Figure 4.2.11: DS-FSW-1855 fracture appearance.

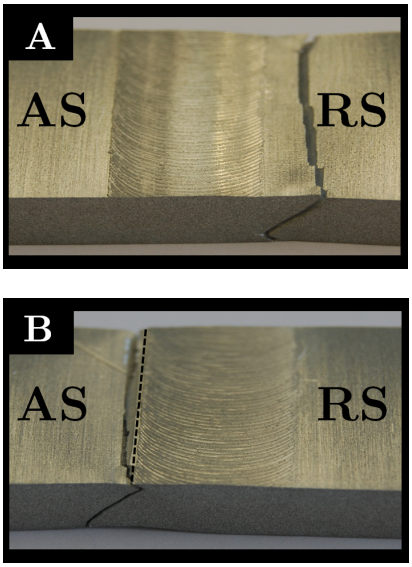

Figure 4.2.12: DS-FSW-1872 fracture appearance.

In all failures, independently of the side preference was possible to observe a significant necking, characteristic of the ductile fracture and intimately related with significant values of elongation. Bellow are presented SEM fractographs performed for one of the fracture surfaces of the DS-FSW-PA-LB-1857 weld; SEM examination revealed large amount of dimples which, as seen, are related with the overload an the ductile nature of fracture.

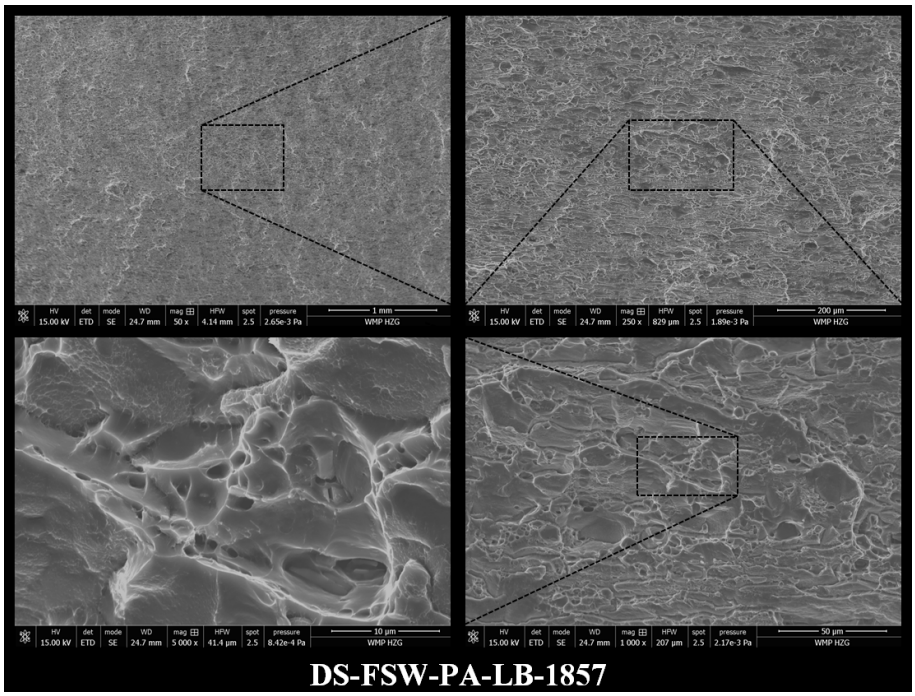

Figure 4.2.13: SEM fractographs of the DS-FSW-PA-LB-1857 fracture surface.

4.2.6 Distortion assessment

Distortion assessment following a similar procedure and layout of that of the conventional FSW (see. 4.1.7) was performed for the best set of double-sided FSW parameters (DS-FSW-PA-LB-1857). Distortion was measured between passes in order to ascertain the influence of each pass on the overall distortion. Markers were placed uniquely on the surface corresponding to the first pass. The distortion assessment and displacement values were obtained when looking to the first pass (first pass upwards).

Just as it happened for the single-side FSW case, both for the x and y directions, low or very low values of distortion, when compared with those of z direction, were found (for both passes); the overall distortion map was then essentially dependent on the distortion values found on the z direction which, inevitably presented very similar features.

Bellow in Fig. 4.2.14 and Fig. 4.2.15 are shown the distortion maps for the z spacial direction after the first and second passes respectively.

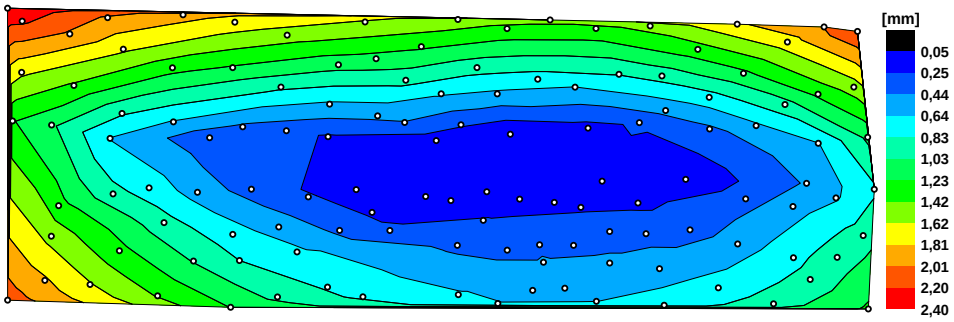

Figure 4.2.14: Distortion distribution (z direction) after the first pass.

Fig. 4.2.14 reveals that higher values of displacement were found on the outer edges of the plates; it

is then possible to ascertain that the first pass was responsible for a state of distortion that essentially consisted of two kinds of distortion; a very wide V-shaped cross-section that followed the x direction (lengthwise) and that was consequently responsible for an almost imperceptible lifting of the outer long edges of the plates (top and bottom in Fig. 4.2.14) and a slight buckling on the lengthwise direction that was responsible for a visually imperceptible lifting of the outer short edges of the welded set of plates (left and right sides of the Fig. 4.2.14). This kind of distortion, roughly speaking, in a boat-like shape, was something expected since just half of the thickness was welded and the vertical load and residual stresses derived from the welding process have the natural tendency to generate tensile stresses on upper surface which are ultimately responsible for lifting the outer edges once the clamping system was loosened.

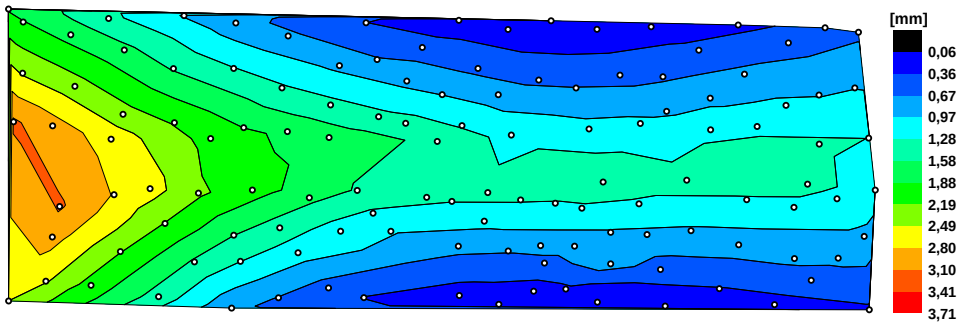

Figure 4.2.15: Distortion distribution (z direction) after the second pass.

After the second pass, Fig. 4.2.15 there seemed to be a compensatory effect relatively to the distortion obtained after the first pass. Unlike the displacement distribution of the first pass the lower values of displacement were observed on the outer edges of the set of plates being the highest values found along the joint line and particularly on the finish point (FP) of the second pass. It should be recalled that the distortion map presented in Fig. 4.2.15 was obtained when looking at the first pass and that consequently higher values along the joint line (as a consequence of the contact of outer edges - x direction) are a consequence of the wide V-shaped cross-section that resulted from the second pass and which is responsible for compensating the distortion effect of the first pass. A longer dwelling time of the tool in the workpiece, resulting from the period immediately after the welding process was completed and the total removal of the tool, led to higher heat input supplied and longer thermal cycles on the finish point region of the second pass which may be the cause of the higher displacements on the particular region. Below are presented the 3D distortion representations of the set of plates after the first and second passes. The surface displayed upwards is relative to the pass A.

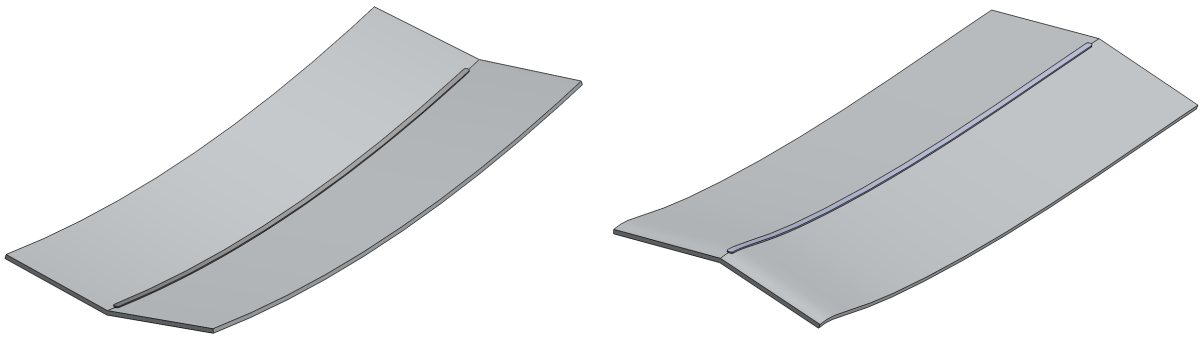

Figure 4.2.16: Schematic representation of the distortion involved: pass A (left), pass B (right)

Both the conventional and double-sided FSW distortion measurements revealed that the original shape

of the set of plates was not greatly affected by the welding processes. Although distortion assessment on double-sided FSW showed a compensatory effected of displacements between the different passes the final product was prone to be a bit more deformed than conventional FSW, Fig. 4.2.17 and Fig. 4.2.18.

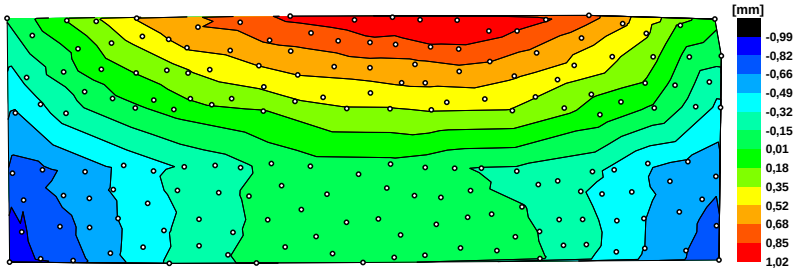

Figure 4.2.17: Distortion map (z direction) FSW

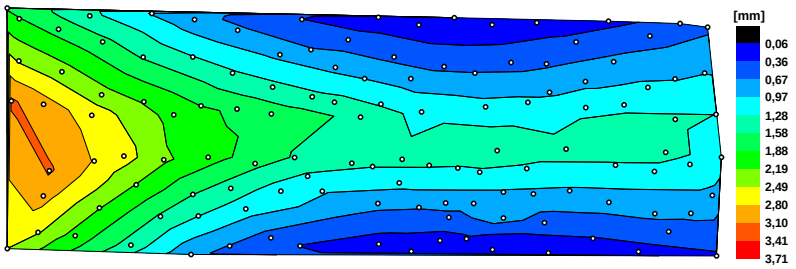

Figure 4.2.18: Distortion map (z direction) DS-FSW

Chapter 5

Conclusion

From the experimental work carried out it was possible to conclude that:

FSW

- For the conventional FSW process, higher welding speeds combined with low or insufficient rotational speed, leading, consequently to lower values of heat input, were responsible for lack of complete material intermixing where volumetric defects of significant size could be found in the upper region of the stir zone;
- For a constant vertical load an increase of the weld pitch led to better material intermixing; the same effect could be observed when increasing the vertical load for a given weld pitch; both cases were intimately responsible for an increase of the heat input value;
- Successfully mixed welds presented the characteristic "W" transverse hardness profiles where the lower hardness values were expectedly found in the HAZ; 80.2% was the hardness efficiency value achieved for the best set of parameters - 5 mm/s, 700 rpm and 25 kN;
- As the heat input values were successively increased greater heat-affected areas and lower absolute hardness values were found;
- A clear tendency for improvement of mechanical properties when the heat input value was successfully increased was observed;
- For the best set of parameters, resulting in an heat input of 0.60 kJ/mm, welding efficiency values of 80.4%, 93.7% and 43.3% for the yield strength, ultimate strength and elongation tensile properties were reached. Elongation efficiency values were systematically the lower of the mechanical properties being critical parameter;
- A global difference of 27.2°C, corresponding to 9.1%, was found between the two sides of the welding process being the retreating side the hottest. No difference on the cross-section microstructure and HAZ size was possible to be observed tough;
- Fracture analysis revealed a tendency for failure occur on the retreating side of the welding process. Welds presenting good material intermixing broke in the HAZ presenting ductile fracture features (dimples) when subjected to SEM. Insufficiently material mixed welds, in contrast, revealed a fragile fracture that occurred through the tool shoulder influence (stir zone);

- Distortion assessment revealed that the welding process barely had influence on the geometric state of the plates. Very low values of relative displacement were found within a set of plates being the real distortion virtually impossible to notice by visual inspection.

DS-FSW

- For all the set of parameters performed good material intermixing and homogeneous microstructure were observed;

- The transverse hardness profiles revealed the characteristic "W" shape on the three indentation lines performed. The middle indentation line, corresponding to half of the thickness, presented the lower hardness values on its HAZ, which, in general and in terms of weld efficiency proved to be slightly higher than those of the FSW. For the best set of parameters, 9 mm/s, 1100 rpm and 15 kN, a welding efficiency, in terms of hardness values, of 86.7% was achieved which corresponded to an improvement of approximately 7.5% when compared with the conventional FSW;

- As for the conventional FSW case, an increase of the heat input value was responsible for greater heat-affected zones combined with lower hardness values;

- For the best set of parameters, resulting in a global heat input value of 0.46 kJ/mm, welding efficiency values of 93.5%, 100.7% and 65.2% for the yield strength, ultimate strength and elongation tensile properties were achieved. Those values revealed a significant improvement on the mechanical properties when compared with the single-sided FSW process; an improvement, in terms of percentage values of 14.0%, 7.0% and 33.6% for, respectively, the yield strength, ultimate strength and elongation were found;

- As observed for the conventional FSW process, elongation values appeared as the critical ones since, a modest maximum efficiency value of only 65.2% was possible to be observed. A clear tendency of elongation improvement as the global heat input value was successively decrease was also uncovered. Yield, and more particularly, ultimate strength did not seem to be significantly affected by the welding process since, high ($\sim$92%) for the yield strength or even very high ($\sim$99%) for the ultimate strength, efficiency values were obtained;

- Temperature measurements carried out during the DS-FSW process did not revealed relevant differences between the temperatures registered in the two sides of the process - advancing and retreating. Was possible to verify, however, that a narrower band of affected material is obtained for the DS-FSW when compared with the single-sided FSW, something expected since the DS-FSW tool had smaller dimensions.

- Tensile failure occurred, with no exception, on the HAZ along the outer trailing line left by the tool shoulder on the advancing side of either the first or second pass; a stress concentration factor arising from a notch effect on the advancing side could be a possible explanation for the welding side preference, however no conclusive hypotheses concerning the pass preference was possible to be drawn;

- Distortion measurements performed for DS-FSW process revealed that the welding process had very few influence on the original geometrical state of the set of plates; a compensatory effect on the distortion was, however, observed between the two passes being the overall distortion a result from both individual distortions.

Future work

To complement the experimental work carried out a number of new experiments and process analysis could and should be done in the near future. Although significantly satisfactory experimental results were already obtained, certain aspects concerning the study of welding parameters itself, for both the FSW and DS-FSW could be, naturally, still be subjected to an attempt of weld properties enhancement through refinement on the ideal set of parameters, with special attention those leading to higher values of heat input (FSW) aiming to an improvement of the elongation efficiency values.

Since the process in study has great industrial applications and deals with structural components subjected to severe operating conditions, fatigue test and residual stresses assessment of the performed welds must be carried out in order to have a better understanding of its properties when subjected to real operating conditions; as mentioned at the beginning of this document questions concerning the process productivity must be also assessed something that can be relatively easy to do by a tool wear evaluation when subjected to real (industrial) welding process.

[blank page]

Bibliography

[1] B.T. Gibson, D.H. Lammlein, T.J. Prater, W.R. Longhurst, C.D. Cox, M.C. Ballun, K.J. Dharmaraj, G.E. Cook, and A.M. Strauss. Friction stir welding: Process, automation, and control. *Journal of Manufacturing Processes*, 16(1):56–73, January 2014.

[2] J.R. Kissell. Aluminum Alloys. In *Handbook of Materials for Product Design*, pages 2.1–2.1178. McGrawHill, 2001.

[3] T. Dursun and C. Soutis. Recent developments in advanced aircraft aluminium alloys. *Materials & Design*, 56:862–871, April 2014.

[4] FC Campbell. Manufacturing Technology for Aerospace Structural Materials. 2006.

[5] P. A. Rometsch, Y. Zhanz, and S. Knight. Heat treatment of 7xxx series aluminium alloys - Some recent developments. *Transactions of Nonferrous Metals Society of China*, 24(7):2003–2017, July 2014.

[6] F. Song, X. Zhang, S. Liu, Q. Tan, and D. Li. The effect of quench rate and overageing temper on the corrosion behaviour of AA7050. *Corrosion Science*, 78:276–286, January 2014.

[7] R.S. Mishra and Z.Y. Ma. Friction stir welding and processing. *Materials Science and Engineering: R: Reports*, 50(1-2):1–78, August 2005.

[8] P L Threadgill, a J Leonard, H R Shercliff, and P J Withers. Friction stir welding of aluminium alloys. *International Materials Reviews*, 54(2):49–93, March 2009.

[9] R. Nandan, T. Debroy, and H.K.D.H. Bhadeshia. Recent advances in friction-stir welding - Process, weldment structure and properties. *Progress in Materials Science*, 53(6):980–1023, August 2008.

[10] C.D. Sorensen, T.W Nelson, and S.M. Packer. Tool Material Testing for FSW of High-Temperature Alloys. In *Proceedings of the Third International Symposium on Friction Stir Welding*, Kobe, Japan, 2001.

[11] C.G. Rhodes, M.W. Mahoney, W.H. Bingel, R.A. Spurling, and C.C. Bampton. Effects of friction stir welding on microstructure of 7075 aluminum. *Scripta Materialia*, 36(1):69–75, January 1997.

[12] G. Liu, L.E. Murr, C-S. Niou, J.C. McClure, and F.R. Vega. Microstructural aspects of the friction-stir welding of 6061-T6 aluminum. *Scripta Materialia*, 37(3):355–361, August 1997.

[13] K.V. Jata and S.L. Semiatin. Continuous dynamic recrystallization during friction stir welding of high strength aluminum alloys. *Scripta Materialia*, 43(8):743–749, September 2000.

[14] S Benavides, Y Li, L.E Murr, D Brown, and J.C McClure. Low-temperature friction-stir welding of 2024 aluminum. *Scripta Materialia*, 41(8):809–815, September 1999.

[15] W. M. Thomas and R.E. Dolby. Proceedings of the Sixth International Conference on Trends in Welding Research. *ASM International*, pages 203–211, 2003.

[16] Y.H. Zhao, S.B. Lin, F.X. Qu, and L. Wu. Influence of pin geometry on material flow in friction stir welding process. *Materials Science and Technology*, pages 45–50, 2006.

[17] G. Buffa, J. Hua, R Shivpuri, and L. Fratini. Design of the friction stir welding tool using the continuum based FEM model. *Mater Sci Eng A*, pages 381–8, 2006.

[18] M. W. Mahoney, C. G. Rhodes, J. G. Flintoff, W. H. Bingel, and R. A. Spurling. Properties of friction-stir-welded 7075 T651 aluminum. *Metallurgical and Materials Transactions A*, 29(7):1955–1964, July 1998.

[19] Yutaka S. Sato, Hiroyuki Kokawa, Masatoshi Enmoto, and Shigetoshi Jogan. Microstructural evolution of 6063 aluminum during friction-stir welding. *Metallurgical and Materials Transactions A*, 30(9):2429–2437, September 1999.

[20] Y. S. Sato, M. Urata, and H. Kokawa. Parameters controlling microstructure and hardness during friction-stir welding of precipitation-hardenable aluminum alloy 6063. *Metallurgical and Materials Transactions A*, 33(3):625–635, March 2002.

[21] Y. J. Kwon, N. Saito, and I. Shigematsu. Friction stir process as a new manufacturing technique of ultrafine grained aluminum alloy. *Journal of Materials Science Letters*, 21(19):1473–1476, 2002.

[22] T. Hashimoto, S. Jyogan, K. Nakata, Y.G. Kim, and M. Ushio. FSW Joints of High Strength Aluminium Alloys. In *Proceedings of the First International Symposium on Friction Stir Welding*, Thousand Oaks, CA, USA, 1999.

[23] W.J. Arbegast and P.J. Hartley. Proceedings of the Fifth International Conference on Trends in Welding Research. pages 541–546, Pine Mountain.

[24] P.L. Threadgill. Friction stir welds in aluminium alloys - preliminary microstructural assessment. *TWI Bulletin*.

[25] P.L. Threadgill. Terminology in friction stir welding. *Science and Technology of Welding and Joining*, 12(4):357–60, 2007.

[26] Specification for friction stir welding of aluminum alloys for aerospace applications. *American Welding Society*, 2006.

[27] J.-Q Su, T.W Nelson, R Mishra, and M Mahoney. Microstructural investigation of friction stir welded 7050-T651 aluminium. *Acta Materialia*, 51(3):713–729, February 2003.

[28] K.N. Krishnan. On the formation of onion rings in friction stir welds. *Materials Science and Engineering: A*, 327(2):246–251, April 2002.

[29] Ying Li, L.E Murr, and J.C McClure. Flow visualization and residual microstructures associated with the friction-stir welding of 2024 aluminum to 6061 aluminum. *Materials Science and Engineering: A*, 271(1-2):213–223, November 1999.

[30] Y Kwon. Mechanical properties of fine-grained aluminum alloy produced by friction stir process. *Scripta Materialia*, 49(8):785–789, October 2003.

[31] I. Charit, R. S. Mishra, Y. T. Zhu, T.G. Langdon, R. Z. Valiev, S.L. Semiatin, D. H. Shin, and T. C. Lowe. Ultrafine Grained Materials III. *TMS*, 2004.

[32] Z.Y Ma, R.S Mishra, and M.W Mahoney. Superplastic deformation behaviour of friction stir processed 7075Al alloy. *Acta Materialia*, 50(17):4419–4430, October 2002.

[33] M.W. Mahoney, R.S. Mishra, T.W Nelson, J. Flintoff, R. Islamgaliev, and Y. Hovansky. Friction Stir Welding and Processing. *TMS*, page 183, 2001.

[34] K.V. Jata, K.K. Sankaran, and J.J. Ruschau. Friction-Stir Welding Effects on Microstructure and Fatigue of Aluminum Alloy 7050-T7451. *Metallurgical and Materials Transactions A*, 31 A:2000–2181, 2000.

[35] Y.S. Sato, S.H.C. Park, and H. Kokawa. Microstructural Factors governing Hardness in Friction-Stir-Welds of Solid-Solution-Hardened Al Alloys. *Metallurgical and Materials Transactions A*, 32A-12:3033–3042, 2001.

[36] L.-E. Svensson, L. Karlsson, H. Larsson, B. Karlsson, M. Fazzini, and J. Karlsson. Microstructure and mechanical properties of friction stir welded aluminium alloys with special reference to AA 5083 and AA 6082. *Science and Technology of Welding and Joining*, 5(5):285–296, October 2000.

[37] R. Brown, W. Tang, and A.P. Reynolds. Multi-pass friction stir welding in alloy 7050-T7451: Effects on weld response variables and on weld properties. *Materials Science and Engineering: A*, 513-514:115–121, July 2009.

[38] J. Yan, M. A. Sutton, and A. P. Reynolds. Process - structure - property relationships for nugget and heat affected zone regions of AA2524 - T351 friction stir welds. *Science and Technology of Welding and Joining*, 10(6):725–736, December 2005.

[39] A. J. Leonard and S. A. Lockyer. Flaws in Friction Stir Welds. In *Fourth International Symposium on Friction Stir Welding*, Park City, UT, USA.

[40] H. Okamura, K. Aota, M. Sakamoto, M. Ezumi, and K. Ikeuchi. Behaviour of oxides during friction stir welding of aluminium alloy and their effect on its mechanical properties. *Weld Int.*, 16:266–275, 2002.

[41] F. Palm, H. Steiger, and U. Hennebohle. Highest FSW Joints Properties versus FSW Process Stability. In *Fourth International Symposium on Friction Stir Welding*, Park City, UT, USA.

[42] B. K. Christner and G. D. Sylva. Friction stir weld developments for aerospace applications. In *Proc. Conf. ICAWT*, pages 359–368, Columbus, OH, USA, 1996.

[43] M. James and M. Mahoney. Proceedings of the First International Symposium on Friction Stir Welding. In *First International Symposium on Friction Stir Welding*, Thousand Oaks, CA, USA, 1999.

[44] C.D. Donne, E. Lima, J.Wegener, A. Pyzalla, and T. Buslaps. Proceedings of the Third International Symposium on Friction Stir Welding. Kobe, Japan, 2001.

[45] M. Peel, A. Steuwer, M. Preuss, and P.J. Withers. Microstructure, mechanical properties and residual stresses as a function of welding speed in aluminium AA5083 friction stir welds. *Acta Materialia*, 51(16):4791–4801, September 2003.

[46] G. Bussu and P.E. Irving. Fatigue Performance of Friction Stir Welded 2024-T351. In *First International Symposium on Friction StirWelding*, Thousand Oaks, CA, USA, 1999.

[47] H. Hori, S. Makita, and H. Hino. Friction Stir Welding of Rolling Stock for Subway. In *Proceedings of the First International Symposium on Friction StirWelding*, Thousand Oaks, CA, USA.

[48] C. Dalle Donne, G. Biallas, T. Ghidini, and G. Raimbeaux. Effect of Weld Imperfections and Residual Stresses on the Fatigue Crack Propagation in Friction Stir Welded Joints. In *Second International Symposium on Friction Stir Welding*, Gothenburg, Sweden, 2000.

[49] M. Cabibbo, A. Forcellese, M. El Mehtedi, and M. Simoncini. Double side friction stir welding of AA6082 sheets: Microstructure and nanoindentation characterization. *Materials Science and Engineering: A*, 590:209–217, January 2014.

[50] H. Wu, Ying-Chun Chen, D. Strong, and P. Prangnell. Stationary Shoulder FSW for Joining High Strength Aluminum Alloys. *Journal of Materials Processing Technology*, February 2015.

[51] W.Y. Li, T. Fu, L. Hütsch, J. Hilgert, F.F. Wang, J.F. dos Santos, and N. Huber. Effects of tool rotational and welding speed on microstructure and mechanical properties of bobbin-tool friction-stir welded Mg AZ31. *Materials & Design*, 64:714–720, December 2014.

[52] F.F. Wang, W.Y. Li, J.J. Shen, S.Y. Hu, J.L. Li, J.F. dos Santos, and N. Huber. Effect of tool rotational speed on the microstructure and mechanical properties of bobbin tool friction stir welding of Al-Li alloy. *Materials & Design*, pages 1–2, July 2015.

[53] Huijie Zhang, Min Wang, Xiao Zhang, and Guangxin Yang. Microstructural characteristics and mechanical properties of bobbin tool friction stir welded 2A14-T6 aluminum alloy. *Materials & Design*, 65:559–566, January 2015.

[54] M. Skinner and R.L. Edwards. Improvements to the FSW Process Using the Self-Reacting Technology. *Materials Science Forum*, 426-432:2849–2854, August 2003.

[55] CES EduPack, 2014.

[56] J. W. Pew, T. W. Nelson, and C. D. Sorensen. Torque based weld power model for friction stir welding. *Science and Technology of Welding and Joining*, 12(4):341–347, May 2007.

[57] G. Biallas and Et Al. Mechanical Properties and corrosion behaviour of friction stir welded 2024-T6. In *First International Conferece on Friction Stir Welds*, Thousand Oaks, CA, USA, 1999.

[58] F. Rui-dong, S. Zeng-qiang, S. Rui-cheng, L. Ying, L. Hui-jie, and L. Lei. Improvement of weld temperature distribution and mechanical properties of 7050 aluminum alloy butt joints by submerged friction stir welding. *Materials & Design*, 32(10):4825–4831, December 2011.

Annexes

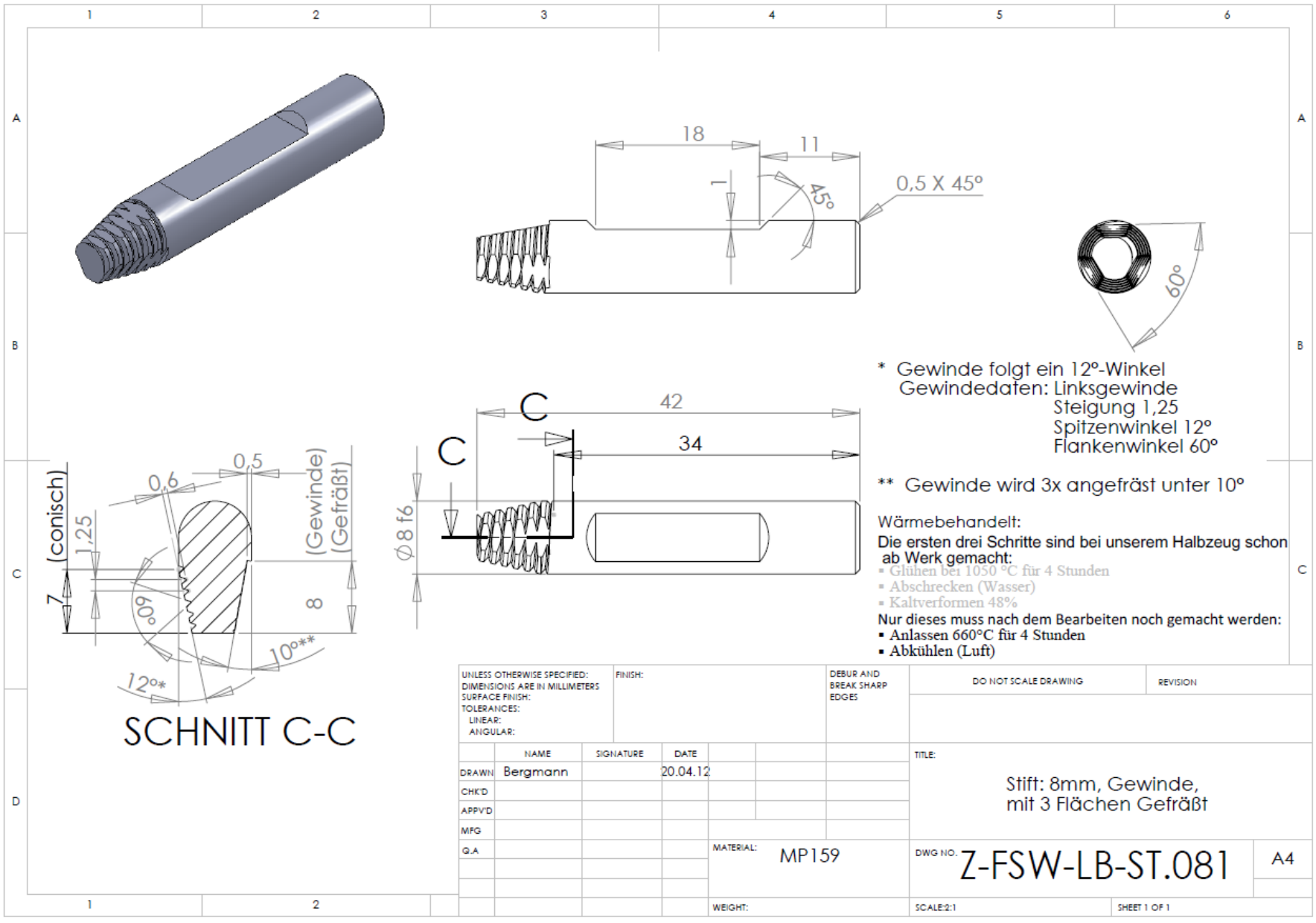

Technical drawing of the FSW tool (probe).

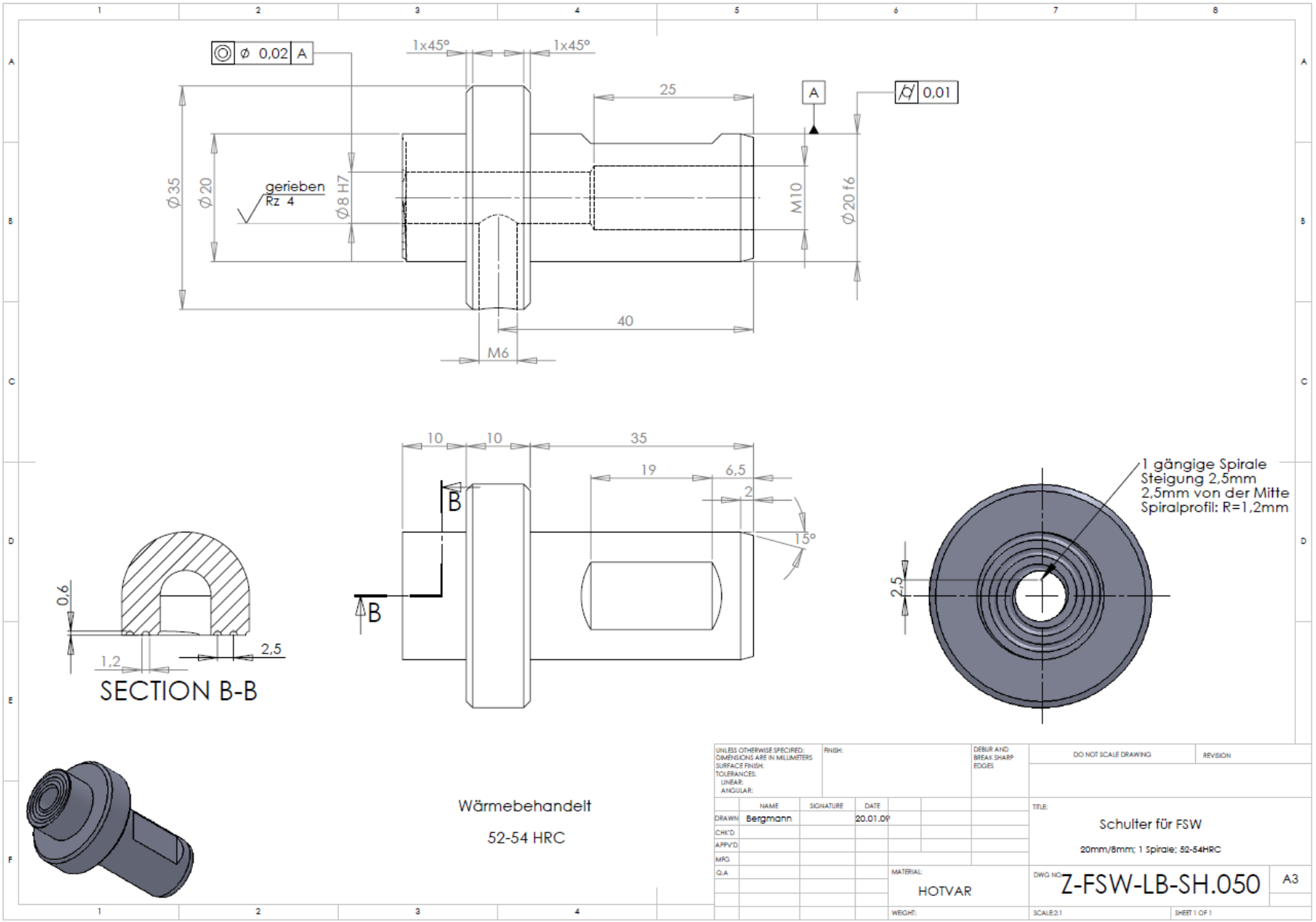

Technical drawing of the FSW tool (shoulder).

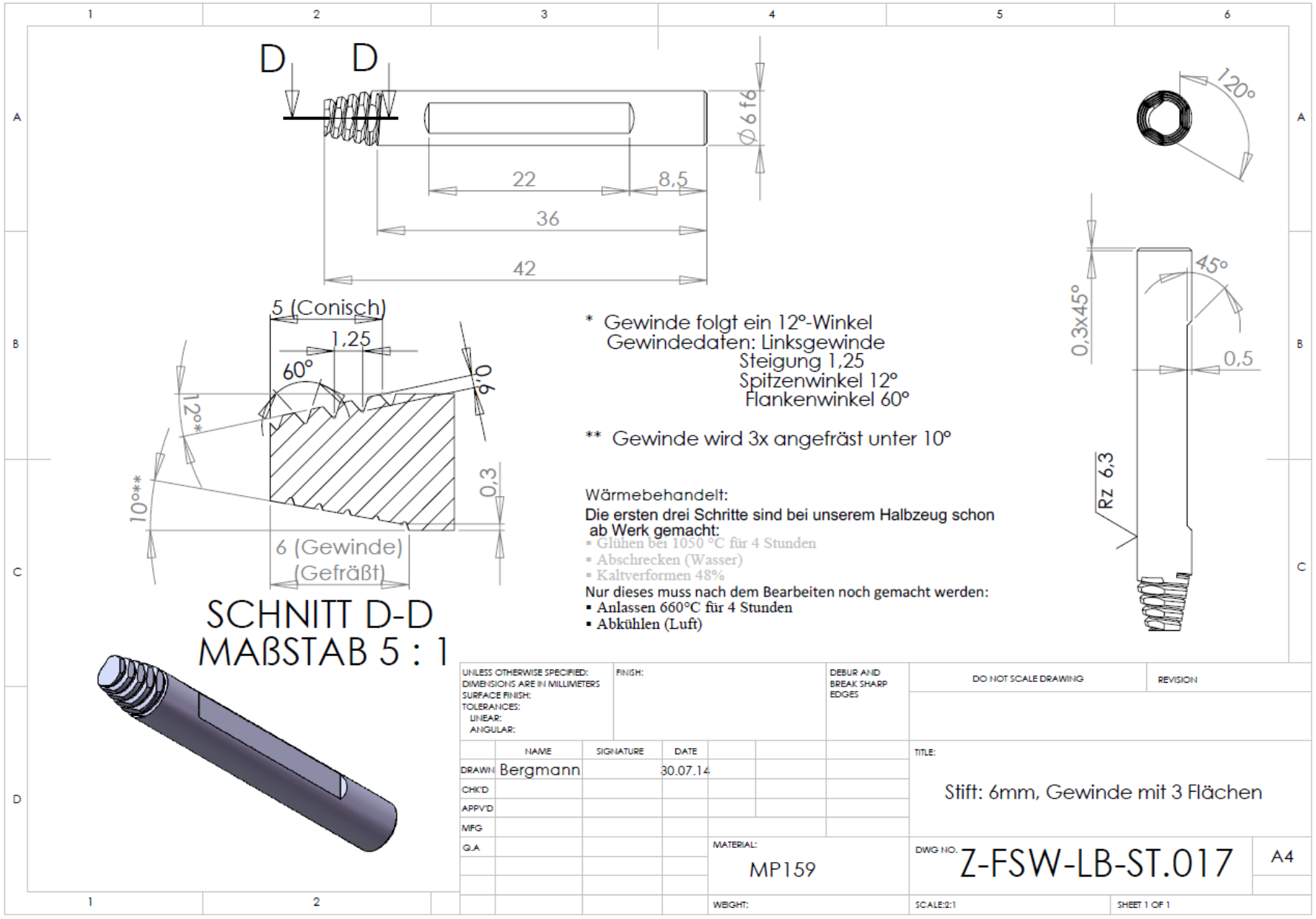

Technical drawing of the DS-FSW tool (probe).

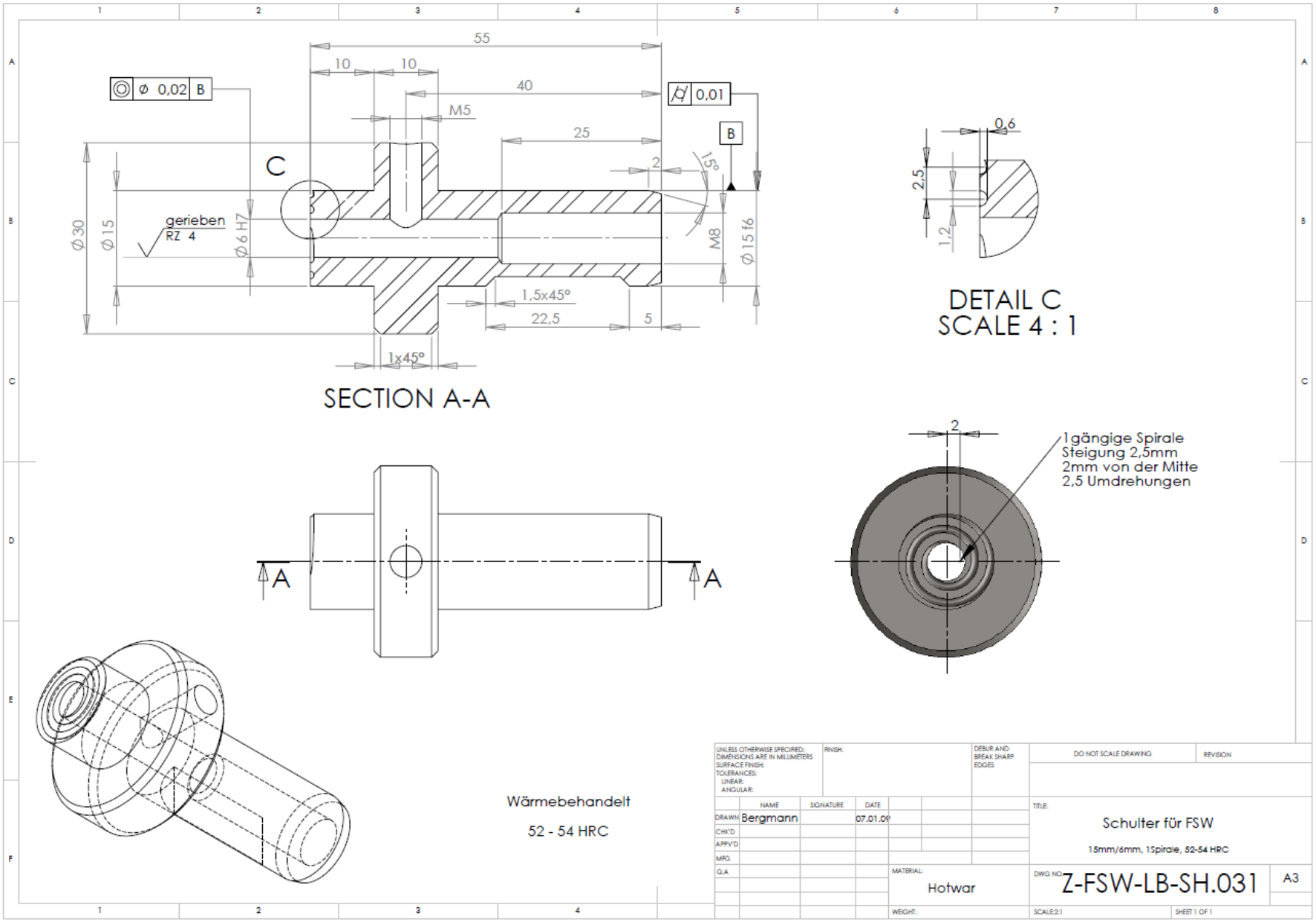

Technical drawing of the DS-FSW tool (shoulder).

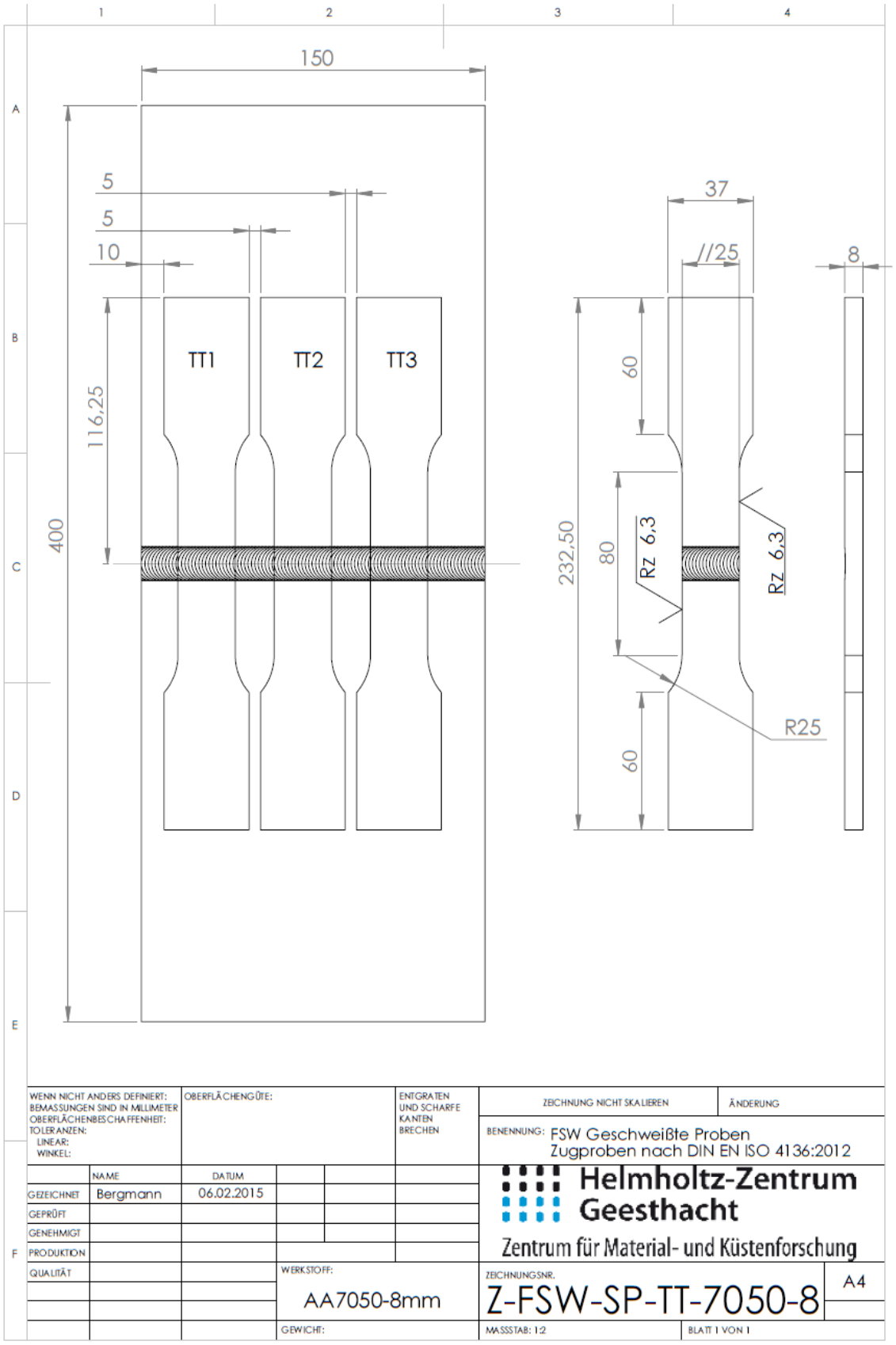

Technical drawing of the tensile specimens (FSW & DS-FSW).

[blank page]